Annex to

Design Requirements and Guidelines Level 1 (DRG1)

Structural Material Database
Article 2. Metallic Material Database

Annex 3. Final Report on "ITER Coil Casing and Intercoil Structures" (FzK)

Final Report on "ITER Coil Casing and Intercoil Structures"

ITER Task No. N11TT89

Table of Contents

1. Overview

Within this present ITER technology task (ITER contract Task No. N11TT89) lasted between July 1997 and June 2000 several materials and structural related problems dealing with ITER model coils and full size mock-ups were investigated. The Report includes also the final part of the investigation results with respect to fatigue crack growth rate measurements of central solenoid (CS) jacket materials which were the candidate materials of Type 316LN and the currently used Incoloy 908. By using a new, recently developed evaluation software it was possible to update these results and finalize the investigations. Besides the material related problems, also important critical components of the Toroidal field model coil (TFMC) were tested with respect to their operational boundary conditions. Within this context the sliding properties of the insulated TFMC superconductor, housed in a representative clamping system were determined at liquid helium environment. Another important aspect was also the determination of the structural behavior of the explosion bonded material combination of copper and Incoloy 908 at cryogenic temperatures in as received and heat treated condition. In addition, to elucidate the stress accelerated grain boundary oxygen (SAGBO) phenomenon heat treatment investigations with TFMC superconductor samples consisting of Incoloy 908 jacket were performed to obtain basic data of oxygen concentration changes at the process environment during the heat treatment action.
Wrought and forged Type 316LN materials from the production line of TFMC coil and full size mock-ups were investigated according to the industrial progress. For weld wire selection, investigations with respect to optimum combination between weld filler materials mechanical performance at 7 K and the industrial weld process were finalized.
The procured Type 316LN material for intercoil structures of TFMC, the cryogenic mechanical properties were determined at 7 K. Also within this context a thick section weld material was investigated with respect to the fatigue life performance.
A data base for the developed new cryogenic structural material, a modified Type 316LN cast steel material, foreseen for the use of moderate stressed parts of the ITER full size coil casing was established. Preliminary fatigue life tests were also conducted at 7 K with the existing reserve CS jacket weldments of Type 316LN material.
For the wedge plates of the ITER coils the friction coefficient at 7 K were determined using a newly designed special experimental setup.
The present Report is so far a compilation and the updating of the several intermediate Reports within the current framework of the ITER Technology Task.

2. Fatigue crack growth rate results with CS superconductor's jacket material

Subject of this chapter is the representation of cryogenic temperature measurement results with respect to Fatigue Crack Growth Rates (FCGR) of Type 316LN and Incoloy 908 base metals used as jacket materials for ITER CS superconductors. These investigations were carried out at load ratios R = 0.1 and R = 0.4 with aged and unaged jacket sections of Type 316LN (Valinox) and aged Incoloy 908 materials using small size ASTM standard CT specimens machined from an industrially manufactured jacket section bars. The acquired data of present tests which were recently evaluated using the below represented procedure were further elucidated using a new type of evaluation technique. In addition, the FCGR properties of butt weld zone of the extruded sections for aged Incoloy 908 are determined, too.

2.1 Method of Test

Small size ASTM proportional specimens machined from the provided jacket sections of CSMC superconductors were used for these measurements. All tests were performed at 7 K under Helium gas environment of about 50 mbar. The servo - hydraulic machine MTS model 810 capable to load the specimen at 40 Hz frequency was used for these tests in a helium flow cryostat equipped with a built in fiberscope (magnification 22 x). **Figure 1** shows the drawing of the used FCGR specimens.

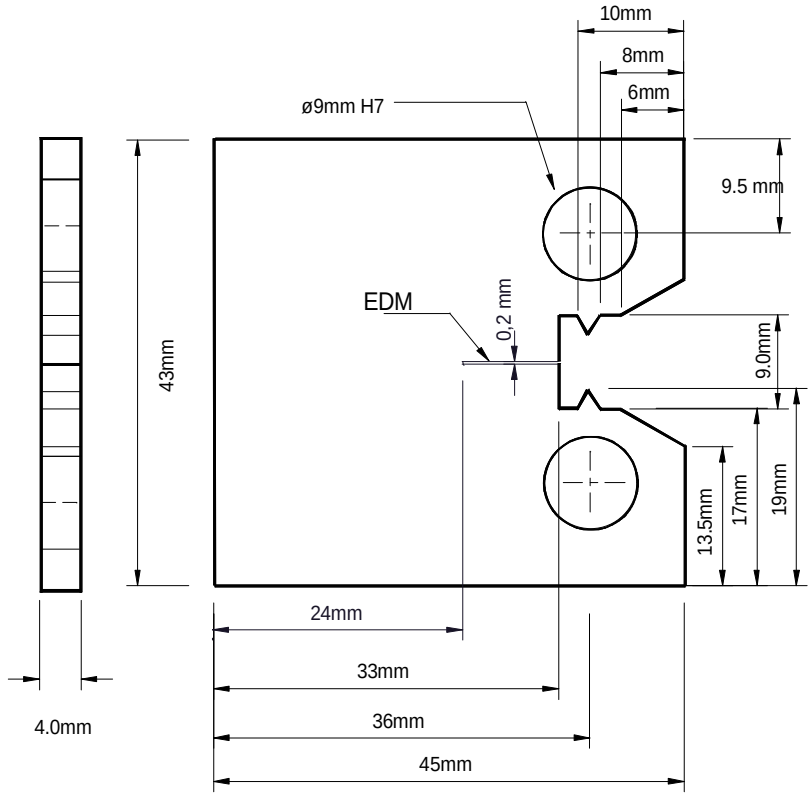

Figure 1 ASTM proportional small compact tension specimen machined from the jacket sections in T - L (transverse-long, according to ASTM designation) orientation. Crack length to width (a/W) ratio is 0.33. In several cases especially for Incoloy 908 material it was not possible to meet the 4 mm specimen thickness owing to the thinner wall sections of the available extruded CS jacket samples.

For the present tests, the CT specimens had an initial a/W ratio of 0.33 thus allowing a crack propagation of ca. 10 mm into the specimens width. The crack initiation were carried out after cool down of the specimen at a ΔK level around 23 MPa$\sqrt{m}$ and at R=0.1. During this stage of

cycling at 40 Hz the machine frequency was slowed down after each 5000 cycle to 0.1 Hz to acquire a load-displacement line using a high resolution stiff extensometer attached at the load line of the specimen coupled to an 18 bit data acquisition system. Using the determined slope, the crack lengths were calculated by the compliance equation with the input parameters Young's modulus and the specimen thickness. After comparing the calculated crack length with the observed crack initiation position the crack length was adjusted if necessary by trimming the Young's modulus value. After this setup procedure the ΔK level was decreased and the FCGR test was started at constant load range, either at R=0.1 or R=0.4. All follow up crack lengths were calculated during the cycling by the determined particular slopes with the use of the experimentally determined compliance line. In the initial stage of the software development the comparison of observed several crack lengths by the use of cryogenic proof fiberscope and the calculated crack lengths using the extensometer yielded during the crack propagation a difference less than 50µm between these two independent techniques thus ensuring a high degree of confidence. The output of the results were saved in a file in form of 11 columns table for the purpose of later data processing. **Figure 2** shows an example of a data output for a FCGR test performed with the compact tension specimen at 7 K.

Material tested at: 2/12/1998 File = V_C33_1.fat

No	a/W	crack	slope	REG.	P-min	P-max	cycle	^K	^K-mean	da/dN
0	0.351	12.623	48212.76	99.9700	0.2200	2.200	0	16.703		
1	0.358	12.871	46683.16	99.9824	0.2200	2.200	10018	17.001	16.852	2.477e-05
2	0.369	13.281	44268.01	99.9703	0.2200	2.200	19924	17.508	17.255	4.136e-05
3	0.378	13.594	42504.87	99.9726	0.2200	2.200	30038	17.908	17.708	3.103e-05
4	0.389	14.005	40302.00	99.9711	0.2200	2.200	40060	18.449	18.179	4.100e-05
5	0.402	14.483	37880.51	99.9663	0.2200	2.200	50021	19.106	18.777	4.797e-05
6	0.413	14.853	36099.63	99.9746	0.2200	2.200	60021	19.636	19.371	3.703e-05
7	0.425	15.318	33975.32	99.9892	0.2200	2.200	70035	20.332	19.984	4.639e-05
8	0.439	15.812	31840.88	99.9831	0.2200	2.200	80035	21.112	20.722	4.939e-05
9	0.456	16.430	29334.01	99.9485	0.2200	2.200	90019	22.154	21.633	6.195e-05
10	0.473	17.014	27123.71	99.9834	0.2200	2.200	100026	23.213	22.684	5.831e-05
11	0.494	17.777	24439.91	99.9951	0.2200	2.200	100040	24.726	23.970	5.450e-02
12	0.515	18.527	22009.19	99.9959	0.2200	2.200	120053	26.379	25.552	3.747e-05
13	0.526	18.922	20805.08	99.9943	0.2200	2.200	125049	27.325	26.852	7.904e-05
14	0.536	19.284	19744.08	99.9949	0.2200	2.200	130038	28.244	27.784	7.259e-05
15	0.550	19.812	18267.80	99.9973	0.2200	2.200	135038	29.682	28.963	1.056e-04
16	0.563	20.259	17078.41	99.9954	0.2200	2.200	140053	31.002	30.342	8.927e-05
17	0.578	20.790	15738.96	99.9949	0.2200	2.200	145060	32.701	31.851	1.060e-04
18	0.594	21.387	14319.29	99.9957	0.2200	2.200	150026	34.812	33.756	1.202e-04

Figure 2 FCGR test results at 7 K of a CT specimen consisting of Type 316LN (Valinox) material machined from the jacket in T-L orientation after compaction (unaged). File code is V_C33_1 with a load ratio of R = 0.1

2.2 Tested materials and test conditions

Table 1 below gives the saved file codes of all tested specimens with respect to base metal, their test conditions, and bar numbers of the jacket sections from which the specimens were machined. As shown in **Table 1** four specimens of Type 316LN were tested at 7 K also in unaged condition at two different load ratio levels. This was conducted to determine the possible effect of the aging on the stainless steel material. All tested, Type 316LN materials were base metals machined from the extruded jacket sections. Furthermore, to determine the effect of the additional bending and straightening after compaction of the extruded bars specimens were also tested which were machined immediately after the compaction stage without any further processing. For Incoloy 908 base metal, the effect of load ratio and the bending/straightening was investigated at 7 K with four specimens machined from two different bars. In addition, to characterize the cyclic properties of the superconducting conduit weldments for the ITER central solenoid model coil small size aged (650°C / 200 h) compact tension specimens were machined from the produced Incoloy 908 tubes. The crack plane of the tested four specimens from two production bars were prepared carefully by etching and proper positioning of the notch in long transverse (L-T) orientation inside the orbital weld seam. The crack propagation in case of this welded specimens were performed exactly at the

center of the weld zone. In **Table 1** the compact tension specimens thickness of the tested Incoloy 908 orbital welded tubes are also given as an additional information to show that only such small size specimens were possible to machine from the provided bars. All other specimens had a thickness of 4 mm as given by the **Figure 1**.

Table 1. Condition of materials for the carried out FCGR tests at 7 K

Type 316LN (Valinox)				**Incoloy 908**			
File code	Bar No	Condition	Load ratio R	File code	Bar No	Condition	Load ratio R
V_B37_1	37	compacted/ bent/aged	0.1	I_C23_1 base	23	Compacted/ aged	0.1
V_B37_2	37	compacted/ bent/aged	0.1	I_C23_2 base	23	Compacted/ aged	0.4
V_B37_3	37	compacted/ bent/aged	0.1	I_C23_3 base	23	Compacted/ aged	0.4
V_B37_4	37	compacted/ bent/aged	0.1	I_B2_1 base	2	Compacted/ bent/aged	0.1
V_B37_5	37	compacted/ bent/aged	0.4	IW-B18c Weld zone Thickness B = 2.97 mm	18	Compacted/ bent/aged	
V_B37_6	37	compacted/ bent/aged	0.4	IW-B18a Weld zone Thickness B = 3.45 mm	18	Compacted/ bent/aged	
V_C33_1	33	compacted	0.1	IW-C11a Weld zone Thickness B = 2.78 mm	11	Compacted/ aged	
V_C33_2	33	compacted	0.4	IW-C11-1 Weld zone Thickness B = 3.34 mm	11	Compacted/ aged	
V_B31_1	31	compacted/ bent	0.1				
V_B31_2	31	compacted/ bent	0.4				

2.3 Results of the FCGR measurements with jacket materials

Based on 11 columns Table as given by the example of **Figure 2**, da/dN versus ΔK plots have been produced to show the cyclic crack growth properties of the investigated jacket materials. **Figure 3** shows the first set of these results performed with 4 identical specimens of Type 316LN (Valinox) to cover up the resulting specimen to specimen variations if any during these investigations.

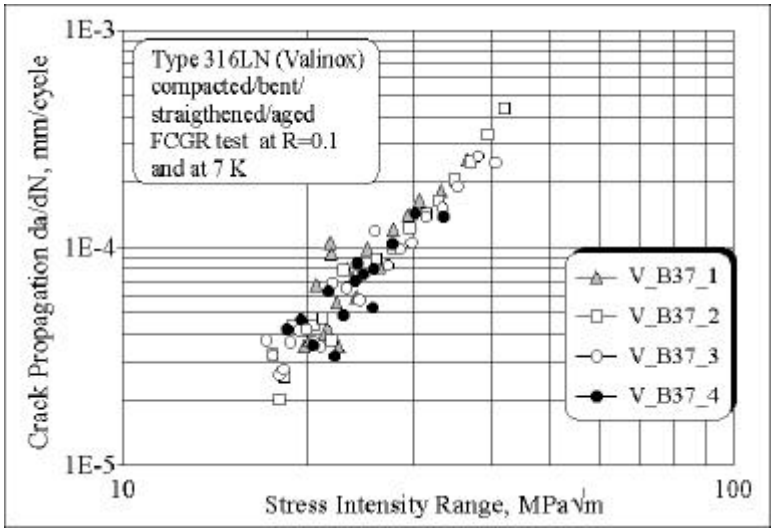

Figure 3. FCGR diagram of Type 316LN (Valinox) aged jacket material tested with four specimens at 7 K and at a load ratio of 0.1. Bar number of this jacket section is 37 and the jacket was bent and straightened after the compaction process prior to the aging.

To determine the Paris line constants the data has been evaluated by a software which allowed to determine the equation constants either by logarithmic regression procedure or by a drawn eye line. The diagram given in **Figure 3** results in m and C_0 values using logarithmic regression procedure to m = 2.394 and C_0 = 3.86 10^{-8} mm/cycle. The determined statistical regression coefficient with 56 % refer to the large scatter nature of such measurements. Therefore, in some cases with plotted data of high scatter the drawn eye line has been used as reference for the determination of the Paris constants.

The obvious large scatter especially in the range between 20 to 25 MPa√m is most probable the result of crack closure effects around the crack tip at the low load ratio level of 0.1. Testing of the same material at higher load ratio (0.4) as given in **Figure 4** shows less scatter owing to the less pronouncing effect of crack closure, because the steady high tension component at the crack tip. The value of determined Paris constants with m = 2.572 and C_0 = 2.41 10^{-8} mm/cycle at R = 0.4 shows about 10 - 15 % higher crack growth rate compared to the case with R = 0.1.

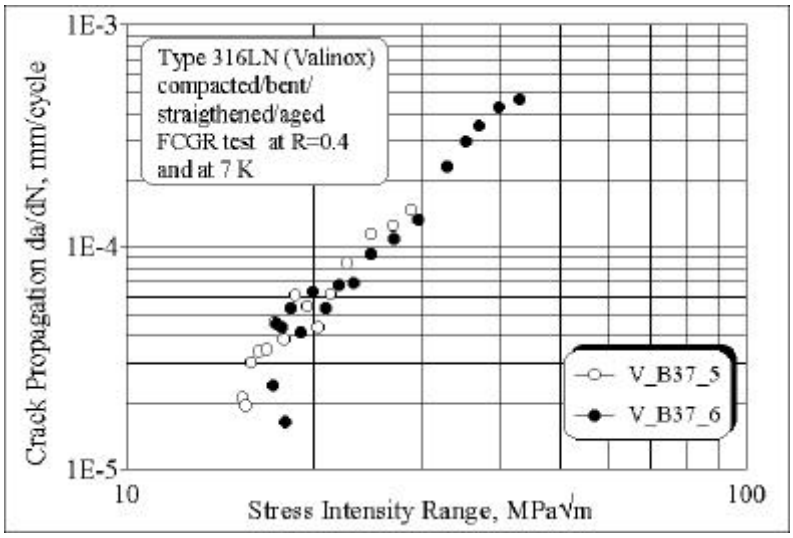

Figure 4. FCGR diagram of Type 316LN (Valinox) aged jacket material tested with two specimens at 7 K and at a load ratio of 0.4. Bar number of the jacket section is 37 and the jacket was bent and straightened after the compaction process prior to the aging.

The tests performed with Type 316LN material consisting of unaged specimens at R=0.1 are shown in the next diagram given by the **Figure 5**. This diagram shows the FCGR results with both unaged specimens one being only compacted, whilst the other one additionally bent and straightened afterwards. Obviously there is no difference between these two conditions. In addition, the determined Paris constants m=2.282 and C_0 =4.58 10^{-8} mm/cycle confirm also the marginal degradation effect with respect to FCGR process after aging of this material.

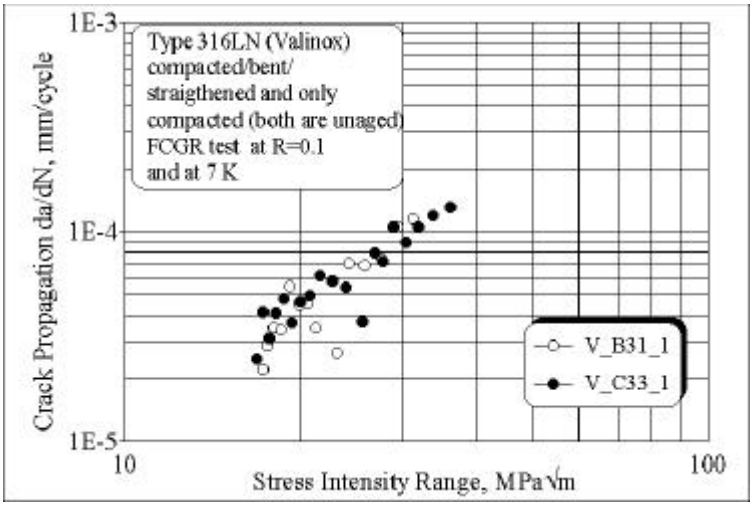

Figure 5. FCGR diagram of Type 316LN (Valinox) unaged jacket material tested with two specimens at 7 K and at a load ratio of 0.1. Bar numbers are 31 for the jacket section compacted bent and straightened and number 33 only compacted

From the same bars No 31 (compacted/bent/straightened) and No 33 (only compacted) FCGR investigations were performed in unaged condition at a higher load ratio level of R = 0.4. The results of these findings are given in the diagram of **Figure 6**. The determined Paris constants with m= 2.584 and C_0 = 2.6 10^{-8} mm/cycle shows a circa 10 % higher fatigue growth rate compared to the case with R = 0.1 load ratio.

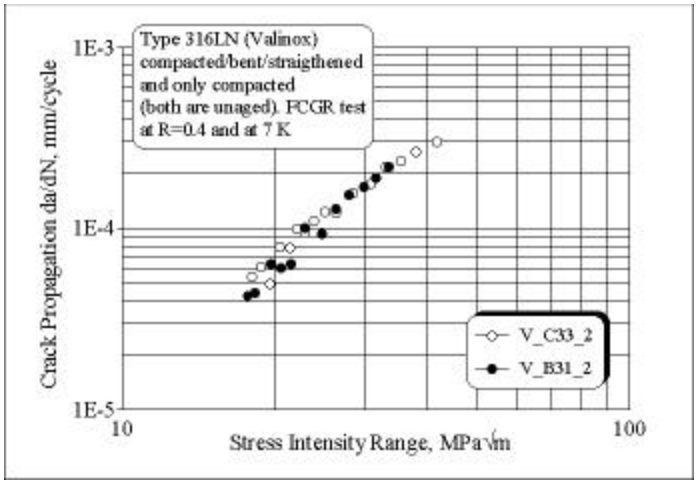

Figure 6. FCGR diagram of Type 316LN (Valinox) unaged jacket material tested with two specimens at 7 K and at a load ratio of 0.4. Bar number given as No 31 for the jacket section is compacted, bent, and straightened, whilst the bar with No 33 only compacted.

For the aged jacket material Incoloy 908 FCGR tests are carried out only for two conditions at two load ratio levels. At load ratio level R = 0.1 only a slightly lower FCGR has been determined after the manufacturing stage compaction, bending, and straightening compared to the case with only compacted, whilst at load level R=0.4 no obvious difference could be found for both cases.

Figures 7 shows the da/dN versus stress intensity factor ranges at 7 K of the jacket material from bar No 23 and 2. The determined Paris constants with m = 3.892 and C_0 = 7.02 10^{-11} mm/cycle are in line with the former determined values (m = 3.95 and C_0 = 7.29 10^{-11} mm/cycle) given in the Report [1].

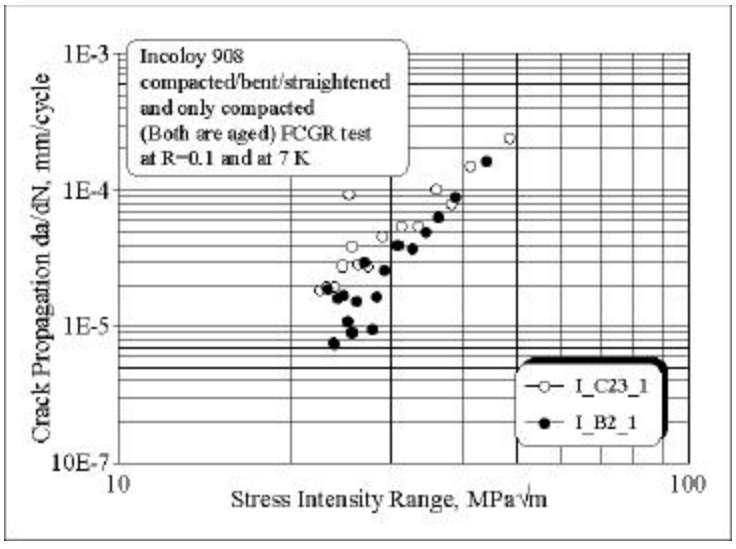

Figure 7. FCGR diagram of Incoloy 908 aged jacket base material tested with two specimens at 7 K and at a load ratio of 0.1. Bar numbers of the jacket sections are 23(compacted) and 2 (compacted, bent, and straightened).

Figure 8 gives the obtained results with the aged Incoloy 908 base metal at load ratio R = 0.4. The determined Paris constant values with m = 3.886 and C_0 = 10.4 10^{-11} mm/cycle confirm

the marginal difference of the load ratio effect between R=0.1 and R= 0.4 in case of aged Incoloy 908 base materials.

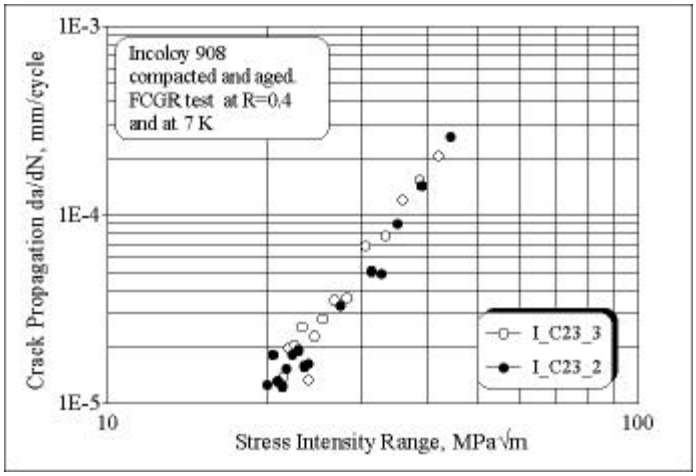

Figure 8. FCGR diagram of Incoloy 908 aged jacket base material tested with two specimens at 7 K and at a load ratio of 0.4. Bar numbers of both jacket sections are 23 (only compacted).

Figure 9 gives the obtained test results of four specimens with the aged Incoloy 908 weld metal at load ratio R = 0.1. The determined Paris constant values with m = 4.32 and C_0 = 2.38 10^{-11} mm/cycle reveal that the weld metal differs little from the base metal. For comparison reason also the base metal plots are given inside this particular diagram. The weld metal values give the upper range of the base metal FCGR line.

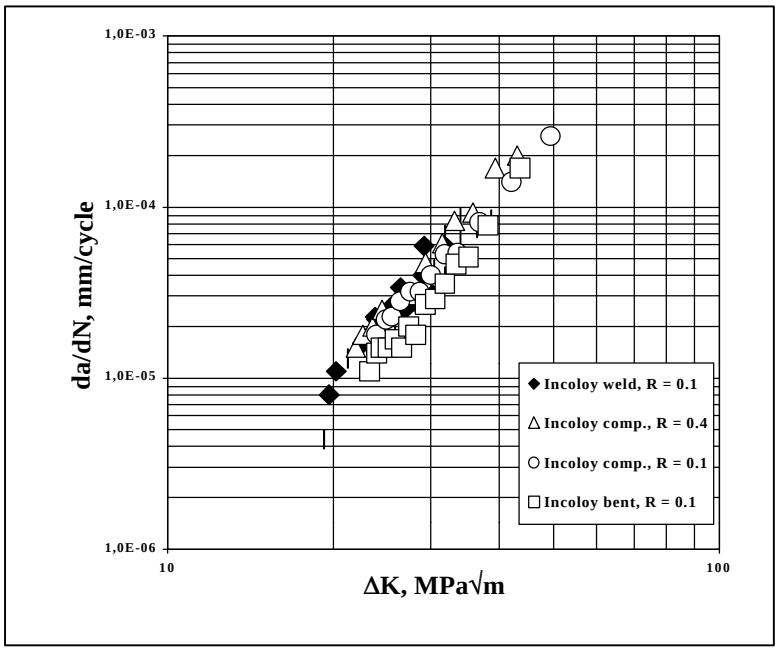

Figure 9. FCGR diagram of Incoloy 908 aged jacket base materials of different conditions in comparison with Incoloy 908 weld metal tested with four specimens at 7 K and at a load ratio of 0.1.

2.4 Final evaluation of the FCGR data and conclusion

The saved data with respect to jacket materials were smoothened using a new evaluation technique and the results of this data sets are plotted into a new diagram. All subsequent FCGR measurements are also evaluated using this new method based on a developed novel software. **Figure 10** shows the compiled values of Type 316LN aged and unaged materials along with aged Incoloy 908 jacket material. So far Incoloy 908 (Base and weld) has a significant higher resistance against fatigue crack propagation compared to the extruded Type 316LN (base) aged jacket materials (Valinox).

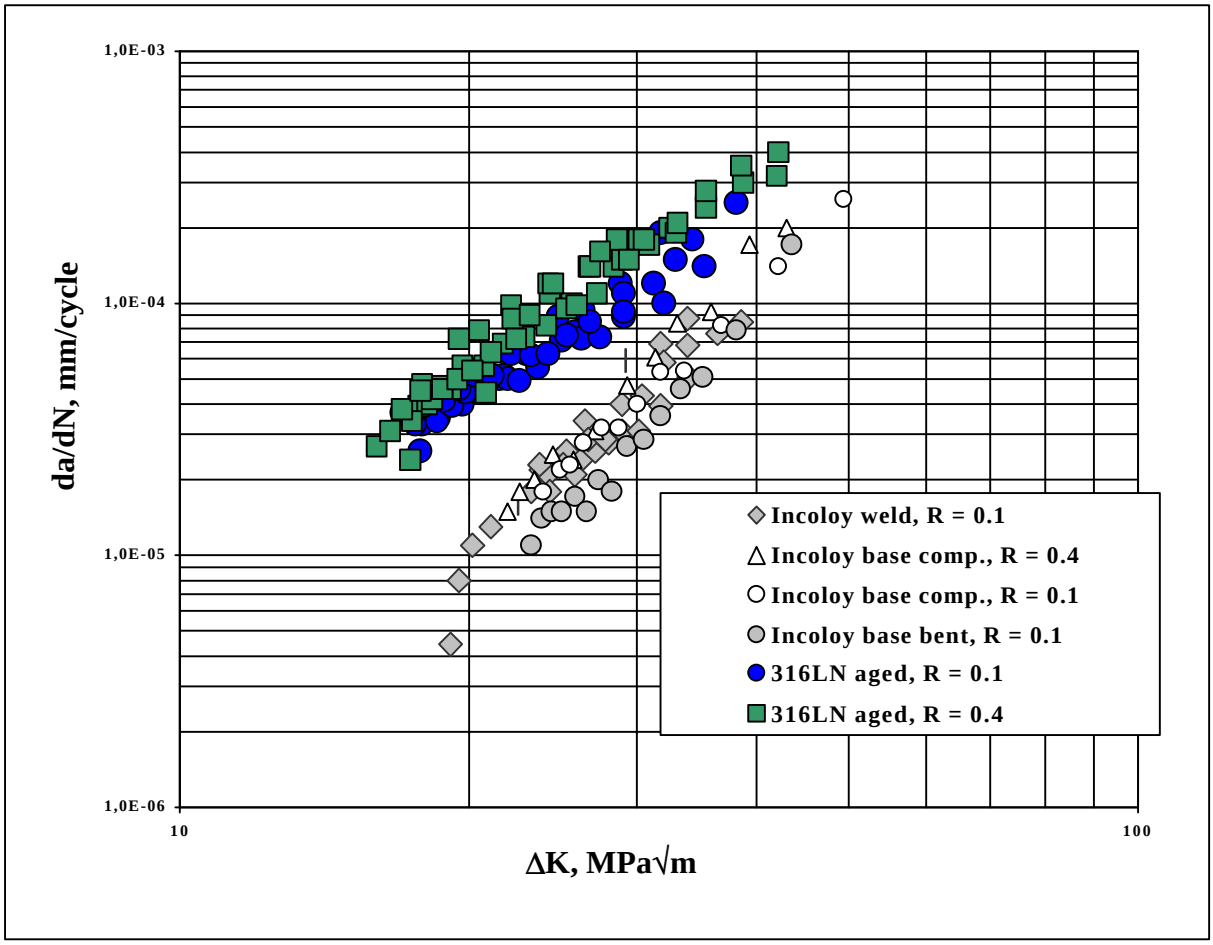

Figure 10. FCGR diagram of Incoloy 908 aged base and weld jacket materials of different conditions in comparison with Type 316LN (base) aged jacket materials (Valinox) at 7 K and at various load ratios.

Table 2 gives the compilation of all determined Paris constants (linear range of the log-log plots) for the performed FCGR measurements.

Table 2. Paris constants of FCGR tests obtained for the two different jacket materials of Type 316LN (Valinox) and Incoloy 908 at 7 K

Material	Jacket sample production details	Load ratio, R	m	C_0 mm/cycle
316LN base	Compacted/bent/straightened [aged]	0.1	2.394	$3.86\ 10^{-8}$
316LN base	Compacted/bent/straightened [aged]	0.4	2.572	$2.41\ 10^{-8}$
316LN base	Compacted/bent/straightened or compacted [unaged]	0.1	2.282	$4.58\ 10^{-8}$
316LN base	Compacted/bent/straightened or compacted [unaged]	0.4	2.584	$2.6\ 10^{-8}$
Incoloy 908 base	Compacted/bent/straightened or compacted [aged]	0.1	3.892	$7.02\ 10^{-11}$
Incoloy 908 base	Compacted/bent/straightened or compacted [aged]	0.4	3.886	$10.4\ 10^{-11}$
Incoloy 908 weld	Compacted/bent/straightened or compacted [aged]	0.1	4.32	$2.38\ 10^{-11}$

3. Shear tests with epoxy insulated TFMC jacket samples at 77

3.1 Background

To determine the slipping and shear strength capacity of an epoxy/ GFRP/Kapton insulated TFMC jacket consisting of Type 316LN steel, samples were prepared by Ansaldo, Genoa foreseen for tests at 77 K in submerged liquid nitrogen at Forschungszentrum Karlsruhe. The sample typical dimensions and the geometry are given in **Figure 11**. Altogether 8 samples were provided to FZK to carry out these cryogenic tests.

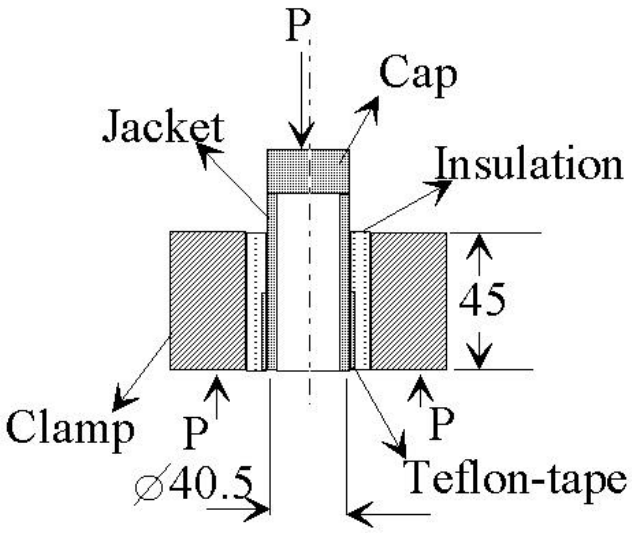

Figure 11. Schematic view of the test sample. The letter P indicates the position of the acting force which introduces shear stresses in the insulation.

3.2 Experimental setup

A specially designed test fixture was placed in the 200 kN cryogenic rig. A simple polystyrene insulated open tank was used as LN2 reservoir which could be moved up and down by the electrical control panel of the big LHe cryostat beneath the 4 K rig. The **Figures 12 and 13** below show the various stages of this test procedure.

Figure 12. Designed test fixture capable to act as a compression rig. The sample is positioned centrally and the averaged displacement are acquired by using two high resolution extensometers positioned in 180°.

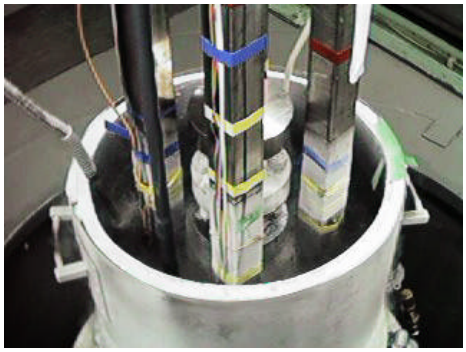

Figure 13. Built in test fixture inside the 4 K rig of the 200 kN screw driven tensile machine. The circular LN2 tank is moved upwards, whilst LN2 is filled from a second tank. Picture shows an overall view of the test facility during the cool down process. The cool down of the samples from 295 K to 77 K took about 45 minutes.

The sample shear area was prepared by Ansaldo, Genoa. Nearly half of the area of the jacket was covered with a Teflon tape to ensure slipping. The tests should give information about the crack penetration during the sample shear loading. The major interest of these tests were to confirm that a starting crack should not penetrate through the insulation in transverse direction.

3.3 Results of the measurements

The diagrams below given by the **Figures 14 and 15** show the results of the load – displacement curves for the samples of No 3 and No 9. The displacements were computed directly by the data acquisition software using the average of the two extensometers.

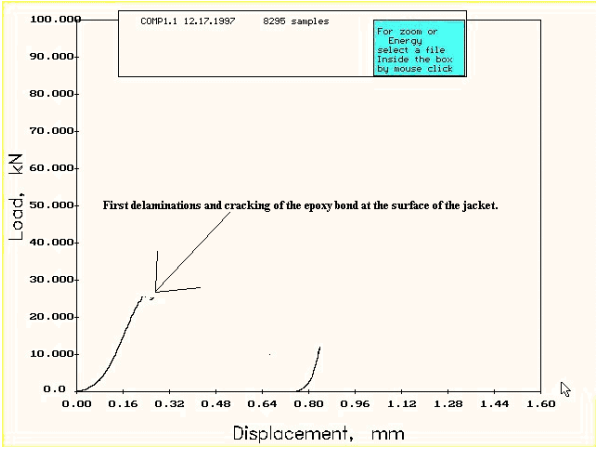

Figure 14. Compression load versus the average displacement of the sample No 3 at 77 K. The total achieved load is about 25 kN, which corresponds to 4.3 MPa considering a shear area of 5725 mm^2.

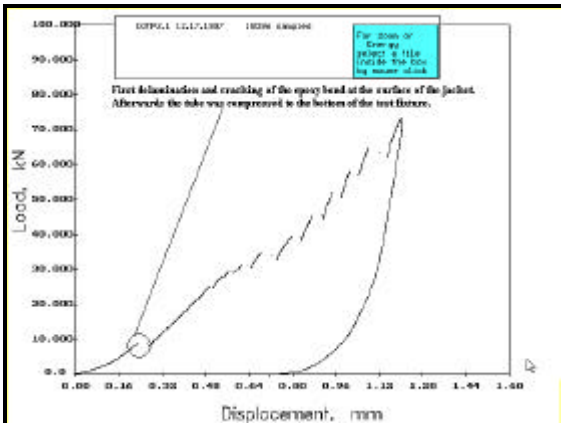

Figure 15. Compression load versus the average displacement of the sample No 9 at 77 K. The total achieved load is circa 10 kN, which corresponds to 1.75 MPa considering a shear area of 5725 mm^2.
After debonding, the load starts to increase continuously because the jacket tube was compressed between the hard steel plates of the fixture. The load drops is a result of crushing of the epoxy pieces between tube and bottom steel plate

Table 3 gives the compiled data of all evaluated results with respect of the maximum shear stress.

Table 3. Measured maximum stress of the nine individual samples at 77 K

Sample No	1	2	3	4	5	7	8	9
Stress, MPa	1.92	3.49	4.3	1.75	4.54	3.49	~0.0*	1.75

* Sample No 8 slided immediately after loading. The shear strength is nearly zero in that case.

For the reason of confirmation the sample No 3 has been released from the two compressed clamps by cutting the two bolts. Immediately after the cut the jacket moved away without any external force. The optical examination using a Zeiss 50 x magnification stereo microscope revealed a damage free kapton epoxy surface. Only some small microcracks could be detected in the vicinity of GFRP/epoxy surface. These were near surface cracks and may be tolerable according to our viewpoint.
Figure 16 shows the photography of the debonded jacket surface in case of sample No 3.

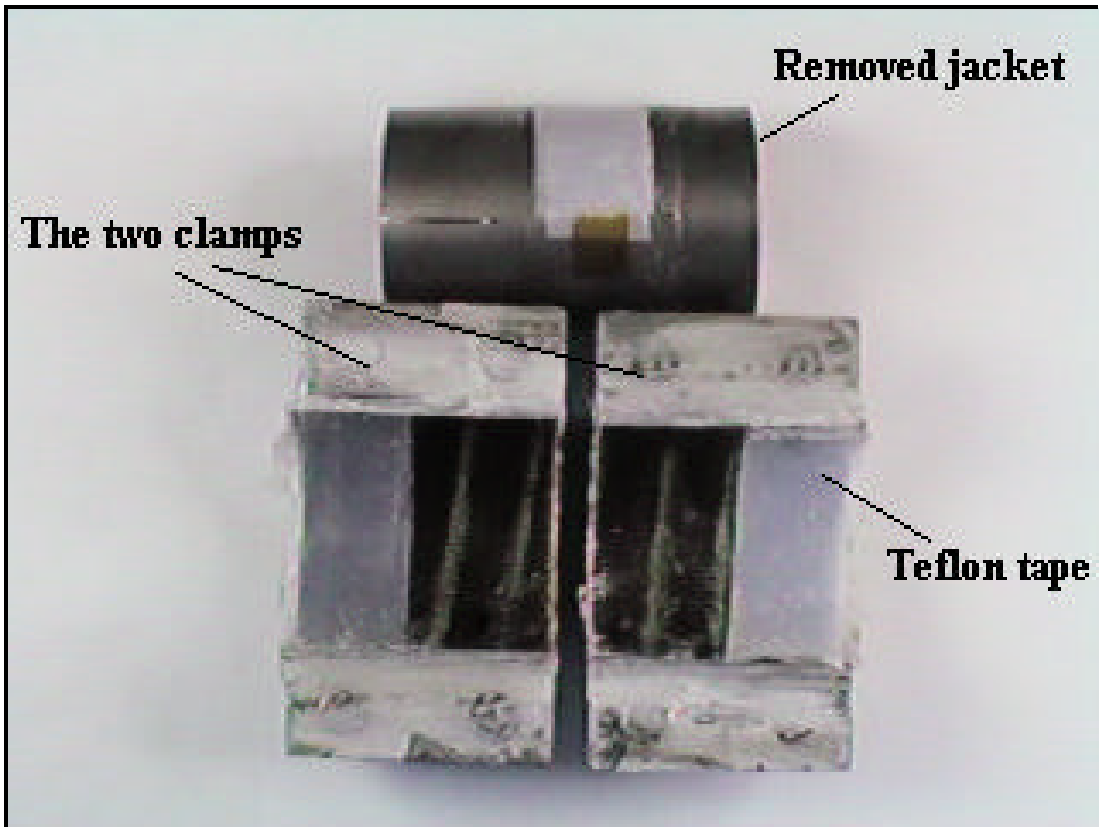

Figure 16. The released jacket from the clamps show clearly the debonding of the epoxy on the surface of the jacket.

3. 4 Conclusion

As an end result one can conclude that all 8 shear samples could be tested successfully without any major problem. The achieved shear strengths are within a bandwidth of approximately 1.7 - 4.5 MPa. The debonding of the epoxy occured on the surface of the jacket. The optical inspection of the debonded area showed only some minor microcracks at the GFRP/epoxy site, however, not at the Kapton/epoxy site.

4. Investigations on sliding behavior of the insulated TFMC jacket structure at 4.2 K

4.1 Background

To determine the sliding behavior of the TFMC jacket a component was manufactured by Ansaldo, Genoa. This component consisted of the original jacket covered partly with a Teflon tape prior to the epoxy/GFRP/Kapton insulation. By a special clamping arrangement it was possible to pull out the jacket by tensile loading in the 4 K rig of the 200 kN cryogenic tensile test facility. Three strain gauges and one displacement transducer were placed in specific positions to obtain a maximum of information during the test. This test assembly was foreseen as far as possible to simulate the TFMC's jacket under operation.

4.2 Test sample

The manufactured test sample was designed with respect to the spatial conditions of the already existing test facility's 4 K rig. Before assembling the jacket into the epoxy cured clamping arrangement the structure (two jackets) was sent to Forschungszentrum for the strain gauge bonding at the specific positions inside and outside of the tube. Two strain gauges inside the tube at 80 mm and at 170 mm depth (distance from the bottom) have been processed by special tooling technique. Attention was paid during the strain gauge bonding the uniaxial orientation of both strain gauges for the reason of similar signal output behavior during the tensile loading. A third strain gauge was placed outside of the jacket at insulation free region for the reason to have a reference signal, free of secondary structures clamped or bonded to the jacket.

In addition, it was foreseen to design two symmetrical rods placed at 180° position between the free moving ends of the sample for the reason of displacement measurements during the loading. The displacement during the loading was recognized as the control parameter at the test. The reason for the placing of two transducers at 180° position was to average the signals owing to the straightening of the possible bent jacket inside this assembly. However, for some certain reason both manufactured samples had at the arrival to Forschungszentrum only the possibility of placing one transducer for displacement measurements because of lacking of the second rod. Therefore, the test was performed only by monitoring of the three strain gauge signals, one displacement signal, and the load signal which means a total of 5 signals.

Figure 17 and 18 show the arrangement of the sample illustrated by the schematic drawing.

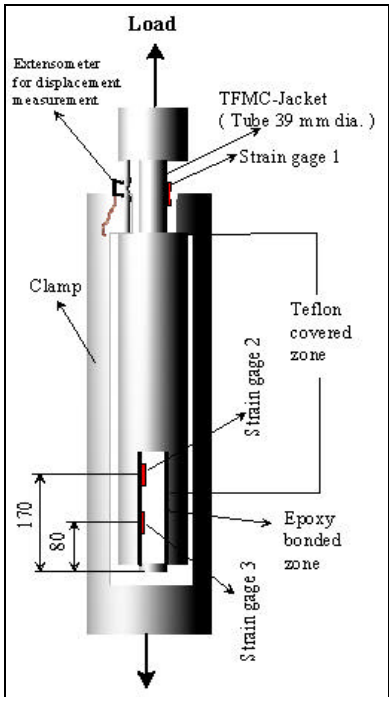

Figure 17. Schematic illustration of the test sample. The Teflon covered zone was foreseen for the sliding and this was the most important point to be clarified during the loading.

Figure 18. Original sample before the assembling procedure.

Before the start of these tests with the original sample several simulation tests were necessary to check the signals, acquire them, and evaluate them for their validity. An existing software was therefore upgraded for the reason to acquire at real time all 5 signals and plot into a diagram for being able to control the system during the loading. To check the performance of the strain gauges 4 strain gauges were bonded using a simple arrangement of a square section tensile test specimen. The strain gauges were symmetrically positioned and the specimen was loaded at room temperature up to 100 MPa stress. In addition, an extensometer was positioned outside the gauge length to check the output signals required by the software. All four particular strain gauges had a grid length of 6 mm and were wired to a full bridge circuit with three other same type strain gauges for a Wheatstone Kelvin type arrangement. The same passive strain gauge set up was later used for the test sample at 4.2 K.

4.3 Results and discussion

The tests with the room temperature strain gauge set up arrangement served as the basis of the further tests with the original test sample. **Figure 19** shows the simulation results with the room temperature strain gauge experimental set up.

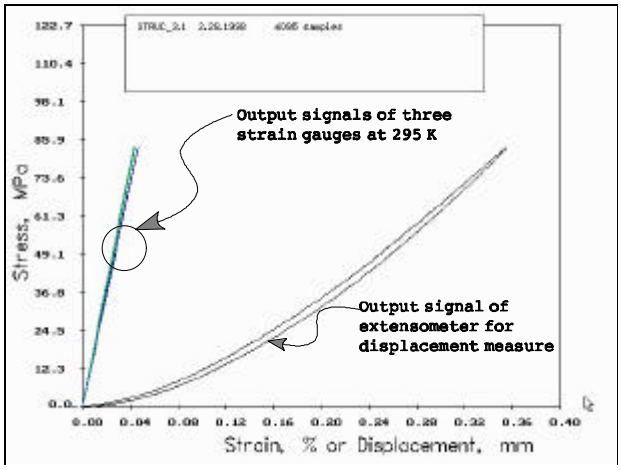

Figure 19. The output of three strain gauges result accurately the material's Young's modulus (180-185 GPa as valid for Type 304 material). The curve of the extensometer reflects the fact that the displacement measurement was carried out outside the gauge section and therefore it determines the compliance of the entire system (machine plus specimen).

The obtained strain gauge results was used as calibration factors for the used strain gauges of the test sample. In addition, these calibration factors were also corrected with the determined low temperature correction factors of previous tests with similar type strain gauge arrangements.

After checking the signals of the assembled test sample, the sample was cooled down to 4.2 K and was entirely submerged into the LHe. The screw driven 200 kN test machine was controlled manually by push buttons up and down which means loading or unloading. The real time record of load versus strain gauges No. 1, No. 2, No. 3, and the Extensometer were displayed on the monitor. Meanwhile all acquired data were saved onto the HDD for later digital data evaluation. **Figure 20** shows the evaluated data of this loading procedure. In fact, the strain gauge No. 1 shows clearly the bending related signal output, whilst the other two strain gauges do not show this phenomenon. The extensometer, on the other hand, shows also the bent situation of the jacket. The initial portion of the displacement is therefore synchronous with the output signal of strain gauge No. 1 with the only exception that in case of strain gauge output the compression component and for extensometer the tensile component are dominant. This is so far correct owing to the situation that both sensors are outside of the epoxy bonded structure free of the secondary components and acting at ca. 180° facing position. In addition, the as received sample could be visually observed that especially the free upper end was remarkable bent as shown in photography of **Figure 18** (see the non

parallel behavior of the rod and the free jacket, foreseen for the extensometer attachment). For the evaluation of the actual displacement, therefore, the loading/unloading curve (load versus displacement) was corrected by the extension of the linear portion of the curve to 0-load. The estimated total displacement of the sample is ca. 0.42 mm up to the load maximum of 200 MPa. Further elastic calculations of the three strain gauge outputs using the previously determined calibration factors (see **Figure 19**) resulted in following values:

1. An estimated Young's modulus of 250 GPa for the jacket at the strain gauge position No. 1.
2. An estimated Young's modulus of 220 GPa for the jacket at the strain gauge position No. 2.
3. The position of the strain gauge No. 3 has a very high apparent Young's modulus, because the not debonded area of the jacket; i. e. the jacket is covered with the insulation and the epoxy bond of the clamping is still intact, which means that the inserted value of the cross section area into the Young's modulus calculation (tube cross section) is too small in this particular case.

The estimated values in case of the two strain gauges No. 1 and 2 is also high (250 GPa and 220 GPa) owing to the still existing bending strains. This will be shown later that after further loading the determined elastic properties will refer to actual material's structural behavior.
Figure 20 shows the strain gauge signals and the displacement during the first loading of the structure at 4.2 K. Whereas in **Figure 21** the enlarged view of the strain gauge signals during the loading is displayed. Here the strain gauge No. 3 shows the starting of first pop-ins as an evidence of the debonding.

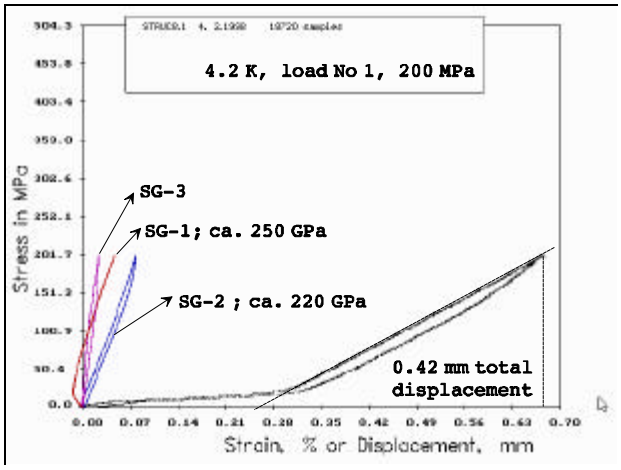

Figure 20. Strain gauge signals and displacement of the test sample at 4.2 K during initial laoding.

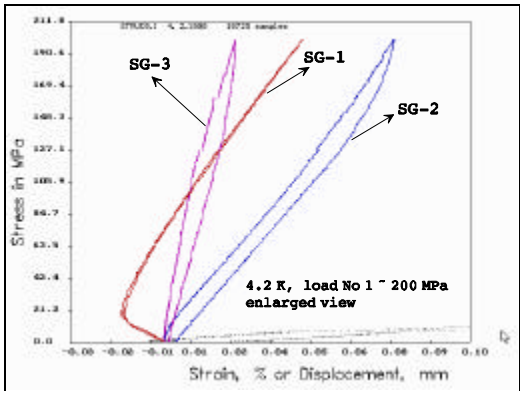

Figure 21. The output signals of the three strain gauges during the first loading of the structure at LHe shown in an enlarged view. Notice the strain gauge No 3 with the pop-ins.

Figure 22 shows the second loading of the sample at 4.2 K . The achieved maximum load was here 374 MPa and the estimated total displacement of the sample after the correction is about 0.88 mm.

The enlarged plots of this diagram shows now clearly the continuation of the debonding acquired by the strain gauge No. 3. The calculated Young's moduli for the three strain gauges deliver using the unloading lines the following results:

1. The value of 220 GPa for strain gauge No. 1 shows still the existing initial compression stress components resulting from the bent jacket.
2. 210 GPa for strain gauge No. 2, a reasonable close value to the material's Young's modulus.
3. The value with 320 GPa indicates the still not fully separated bonding between clamp and jacket structure.

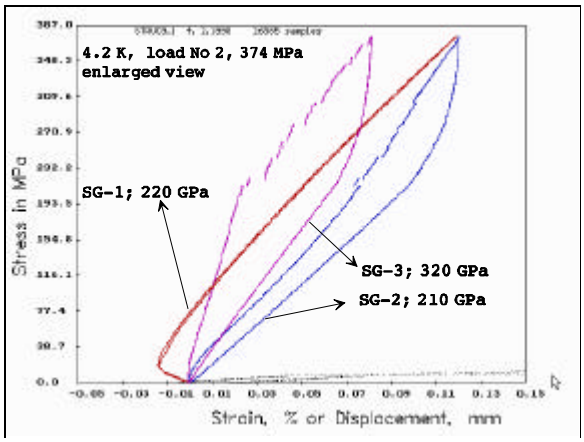

Figure 22. The output signals of the transducers during the second loading of the structure at LHe shown in an enlarged view.

At the third loading of the structure the recorded maximum stress was 552 MPa. The estimated total displacement results in a value of 1.35 mm. During this 3rd loading at 4.2 K further debonding mechanism could be observed. After a big pop-in the bond was assumed to be deteriorated. The unloading curve of strain gauge No. 3 has had now nearly the same slope as the other two strain gauges. All three unloading slopes result in Young's moduli values corresponding to stainless steel 4.2 K values (200-205 GPa). A further loading of the sample (fourth loading) is shown **in Figure 23**. The achieved displacement of 1.36 mm is almost similar to the previous one but the maximum stress is in this case 567 MPa.

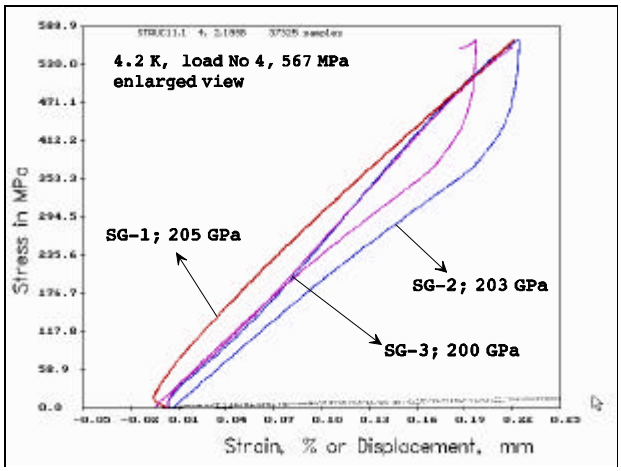

Figure 23. The output signals of the strain gauges during the last loading of the structure at LHe shown in an enlarged view.

The enlarged view for the part of interest (**Figure 23**) with the three strain gauges show a similar type of loading unloading behavior compared to the previous load history. The only exception is the sudden shift of the output signal in case of strain gauge No. 3 at the high stress level. This can be attributed to some movements of debonded epoxy parts in the region of strain gauge No.3, where the strain gauge is still intact and may record all structural

movement events. However, the unloading line of the strain gauge No. 3 gives a slope corresponding to the material's Young's modulus.
All these results indicate that a sliding of the jacket, bandaged with Teflon and insulated by epoxy-glass/Kapton tapes occurs from the initial loading sequence of the structure. A debonding of the epoxy bonded region starts after the loading around the stress level of 125 MPa.
The strain gauge No. 1 shows the same load and unload pattern, which means that it is free from secondary structures influencing the loading/unloading behavior (no hysteresis). Whereas the strain gauge No. 2 and later the strain gauge No. 3 show a remarkable hysteresis owing to the friction of the jacket inside the clamped section. For the reason of verification and confirmation of the debonded sections, the sample has been carefully released from the clamps by means of mechanical machining. The free jacket were analyzed with respect of the deteriorated insulation and the possible cracks inside the insulation region.
Figure 24 shows the photograph of the structure. As analyzed in fact, Teflon was destroyed (clear white area) during the sliding resulting from the loading and unloading sequences. No cracks on the entire epoxy cured region could be detected visually.

Figure 24. Photograph of the structure after the test. The halve of the clamp has been removed.

Finally, **Figure 25** shows a schematic cross section of the Teflon protected region and the corresponding surface where the sliding occurred. The debonding of the epoxy cured insulation occurred thereafter at the interface between insulation and the clamping. The clamps here were foreseen for the shear plate simulation.

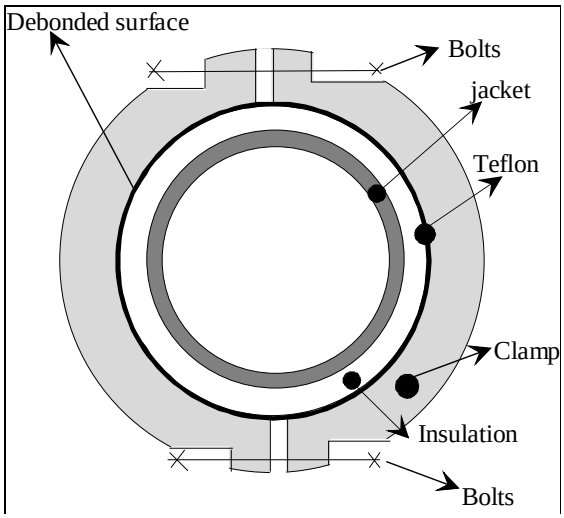

Figure 25. The cross section of the tested sample and the slide region of the jacket. Also the debonding of the jacket occurred at the interface between clamp and insulation

5. Cryogenic mechanical performance of copper / Incoloy 908 explosion bonded joint

5.1 Background

Subject of these investigations were tensile tests of explosion bonded metal /metal joints. Two bulk materials Incoloy 908 and copper explosion joined together to a plate was provided to Forschungszentrum Karlsruhe for detailed mechanical tests. From this plate with an overall dimensions of 410 x 155 x 72 nine asymmetric tensile specimens were machined in vertical orientation. **Figure 26** shows the provided plate consisting of both materials joined together.

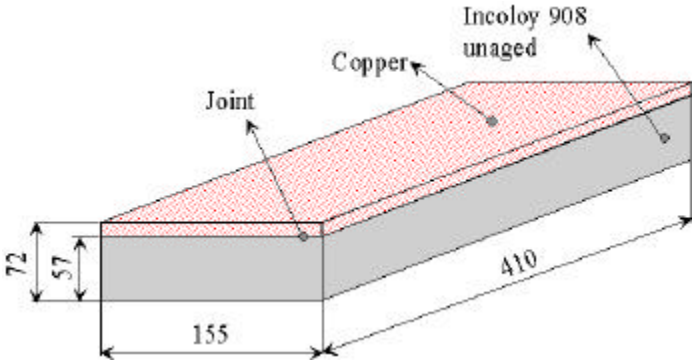

Figure 26. Explosion bonded Incoloy 908 (unaged) with copper plate in as received state.

5.2 Method of test

Figure 27 shows the illustration of a specimen machined from vertical orientation of the plate with the surrounded extensometers ready for test. Four specimens from the machined nine specimens were aged at 650°C for 200 hours at vacuum. The remaining 5 specimens were foreseen for tests in as received condition. From stress-strain curves of the carried out tests and the appearance of the loaded specimens after loading the performance of the bonded joint could be assessed. Altogether 5 tests with unaged specimens were carried out at 295 K and at cryogenic temperature regime. From the aged specimens 2 tests were conducted at room temperature and one measurement has been performed at 7 K.

Figure 27. This illustration gives the conditions of the test and shows the necessary placement of both extensometers for the determination of the bond quality.

5.3 Results with unaged specimens

Prior to the cryogenic tests three specimens in their as received condition (not heat treated) were tested at 295 K to obtain a general information about the bond quality. All three tests showed at room temperature a high performance of this explosion bonded joint. The copper region outside the gauge region started to neck after the general yielding. This means that the bond strength is at least in the same order compared to the copper materials tensile strength; i. e. the copper material is the weakest link within this combination. The following cryogenic tests were conducted also with the unaged specimens at 7 K and at 20 K. Similar results were obtained as in the case of 295 K. However, because of the enhanced strength characteristics of the copper material the bond endured a ca. 50 % more load capacity compared to the cases

with the room temperature tests. **Figure 28** shows the stress-strain measurement results of all five tests.

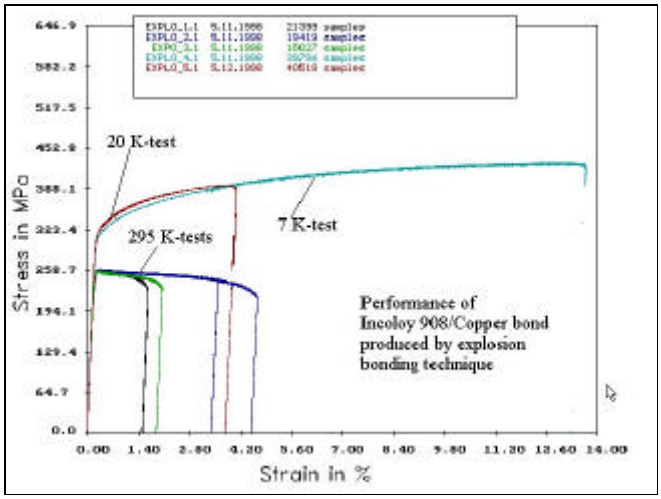

Figure 28. Stress-strain curves of the performed tests with unaged specimens at 295 K and at cryogenic temperatures. No fracture has occurred even after an appreciate amount of allowed necking of the copper material. The bond quality at room temperature as well as at cryogenic temperatures showed to be ideal.

Table 4 gives below the obtained mechanical results of these unaged specimens. The tensile strength is the value which can be seen as maximum permissible stress of the joint section region. However, most probable the stress bearing capacity of this explosion bonded joint is much higher than the ultimate tensile strength value of the copper.

Table 4. Tensile properties of the joint section and the measured ultimate tensile strength as the maximum possible obtainable stress of the unaged Incoloy 908/copper bond considering the specimen's configuration.

File name	Temperature K	Young's modulus GPa	Yield strength MPa	Ultimate tensile strength, MPa
explo_1	295	139	256	259
explo_2	295	134	258	259
expo_3	295	136	255	259
explo_4	7	139	321	429
explo_5	20	142	329	392

5.4 Results with aged specimens

The heat treatment (650°C/200h) of the four specimens conducted at vacuum show a marked oxidation of the Incoloy 908 section compared to copper. The reason of this is the lower standard free energy ΔF° of both nickel and iron, constituents of Incoloy 908, which deoxidizes the copper entirely during the long heat treatment procedure.

Two specimens were tested at 295 K under similar conditions compared to unaged specimens. The stress-strain diagram shows the very soft characteristics of the heat treated copper material. The yield strength of the unaged specimens decrease for nearly a factor of 10. The copper section determines the overall plastic flow behavior. The copper material starts to strain harden after the general yielding. The ultimate tensile strength is also lower compared to the unaged condition. On the surface of the necked specimen one can also easily see the large grains of the copper. The copper grains undergo substantial growth during the aging process. The test performed with one of the aged specimen at 7 K show also that there is almost no difference of the plastic flow behavior compared to 295 K tests. Only the ultimate strength is ca. 45% higher than the room temperature tests. **Table 5** gives the results of these mechanical tests performed with the aged specimens and **Figure 30** gives the complete stress-strain curves of these investigations.

Table 5. Tensile properties of the aged Incoloy 908/copper bond at 295 K and at 7 K.

File name	Temperature K	Young's modulus GPa	Yield strength MPa	Ultimate tensile strength, MPa
explo_6	295	133	28	200
explo_7	295	130	20	201
explo_8	7	--	26	295

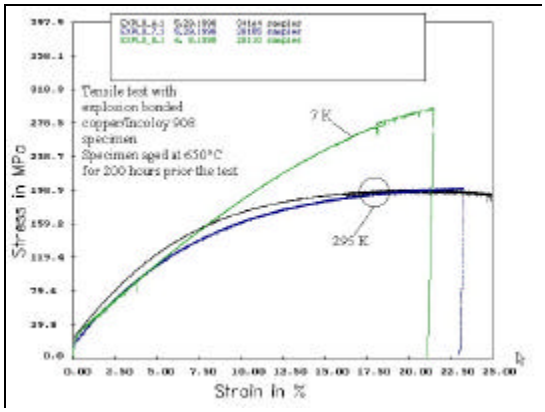

Figure 29. Tensile response of aged copper / Incoloy 908 joint at 295 K and at 7 K.

The diagram given in **Figure 29** shows that between unaged and aged condition the only difference results from the tensile response of the high strain hardening capability of the heat treated copper. **Figure 30** shows the appearance of the tested specimens both in aged and unaged condition. The far right specimen is the aged one before the test. The necking of all specimens after the test show again the copper as weak link.

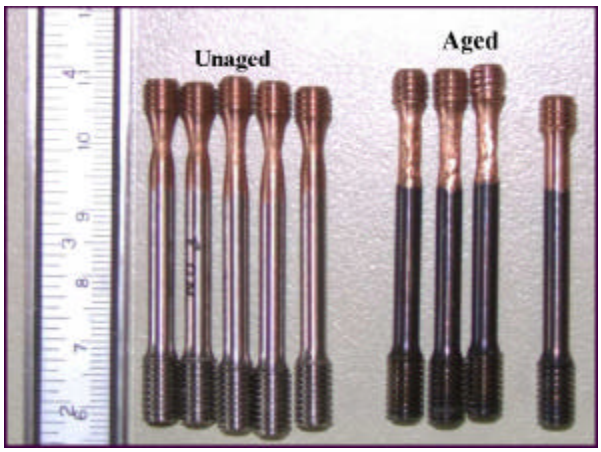

Figure 30. Photography of all specimens. The aged specimens show a clear oxidation after the heat treatment. The large grains of the heat treated specimens refer the grain growth of the copper material during the aging process.

5.5 Conclusion

The conclusion of these tensile tests conducted at room temperature and at cryogenic temperatures show no damage of the joint region in aged and unaged condition. The material copper in both cases at low and at room temperature necks after reaching the general yielding regime. Therefore the material copper determines the overall performance of the explosion bonded joint. The bond can bear therefore at least the stress reached by the ultimate tensile strength of the copper material.

6. Cryogenic mechanical characterization of Type 316LN 90 mm thick Plate, GMAW-, and TIG – weld metal

6.1 Background

Subject of this task is the cryogenic characterization of a 90 mm thick plate Type 316LN material provided by Alstom Company, France. Besides, measurements were made with provided ca. 50 mm thick GMAW (Gas metal arc weld) weld samples as well as with a ca. 11 mm thick TIG welded plate. The carried out tensile and fracture toughness tests comprised mechanical investigations at cryogenic temperatures.

6.2 Test Procedure

The tensile tests have been performed using 4 mm diameter cylindrical specimens with 22 mm reduced section and M6 threaded ends. These tests were carried out with specimens machined from the sample in transverse, longitudinal, and vertical orientations. The positions of the specimens were approximately in 10 and 20 mm depth position of the plate as well as in case of the GMAW-weldment. The TIG weldment of Type 316LN material was a bent U-shaped 11 mm thick plate material foreseen for the cover of radial plate. The tensile specimen for this particular test was machined from the weld transverse orientation. In **Figure 31** the provided plate metal sample and the position of the specimens are illustrated.

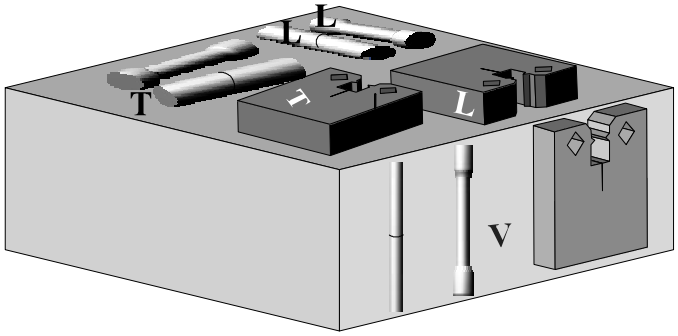

Figure 31. 90 mm thick Type 316LN metal sample and the machined specimens from the plate showing different orientations.

The chemical compositions of the investigated 90 mm thick plate and the GMAW weld metal are given in **Table 6**. In addition, the inclusion content of these both materials were checked according to ASTM E 45 and determined to be zero for the categories of A, B, C, and D.

Table 6. Chemical composition of the investigated 90 mm thick plate Type 316LN and GMAW weld metal

Mat.	C	Si	Mn	P	S	Cr	Mo	Ni	Al	Cu	Nb	Ti	V	B	N
Base	.02	.39	1.65	.029	<.001	17.2	2.78	11.2	.01	.13	.01	<.01	.05	.0008	.1865
GMAW	.03	.38	7.45	.013	.011	20.4	2.85	15.7	<.00	.06	.02	<.01	.15	.001	.1835

For the fracture mechanical tests severely EDM - notched round bars of 6 mm diameter have been used. This recently developed test method (J Evaluation with Tensile Tests, JETT) uses the novel J - evaluation test method proposed by J Rice and developed by Forschungszentrum in close collaboration with Japanese scientists at NIFS, Toki [1]. Altogether 6 JETT specimens approximately from similar positions have been tested in transverse, longitudinal, and vertical orientations. Four 4 mm diameter small JETT specimens from a first GMAW trial weld metal and four additional 6 mm diameter from a second GMAW weld sample were the basis of these weld qualification measurements. In addition, from the bent TIG zone of the U-cover two 6 mm diameter JETT specimens were also prepared for the JETT measurements.
Besides, for the reason of confirmation the obtained fracture toughness results of the 90 mm thick plate were checked with four standard 15 mm thick CT specimens machined from the base metal sample in three different orientations. From the GMAW weld metal two 15 mm thick CT specimens were machined in longitudinal (in welding direction) and weld transverse

orientation. All these results were compared with JETT specimen test results. In addition, attention has been paid for the crack plane orientation during the assessment of the obtained results with standard CT and JETT Type specimens.

6.3 Tensile measurement results

Table 7 gives the results with the carried out tensile tests from different orientations at 7 K. The mechanical test results reveal the significant difference of obtained uniform elongation between vertical and long/transverse orientated specimens. Whereas the yield strength values can be assumed that they are within a natural scatter band. The ultimate tensile strength data seems to be inferior in case of vertical orientated specimens compared to long/transverse machined specimens. The latter two tests carried out up to ~4 % and ~9 % strain was performed for the reason of confirmation of obtained yield strength values and therefore they were not fractured ultimately.

Table 7. Tensile test results of Type 316LN 90 mm thick plate sample at 7 K

Files	Specimen orientation	Young's Modulus, GPa	Yield Strength, MPa	Ultimate tensile strength, MPa	Uniform Elongation, %
90T_V1	Vertical	208	931	1522	31
90T_V2	Vertical	209	890	1512	31
90T_L1	Longitudinal	202	887	1635	49
90T_T1	Transverse	200	903	1608	47
90T-T2	Transverse	199	907	-	-
90T_L2	Longitudinal	ca. 200	900	-	-

Table 8 refers to the measurements of the GMAW sample of the first trial welding procedure. Here also there is a significant difference between weld transverse and weld vertical orientation. This difference, however, results mainly from the performed weld process. The two ca. 50 mm thick Type 316LN plates were rigidly hold during the welding process to avoid distortion. This resulted most probable to high residual stresses during cool down of the final welded sample, thus giving less chance of elongation during tensile testing in weld transverse direction. Similar results were obtained with a second GMAW sample sent by GEC Alstom company. This sample was also welded within the same weld specification process. **Table 9** gives the results of these next measurements.

Table 8. Tensile test results of the first trial GMAW weld sample at 7 K

Specimen orientation	Young's Modulus, GPa	Yield Strength, MPa	Ultimate tensile strength, MPa	Uniform Elongation, %	Reduction of Area, %
Transverse 1	205	1091	1337	8	~9
Transverse 2	203	1107	1278	7.7	~9
Vertical 1	197	1225 *	1502	24	~53
Vertical 2	204	976	1533	30	~60

* Specimen has been accidentally preloaded to ca. 2 % at 7 K before the actual measurement started and therefore it is strain hardened before the test start

Table 9. Tensile test results of the second GMAW weld sample at 7 K

File	Specimen orientation	Young's Modulus, GPa	Yield Strength, MPa	Ultimate tensile strength, MPa	Uniform Elongation, %	Reduction of Area, %
MAG_T3	Transverse	203	977	1165	10	~10
MAGT_L1	Longitudinal	195	1022	1508	49	~50

Higher yield strength values could be confirmed in case of the bent 11 mm thick U-cover sample. The tensile specimen was machined from weld transverse orientation with the weld

zone located in the center of the specimen. Here the 8 mm gauge length extensometer was placed entirely at the weld zone, thus the measurement reveal the weld zone tensile behavior of the TIG weld metal. **Table 10** shows the mechanical characterization of this sample.

Table 10. Tensile test results of Type 316LN TIG weld metal of U-bent section sample at 7 K

File	Specimen orientation	Young's Modulus, GPa	Yield Strength, MPa	Ultimate tensile strength, MPa	Uniform Elongation, %	Reduction of Area, %
U-cover	Transverse	197	1165	1500	30	36

6.4 Fracture toughness measurements

For the fracture toughness measurements of the 90 mm thick Type 316LN plate material, two methods have been applied comprising two different kinds of specimens; Compact tension (CT) and JETT (EDM notched round bar). The plan of machining is illustrated in **Figure 31**. According to this Figure a comparison of these two different type specimens can be done by considering the crack plane orientation. In addition, the CT specimens (63 x 60 x 14) were all side grooved having a groove of 90° angle and a 0.5 mm groove depth. The width and thickness of these specimens were 50 mm and with an effective thickness of 14 mm, respectively. The CT specimens were tested in LHe environment using the 200 kN tensile machine. In **Figure 32** the load-displacement diagram of the CT specimen machined from transverse orientation is given as one typical example of the carried out J-tests. The single specimen unloading compliance method according to ASTM E 813 was used for all these measurements.

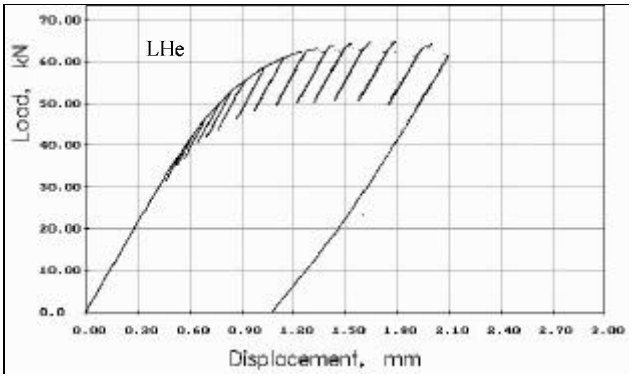

Figure 32. Load-displacement curve of the 15 mm thick side grooved CT specimen measured in liquid Helium at 4.2 K. Specimen was machined from transverse orientation (base metal).

Figure 33 shows the evaluated resistance diagram (J versus physical crack extension) of this test. The intersection of the curve with the 0.2 mm offset shift blunting line results in a critical J value of ca. 500 N/mm. Whereas, the intersection with 0-offset blunting line results in ca. 360 N/mm.

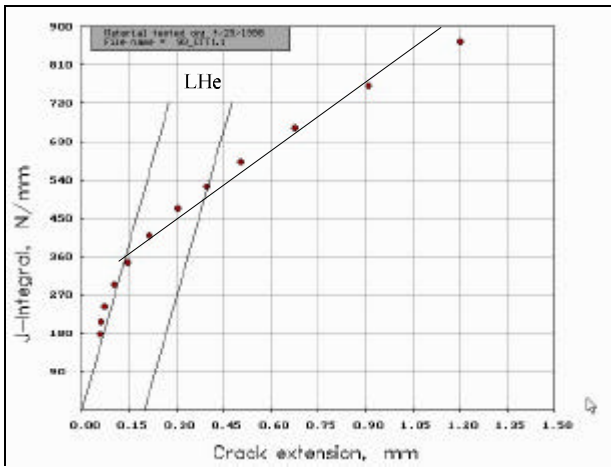

Figure 33. J versus crack extension curve of the 15 mm thick side grooved CT specimen measured in liquid Helium at 4.2 K. Specimen was machined from transverse orientation (base metal).

In the following fracture toughness assessment it was decided to accept the lower value (according to ASTM e 813-81 standard) as worst case and this value was converted to the K_{IC}. In **Table 11** all data obtained from the three orientations are collected together. The corresponding measured JETT results are related to the CT specimen findings considering the crack plane orientation. As obvious there is a large scatter between CT bound measurements in case of vertical machined specimens. The transverse machined CT specimen shows also significant high values compared to the JETT based vertical machined specimen. However, regarding the very high fracture toughness values a large scatter is reasonable.

Table 11. Fracture toughness properties tested with various type of specimens at 4.2 and 7 K.

Files (test code)	K_{IC}, MPa√m, (CT-type), LHe	K_{IC}, MPa√m, (JETT-type), 7 K
90_CTV2	280 Vertical	
90_CTV1	310 Vertical	
90_CTL1	356 Long	
90_CTT1	270 Transverse	
90_JL1 / 90_JL2		278 / 220 Long
90_JT1 / 90_JT2		355 / 314 Transverse
90_JV1 / 90_JV2		217 / 215 Vertical

Figure 34 shows the load-displacement curve of the GMAW weld metal for the CT specimen. The specimen was machined from weld longitudinal orientation. The evaluated diagram J versus crack extension according to ASTM E 813 is shown in **Figure 35**. The 0-offset line intersection point gives a critical J value of 110 N/mm .

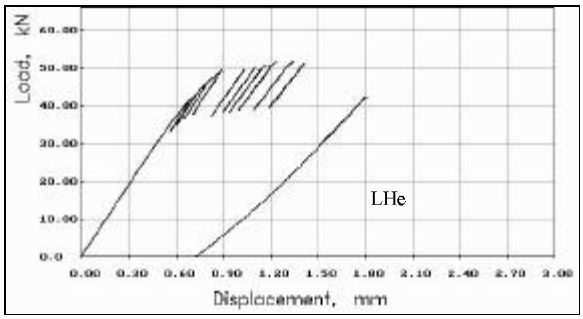

Figure 34. Load-displacement curve of the 15 mm thick side grooved CT specimen (GMAW weld) measured in liquid Helium at 4.2 K. Specimen was machined from weld longitudinal orientation and the crack plane consisted entirely by GMAW weld zone.

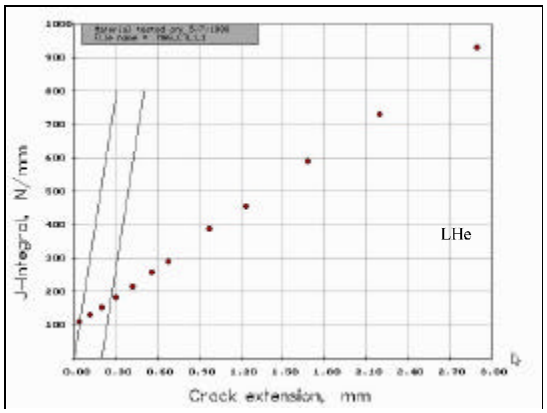

Figure 35. J versus crack extension curve of the 15 mm thick side grooved CT specimen (GMAW weld) measured in liquid Helium at 4.2 K. Specimen was machined from weld longitudinal orientation and the crack plane consisted entirely by GMAW weld zone.

In **Table 12** the former results with the first trial GMAW sample is given which was measured with JETT specimens only. **Table 13** shows, whereas, the results with the second GMAW sample. This measurements were conducted with both type of specimens, CT and

JETT. According to the results given in this Table there is a relatively low scatter indicating the better suitability of the used CT specimen sizes because of the lower toughness regime.
In addition, a JETT test was conducted with the TIG welded U-bent cover material. The EDM notch was located inside the TIG weld zone. Crack plane was in weld longitudinal direction. Two tests have been performed with this material and the obtained fracture toughness results were 180 / 176 MPa√m.

Table 12. Evaluated J - Integral values of the machined specimens from the first trial GMAW weld metal sample at 7 K.

Specimen and the orientation	Critical J - Integral value, N/mm	Converted Fracture toughness K_{IC}, MPa√m
No 1 Transverse	90	136
No 2 Transverse	138	168
No 3 Transverse	132	165
No 4 Transverse	104	147
No 1 Vertical	296	246

Table 13. Fracture toughness properties tested with various type of specimens for the second GMAW weld metal sample at LHe and at 7 K.

File	K_{IC}, MPa√m, (CT-type), 4.2 K	K_{IC}, MPa√m, (JETT-type)
MAG_JT4		172 Transverse
MAG_JT5		165 Transverse
MAG_JL1		162 Long
MAG_JL2		163 long
MAG_CTT1	172 Transverse	
MAG_CTL1	150 Long	

6.5 Conclusion about these plate and weld metal mechanical measurements

The conclusion of this results show for the tensile properties of the plate a yield strength value around 900 MPa considering all three orientations. However, the ultimate tensile strength and the uniform elongation seems to be inferior in vertical orientation compared to long or transverse plate direction.
The GMAW weld sample shows in transverse orientation owing to the welding procedure (the plates were rigidly hold to avoid distortion) a significant lower uniform elongation (~10 %) compared to long or vertical direction (~50 %).
A TIG weldment of a bent 11 mm thick plate showed a high yield strength of 1165 MPa.
Fracture toughness measurements of the 90 mm thick plate were performed with JETT type specimens at 7 K as well as with CT type specimens at LHe temperatures. Depending on direction the obtained results show fracture toughness values between 355 - 215 MPa√m. A scatter between CT type findings (280 - 310 MPa√m) could be determined. Whereas, between JETT type and CT type measurements a reasonable correlation could be determined.
For the GMAW sample the obtained fracture toughness values are in case of transverse ~170 MPa√m, whilst for the longitudinal direction a value between 150-160 MPa√m are determined. A good correlation between CT (4.2 K) and JETT (7 K) in case of the GMAW sample could be also observed.

7. Cryogenic mechanical characterization of Type 316LN radial plate material

7.1 Background

For the determination of the radial plate properties a small block sample has been sent to Forschungszentrum by NOELL company on request by EFDA Team. The sample was foreseen to be investigated at cryogenic temperatures with respect to tensile and fracture properties. The provided block was already milled at the company to outer dimensions of 150 x 100 x 75 from a 130 mm thick forging. The sample is a product of the preliminary production batch for the radial plates of the ITER TFMC. The **Figure 36** below shows the machined specimens from the provided block produced from the heat B73896. The material is designated as Type 316LN and the vendors chemistry is given in **Table 14** as follows:

Table 14. Chemical analysis of the block in wt %

C	Si	Mn	P	S	Cr	Ni	Mo	N	Nb
0.01	0.71	1.50	0.027	0.001	17.26	13.28	2.55	0.16	0.048

Within the context of chemistry the P content seems to be rather high. The limit should be below 0.025 % to minimize the detrimental effects, especially during the welding process.

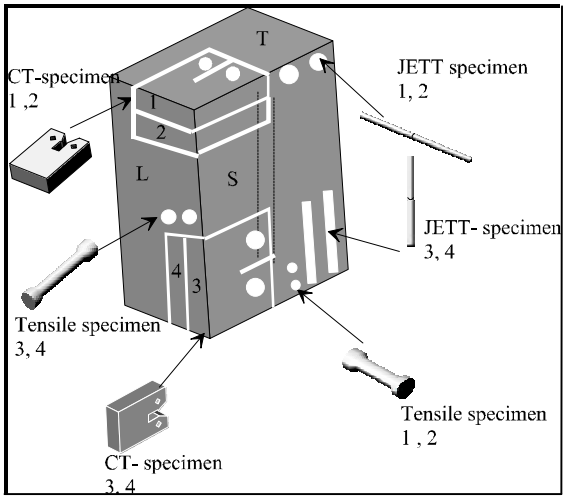

Figure 36. Provided block and the plan of specimen machining with respect to different type of investigations.

7.2 Tensile measurement results

The evaluated mechanical tensile property data evaluated from the test results are given in the following **Table 15**, which includes also the inclusion contents observed on the fracture surface.

Table 15. Tensile properties of the investigated radial plate at 7 K. The inclusion size and the rating has been determined with a stereo microscope on the fractured surface of the specimens

Specimen No	Young's Modulus GPa	Yield strength MPa	Ultimate Tensile strength MPa	Uniform elongation %	Inclusion diameter µm	Inclusion rating Incusion/m m^2
1	208	904	1543	46	1 inclusion has ~130 all others ~150	4
2	192	874	1445	29	~20	2
3	202	972	1521	43	~30	7
4	194	1052	1549	52	~50	2

7.3 Fracture toughness measurements

The first set of these measurements have been performed with severely EDM - notched small round bar specimens machined from the provided block in two orientations as shown in **Figure 37**. The 60 mm long specimens had 6 mm nominal diameter with a 2 mm net diameter of the EDM cut section. The calculated K_{IC} of these measurements from the obtained critical J-integral values and computed by the load-displacement diagrams using the JETT test method are given in the **Table 16**.

Table 16. Fracture toughness results obtained by the EDM notched round bars at 7 K (JETT test method).

Specimens No.	Fracture toughness, MPa√m	Comments
1	190	
2	191	
3	205	
4	179	High inclusion content 50-75 µm

Tests have been also performed with ASTM proportional 15 mm thick compact tension specimens using the single specimen compliance test method to obtain the critical J_{IC} value using the standard test method. For this purpose the screw driven 200 kN test facility has been used. All four specimens were tested in liquid helium at 4.2 K one after the other after the cool down using the multi-specimen rig. The analysis of these tests showed an unusual high degree of resistance against the crack extension of the precracked specimen. The average crack extension of specimens 1 and 2 were ca. 0.6 mm and for the specimens 3 and 4 ca. 0.3 mm. To an exact determination of the fracture toughness using the single specimen evaluation test method in general crack extension lengths of greater than 2 mm is necessary. Therefore, more tests are necessary for a final judgment of the fracture toughness values using the standard test method. However, the obtained results with respect to EDM notched round bar tests could be used for a lower bound estimation. The estimated fracture toughness values obtained from the CT specimen tests are higher than those results obtained by round bar specimens. Presumably, the observed inclusions may affect more effectively the small critical net section of the round bars than the compact tension specimens. In this context the CT specimens show considerably plastic constraints (plane stress behavior) at the plane surfaces of these specimens. The high crack tunneling tendency is also an indication of large plastic constraints as shown in the following photographic appearance (**Figures 37 and 38**) obtained from the broken halves of the specimens. Moreover, these test results do not meet the crack extension profile criterion according to the ASTM standard.

The carefully estimated fracture toughness values from the obtained results of the CT specimen tests give for specimen 1 and 2 a value of 250 MPa√m and for specimen 3 and 4 a value of 300 MPa√m respectively. These values refer to an upper bound estimation.

Figure 37. Obtained crack profile after loading of specimen #1 at 4.2 K. Large crack tunneling

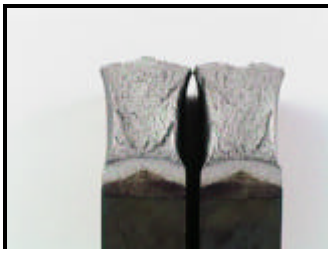

Figure 38. Obtained crack profile after loading of specimen #2 at 4.2 K. Large crack tunneling

7.4 Inclusion content:

Inclusion content were inspected using the broken halves of the four tensile specimens. For this reason the specimens were polished in longitudinal orientation after embedding into the epoxy. The surface of these micrographs were examined under a microscope with 100 x and 50 x magnification. A CCD camera was capable to acquire digital pictures. The **Figures 39 and 40** show the inclusions determined in the structure from the specimens 1 and 2 as an example. Specimen #4 showed so far very small (<10µm) inclusions and because of this reason we didn't took pictures from this specimen. Naturally a further grinding and polishing may show a different micrographic appearance owing to the buried nature of the inclusions. Based on inclusion specification, the inclusion diameters/ratings for specimens 1 and 3 would not be acceptable whilst those for samples 2 and 4 fall within an acceptable limit. However, since all the specimens are from the same block, this radial plate steel would have to be rejected if one holds strictly to the specification. However, the tensile and fracture toughness results show that the forged steel block has reasonable good and acceptable properties and should not be rejected despite some of the adverse inclusion findings.

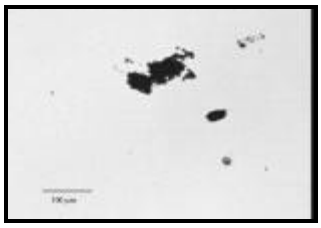

Figure 39. Micrograph showing inclusions under 100 x magnification Specimen # 1

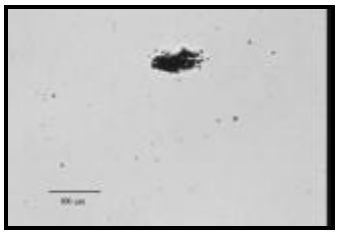

Figure 40. Micrograph showing inclusions under 100 x magnification Specimen # 2

7.5 Conclusion

It could be concluded that the level of the inclusions is a bit higher compared with the purity requirements of this Type 316LN steel for cryogenic application. The level of inclusion may affect adversely the fracture properties of the steel. However, considering the measured yield strength, ultimate tensile strength, and the K_{IC} values it can be concluded that this thick forged steel of Type 316LN may cover the requirements of the current cryogenic application.

8. Cryogenic mechanical properties of Type 316LN commercial weld filler materials

8.1 Background

To characterize the weld filler material 19 samples of ca. 50 mm thick weldments foreseen for the weld filler material qualification of different commercial weld filler wires were provided by Belleli, Italy in as welded and in as heat treated condition (800 °C / 1 h). These welds were performed with 50 mm thick Type 304 plates using selected filler wires appropriate for Type 316LN materials. During this task, measurements were carried out with respect to tensile and fracture properties of the weld metal.

8.2 Samples and specimens

Figure 41 shows the weld metal sample and the position of the machined specimens. The majority of the specimens were machined in weld transverse orientation. Some few tests were also performed in weld longitudinal orientation to confirm the weld transverse results. During the tensile and fracture tests great care was taken to guarantee that no fusion of 304 base metal affected the tested central region of the specimen. To achieve this, small gauge length (8 mm or 4 mm) extensometers were used which were clamped well inside the weld fusion zone. For

fracture toughness tests each individual specimen's crack or notch position were placed in the centerline of the weld fusion zone. **Figure 42** illustrates the specimen under test with the knife edge positions of the extensometers.

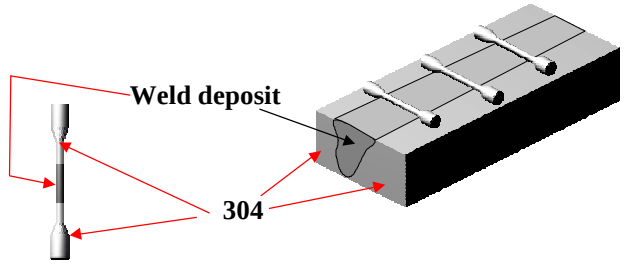

Figure 41. 50 mm thick weld metal sample. Two plates of 50 mm thickness consisting of 304 material were joined together using different commercial filler wires.

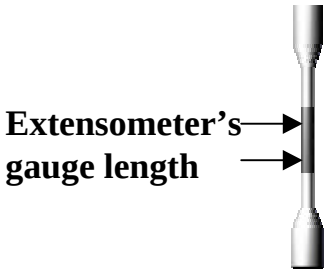

Figure 42. Position of the attached extensometer onto the specimens weld metal section.

Table 17 represents a listing of the used commercial filler wires and their origin.

Table 17. Compiled data of the selected commercial weld filler wires for the investigation of cryogenic weld metal performance

Weld filler wire code	Weld Process and wire size	Vendor	Designation
N° 2684A	GTAW, 1.2	Sandvik	25.22.2LMn
N° 2684B	GTAW cw, 1.2	Esab	316LMn
N° 2677A	SMAW, 4 x 350	Esab	316LMn
N° 2677B	SMAW, 4 x 350	Thyssen	25.22 H
N° 2676B	SAW, 1.6	Sandvik/Soud	25222 LMn/Ind24
N° 2676E	SAW, 3.2	Esab	316LM/Sid.Si
N° 2676F	SAW, 2.4	Sandvik	25.22.2LMn/Sid.Si
N° 2675A	GMAW, 1.2	Siderfil, Esab	316LM

Table 18 shows the chemical composition of the deposited weld metals ordered by the type of the applied weld process.

Table 18. Chemical composition of the deposited heavy weld filler material samples. The chemical analysis of the welds are with spectroscopic sampling technique from the mid of welded zone.

Mat. / Codes	C	Si	Mn	P	S	Cr	Mo	Ni	Al	Cu	Nb	Ti	V	N
GTAW 2684A	.02	.15	4.43	.013	.005	24.5	1.96	20.1	<.00	.07	<.01	.01	.06	.326
GTAW 2684B	.01	.38	7.43	.012	.005	20.0	3.23	15.5	<.00	.06	.02	<.01	.01	.266
SMAW 2677A	.04	.63	6.40	.020	.006	19.0	3.19	15.4	<.00	.11	.01	.03	.04	.227
SMAW 2677B	.04	.36	5.43	.012	.011	25.3	2.37	21.0	<.00	.01	.01	.03	.04	.227
SMAW 2676B	.02	.31	3.70	.016	.007	24.8	2.05	21.4	.04	.08	<.01	<.01	.05	.196
SMAW 2676E	.03	.64	6.31	.017	.005	19.1	3.22	15.4	.00	.11	.01	.01	.08	.222
SAW 2676F	.03	.34	4.52	.016	.007	24.6	2.06	20.7	.01	.06	<.01	.06	.000	.181
GMAW 2675A	.02	.38	7.34	.013	.006	19.8	3.20	15.7	<.00	.06	.02	<.01	.10	.238
SAW 2676H	.03	.36	4.50	.011	.009	24.5	2.1	21.5						.134
SAW 2676G	.03	.50	6.00	.018	.004	20.5	2.48	15.6		.03				.15
SMAW 2677C	.03	.48	3.89	.017	.004	25.4	2.32	21.9						.16

8.4. Tensile and fracture test results

In Table 19 all tensile and fracture test results carried out at 7 K or 4.2 K are compiled. The majority of fracture toughness tests are performed using small scale EDM notched round bars (JETT technique) at 7 K. For the reason of confirmation also two tests were conducted using ASTM standard 15 mm thick compact tension specimens at 4.2 K. In fact, the comparison of both techniques verify that both independent test methods are in line.

Table 19. Tensile and fracture toughness test results of weldments welded with various filler materials appropriate for Type 316LN metals at 4.2 K and at 7 K in as welded and heat treated condition (ht).

Weld process and filler material designation	Young's Modulus GPa	Yield Strength MPa	Ultimate tensile strength MPa	Uniform Elongation %	K_{IC} E-813 MPa√m	K_{IC} JETT MPa√m
GTAW 2684A, as rec.	190	1253	1550	17	-	174/166
GTAW 2684B, as rec.	186	1195	1565	17	-	131/156
SMAW 2677A, as rec.	180	1170	1513	33	-	173/154
SMAW 2677B, as rec.	167	1067	1447	31	-	146
SMAW 2676B, as rec.	136	1029	1155	6**	-	152/114
SMAW 2676E, as rec.	150	1083	1285	25	-	135
SAW 2676F, as rec.	189	1058	1285	25	-	134/134
GMAW 2675A, as rec.	168	1127	1451	27	-	148/171
SAW 2676H, as rec.	181/173	956/951	1359/1301	30/25	-	142/144
SAW 2676G, as rec.	152	934	1372	26	150	163/175
SMAW 2677C, as rec.*	147/166	1032/1022	1389/1378	27/33	122	131
GTAW 2684A, ht.	193	893	1253	16	-	142/195
SMAW 2677A, ht.	182	1162	1373	9	-	87/88
SMAW 2677B, ht.	201	1117	1407	9	-	89/86
GMAW 2675A,ht.	158	1064	1395	17	-	99/120

*Specimens consist of pure weld metal. Tensile specimens were machined in weld longitudinal orientation inside the weld mid zone.

** Massive pores were detected on the fractured surface.

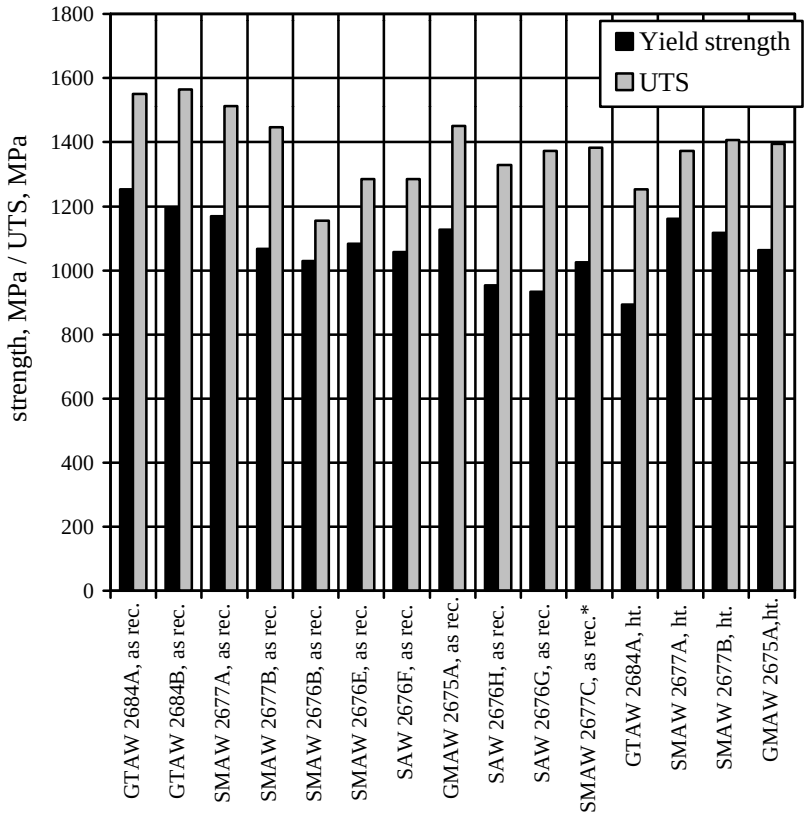

Figure 43. All tensile results shown as bar graph with respect to the cryogenic properties of yield and ultimate tensile strengths. Test temperatures were 7 K

Figures 43 and 44 give the obtained cryogenic mechanical property values in form of bar graphs. The specified ITER values with 1500 MPa for ultimate tensile strength, 1000 MPa for the yield strength, and 130 MPa√m for the fracture toughness were almost achieved with the majority of the weld filler wires. In case of fracture toughness the heat treated specimens could not meet the specified value of 130 MPa√m. Therefore for the further qualifications a heat treatment of the welds were rejected. In addition, the selection of the weld filler wire was guided besides the obtained mechanical values also the weld process handling and the sound weldability of the material.

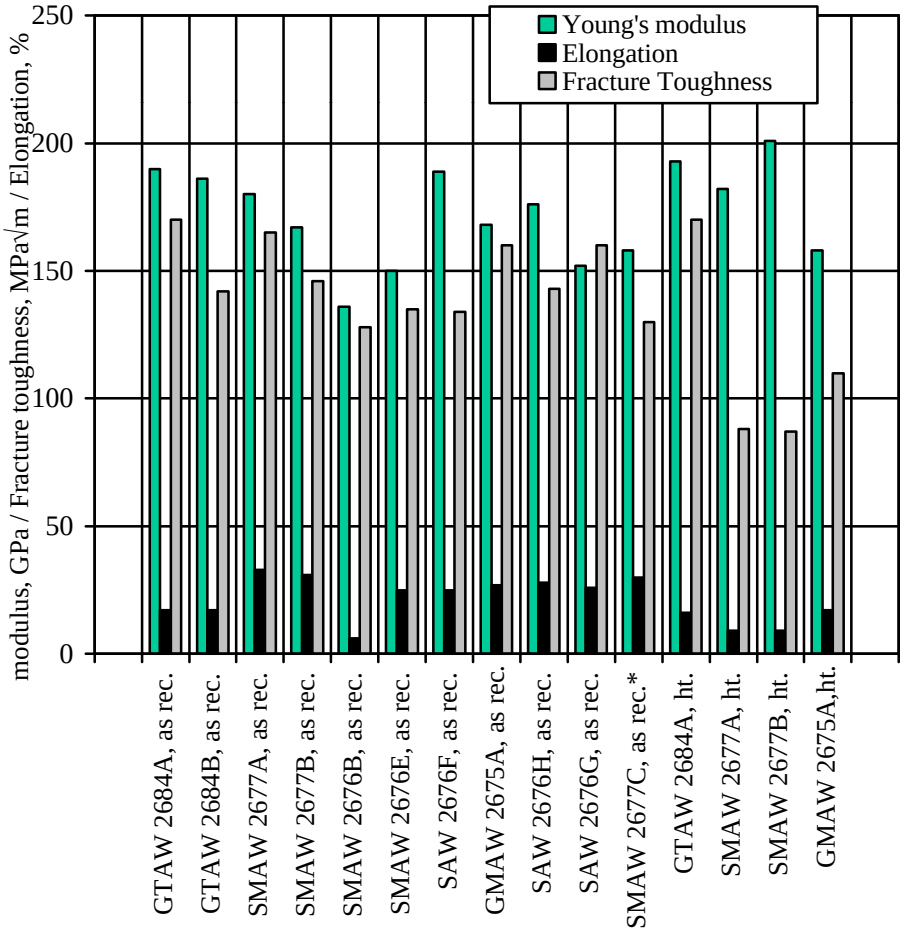

Figure 44. All tensile and fracture results shown as bar graphs with respect to the cryogenic properties of Young's modulus, elongation, and fracture toughness. Test temperatures were 7 K and in case of fracture toughness tests with CT specimens 4.2 K.

Besides the weld filler material qualification also deeply penetrated weld passes of different materials using electron beam (EB) or laser beam weld (LB) processing were measured with respect to their mechanical properties at cryogenic temperatures. These materials were the newly developed fully austenitic nitrogen strengthened cast stainless steel (Model 2) and a heavy forging of Type 316LN material (Model 1). For this action welded samples were provided to Forschungszentrum Karlsruhe where tensile and fracture toughness (JETT) type specimens were machined in weld transverse orientation. **Table 20** gives the measurement results of this particular tests.

Table 20. Tensile and fracture behavior of EB and LB weld passes for cast and forged materials at 7 K.

Weld material samples	Young's Modulus GPa	Yield Strength MPa	Ultimate tensile strength MPa	Uniform Elongation %	K_{IC} JETT MPa√m
Casting EBW zone	133/133	974/862	1179/1177	37/35	193/235
Forging EBW zone	161/198	993/1070	1460/1545	30/50	190/212
Forging LBW zone	187	1077	1521	55	> 220
Casting LBW zone	168	942	1173	17	> 200

As given in **Table 20** the LB-weld zones show in case of forged material a higher elongation at fracture compared to the LB weld material of the cast stainless steel. The reason for this phenomenon is the somewhat lower yield point of the cast material which strains extensively during the loading whereas the weld material (higher yield strength) resists against the straining. The attached extensometer pair inside the weld metal of cast metal specimen show therefore little elongation without a significant necking. **Figure 45** shows the two fractured specimens and the difference of failure positions.

Figure 45. Cast material with the laser beam weld zone of the left hand specimen show marginal necking inside the weld metal and a fracture occurrence outside the weld metal (inside the base metal of the cast steel). The right hand specimen consisting of forged material and the laser beam weld zone shows the fracture event inside the weld metal. The weld metal's yield strength is inferior to the base metal.

Within the weld metal investigation task also fluxed core arc welded (FCAW) weld metals were tested. Two sets of samples were measured with respect to their tensile and fracture properties. These were uphill vertical position (3G) welded two specimens of FCAW samples. **Table 21** gives the results of these measurements. The results with material 2733 refer for one of the specimen a low value for elongation owing to a small embedded pore resulting from the weld process.

Table 21. Tensile and fracture behavior of FCAW weld metals at 7 K.

Weld material samples	Young's Modulus GPa	Yield Strength MPa	Ultimate tensile strength MPa	Uniform Elongation %	K_{IC} JETT MPa√m
FCAW 2733 vertical (nicros) 3G	183 / 195	956 / 925	1168 / 1312	8.2* / 23	170 / 150
FCAW 2739 vertical 3G	164 / 170	948 / 957	1329 / 1364	31 / 30	137 / 124

*A pore in the center of the fractured specimen could be detected, thus leading to low a elongation value.

8.5. Conclusion

The cryogenic mechanical weld metal results show so far properties which meet the specified structural requirements concerning with the design criteria.

9. Cryogenic mechanical investigations on materials of model 1 and model 2 mock-ups for ITER toroidal field coil structures

9.1 Background

Within the framework of EUHT (European Home Team) a R&D task was placed to develop mockups for the TF coil. These activities are firstly; a full scale model of inner upper case leg structure (model 1), and secondly; the full scale model of intermediate OIS region (model 2). To manufacture these parts successfully a material testing program has been initiated to characterize the procured materials at 4 K and establish a data base to demonstrate the technological feasibility with the realization of full scale partial sections of the case and OIS. The selected material was Type AISI 316LN with N = 0.16-0.20 % and reduced level of impurities (Cu, Co, S, and Si). Owing to the reality that only the critical heavy loaded parts of the coil case (e. g. Inner leg section) should fulfill the stringent above given material requirements, the requirements for the upper OIS (yield >420), case outer leg (yield >900 MPa), middle OIS (yield>770 MPa), and lower OIS (yield>410 MPa) could be relaxed to reduce the cost situation. The tested materials were heavy forged samples, and castings (casted in a chromite mould).

9.2 Materials and specimens

The supplied materials for the cryogenic mechanical investigations are given as follows:

- Heavy samples were procured from various manufacturing stages of the 65 t ingot till the final 40 t square tube forging representing the full scale model 1. The relevant samples were machined out from various spatial positions. Ingot was melted by Thyssen, Germany and the forging was processed by R. KIND, Germany using a 6000 t capacity press.
- Representative blocks were machined from different spatial positions of the one ton trial casting representing in thicknesses and in the solidification rate the 25 t full scale model 2 manufactured at Creusot Loire Industries, France.

Figure 46 shows an illustration of the two mock-ups and their main dimensions.

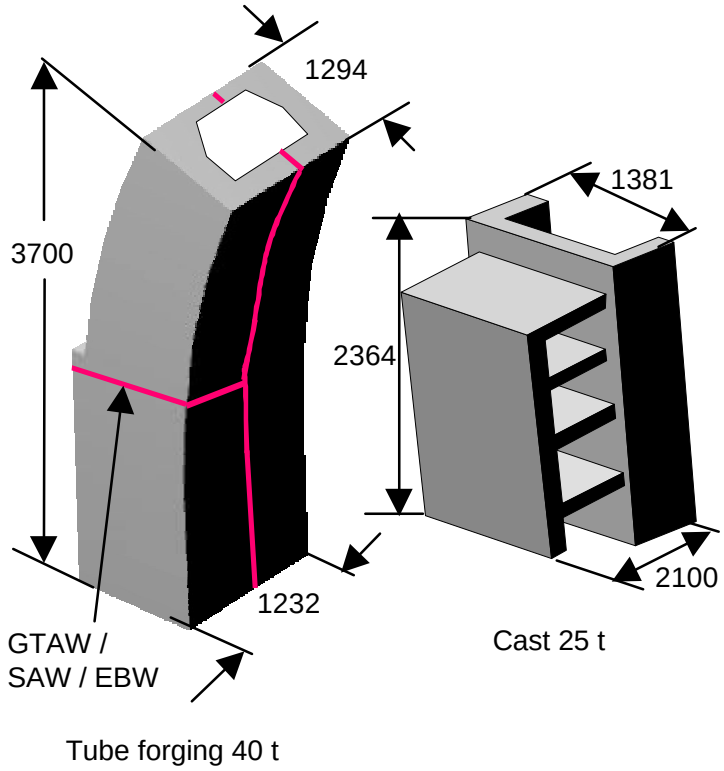

Figure 46. Schematic illustration of the two mock-ups (left hand model1 and right hand model 2).

The chemical compositions of investigated base metals are given in **Table 22**. The type of specimens used for tensile, fracture, and FCGR investigations were as follows:

Round smooth tensile: gauge diameters of 4 mm machined from the plates, of 4 and 12 mm from the 66 t forging, and 4, 12, 18, and 22 mm from one ton cast steel.

Flat tensile: reduced gauge length section of ~2 x ~1.5 mm.

Compact tension (CT): ASTM proportional 63 x 60, with thickness' of 15 and 25 mm. FCGR CT specimens of 40 x 43 x 4 mm. Additionally, for fracture toughness verification of cast steel CT specimens of 109 x 100 x 40 mm.

EDM notched round bar: 50 mm long with a shaft diameter of 6 mm and a net diameter after notching around the girth of about one third of the shaft diameter.

Prior to the manufacturing of 25 t mock-up for model 2 an order of one ton trial casting was placed to investigate all relevant structural properties of this new material. **Figure 47** shows an illustration of the manufactured one ton trial casting.

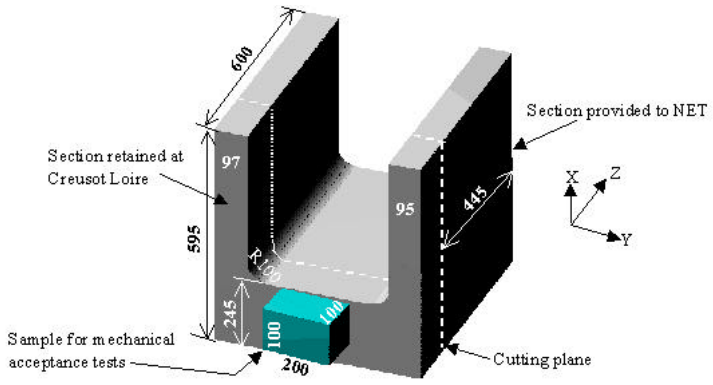

Figure 47. One ton heavy trial casting (model 2) manufactured by Creusot Loire Industry, France. Dimensions are given in mm. The casting process was performed in a chromite mould to accelerate the solidification process using the high thermal conductivity of the chromite sand.

All investigations were carried out either at 7 K or in LHe according to the size of the specimens. Several tensile measurements with specimens having different gauge sections machined from provided samples (cast steel; A, B, T1, and T2 of **Figure 49**) were performed at 7 K and in LHe to ensure a size and test environment independence especially for the cast steel results. **Figure 48** shows the cut section, delivered to EFDA for the removal of various test samples for the reason of mechanical and joining investigations. The Figure gives the spatial location and approximate size of the cut samples.

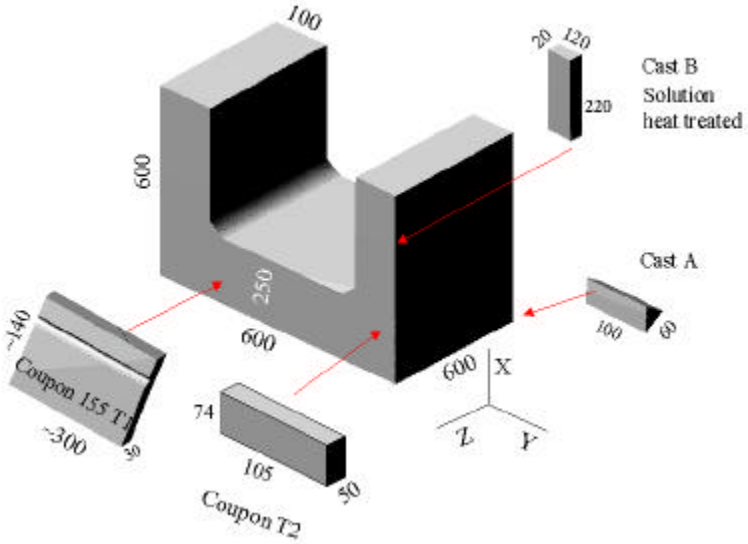

Figure 48. Provided trial casting to EFDA and the cut test coupons foreseen for the mechanical investigations. The coupon designated as Cast A was the first test sample in as received condition.

The tensile tests with 12 mm gauge diameter specimens were performed in LHe using the 200 kN screw driven tensile test machine, whereas the 4 mm gauge diameter specimens were tested at 7 K using the servohydraulic 25 kN capacity machine. The tensile specimens with 18 mm and 22 mm gauge section diameters machined from a sample cut from the cast steel section (T3, at the vicinity of T1 position) were tested at Breda Istituto Scientifico, Milan, Italy using a 1200 kN servo hydraulic capacity machine equipped with a LHe dewar. The data acquisition for all these tests were performed using the procedure with two extensometers attached onto the specimen. **Table 22** gives the results with the chemical composition of the two mock-ups.

Table 22. Chemical composition of the investigated Type 316LN forged and cast stainless steel samples.

Mat. / Codes	C	Si	Mn	P	S	Cr	Mo	Ni	Al	Cu	Nb	Ti	V	N
Forged tube model 1	.018	.37	2.01	.028	.002	17.23	2.52	13.46	.009	n. d.	n. d.	n. d.	.06	.182
Casting model 2	.016	.78	6.00	.022	.005	17.6	3.01	13.9	.005	.182	n. d.	n. d.	.057	.184

9.3 Tensile measurements with cast steel (model 2)

After the initial tensile tests with coupon A and B a clear effect of specimen orientation could be observed. To clarify this phenomenon, explainable from the point of view for cast materials, several tensile specimens have been machined from the coupon T2 accurately in all three spatial orientations. Furthermore, the initial tests revealed a significant scattering of the obtained Young's modulus results at 7 K (between 190 and 100 GPa). Therefore, a discussion arose about a possible effect of specimen size regarding the Young's modulus. The standard tensile specimens used at Forschungszentrum to date have a diameter of 4 mm in the gauge section, which might be not big enough for tensile tests owing to the situation of large grain sizes of the present cast material and possible microporosity. It was thereafter decided to conduct some benchmark tests with large size specimens machined from the same orientation as the ones with 4 mm diameter. After a rough estimation for a feasible geometrical section using the already known material strength values three tensile specimens of 12 mm gauge section diameter has been machined for tests at LHe using the screw driven 200 kN tensile machine at Forschungszentrum Karlsruhe site.

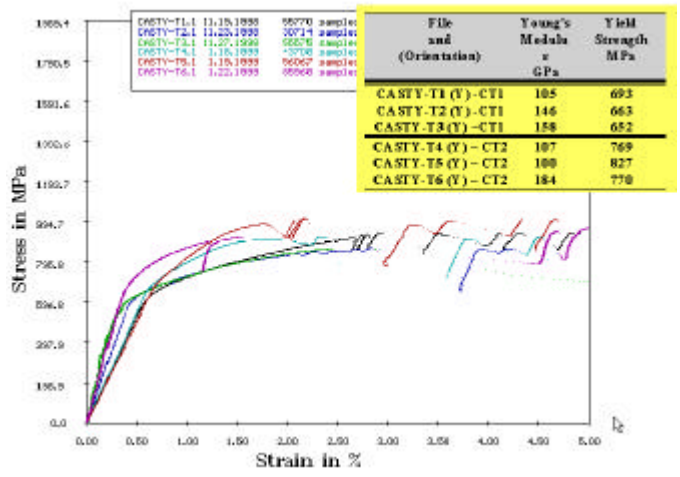

Figure 49. Stress strain test results at 7 K and at 4.2 K for different size specimens. The inserted Table shows the obtained Young's modulus and the yield strength data. The code with CT1 refers to coupon T2 and the one with CT2 refers to coupon 155 T1. Further the files CASTY-T3 and CASTY-T6 are valid for LHe tests performed with 12 mm Ø specimens. All other tests (T1, T2, T4, and T5) are with 4 mm Ø specimens.

After completing the tests with the 12 mm diameter specimens at Forschungszentrum site one could saw that there is no size effect concerning with the yield strength at least up to 12 mm

tensile specimen diameter. The diagram in **Figure 49** shows the original six test results of different size specimens all in Y-orientation and with different specimen diameters.
In consequence, EFDA could successfully negotiate with a material testing laboratory (Istituto Scientifico Breda ISB, Milan) to test at their site even larger size specimens at LHe. ISB is capable to ensure tensile testings of large diameter specimens owing to the fact of the availability of a 1200 kN tensile testing machine equipped with a small double dewar system for LHe tests.

9.4 Tensile tests at Breda, Milan

The available tensile test machine at Breda, Milan was a servo hydraulic 1200 kN capacity unit from DARTEC company. **Figure 50** shows the machine and the cryogenic equipment system under operation. Furthermore, the built in specimens in the 4 K rig are shown also within this **Figure 50**.

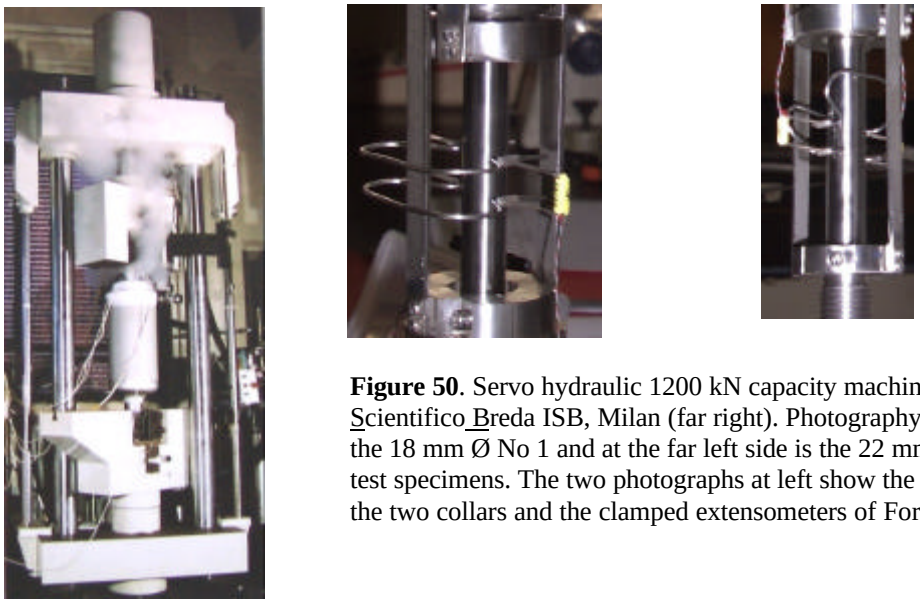

Figure 50. Servo hydraulic 1200 kN capacity machine at Istituto Scientifico Breda ISB, Milan (far right). Photography at the center is the 18 mm Ø No 1 and at the far left side is the 22 mm Ø No 2 tensile test specimens. The two photographs at left show the screwed beams to the two collars and the clamped extensometers of Forschungszentrum.

For this tensile measurement task an order was placed for ISB to conduct four tensile tests in Y and X orientations. To perform these tests two 18 mm diameter and two 22 mm diameter specimens were machined in Y and X orientation at Milan. The tensile test specimens have had near the both ends of upper and lower threads collars where a stiff clamp was screwed before the test (see **Figure 50**). Two long beams attached in each side of these collars were extended out of the LHe /dewar system, thus enabling for the placing of the LVDT (Linear Variable Differential Transducer) displacement measurement gauges. To obtain maximum possible information an independent displacement measurement system was attached directly onto the specimen during these tests as usually conducted by the standard tests at Forschungszentrum. For these reason four special large size, high resolution extensometers have been manufactured. Prior to the tests at ISB site these extensometers were used at Forschungszentrum for the measurements of 12 mm diameter specimens. For the foreseen tests, Forschungszentrum brought also its own data acquisition system consisting of an A/D converter and a Notebook. During the first test owing to the restricted spatial conditions in the 4 K rig the sensitive extensometers failed above the 2 % strain regime. This was probable due to the spring system surrounded from the outer side of double beam system as shown in **Figure 50** (mid photo). The next test with 22 mm diameter specimen used a spring system which was surrounded inside the two beams, thus giving less chance to a failure by malfunctions due a touch during specimens mounting phase (see **Figure 50** at far left).

However, the acquired data in case of specimen No 1 allowed a safe evaluation of the three quantities, Young's modulus, yield strength, and the ultimate tensile strength. In **Figure 51** the acquired stress strain diagram of this first test is given. As shown in this diagram the slope at the initial stage is irregular, most possible by slipping of the pulling rods inside the hydraulic jacks of the machine. After reaching a certain amount of load the system stabilizes and there are no more movements between jack and pulling rods. Otherwise there is no explainable reason why the shown irregular jumps may occur. Same type of a result was also observed by the X-Y chart recorder system of ISB, which is shown in **Figure 52**.

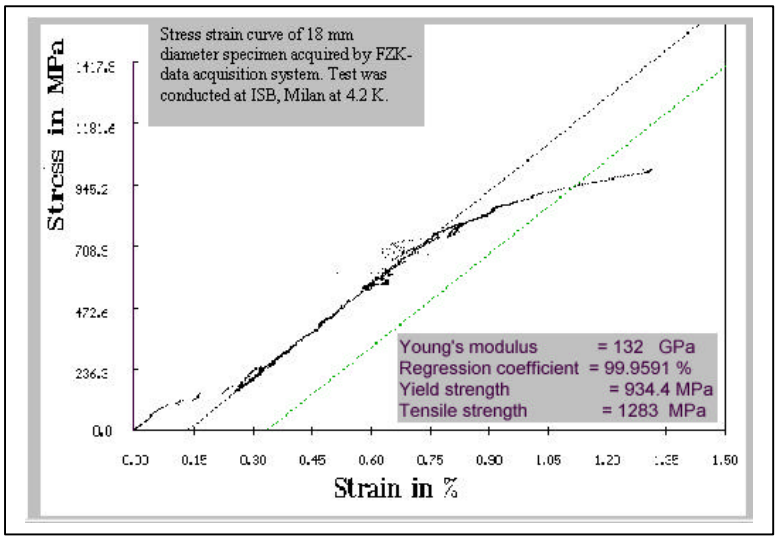

Figure 51. Acquired data of specimen No 1 which was designated at ISB to be in Y-orientation. The Young's modulus has been evaluated inside the linear portion of the slope within an accuracy of +/- 3% using a first order regression analysis taking account of all data inside the linear region between 0.35 and 0.6 % strain.

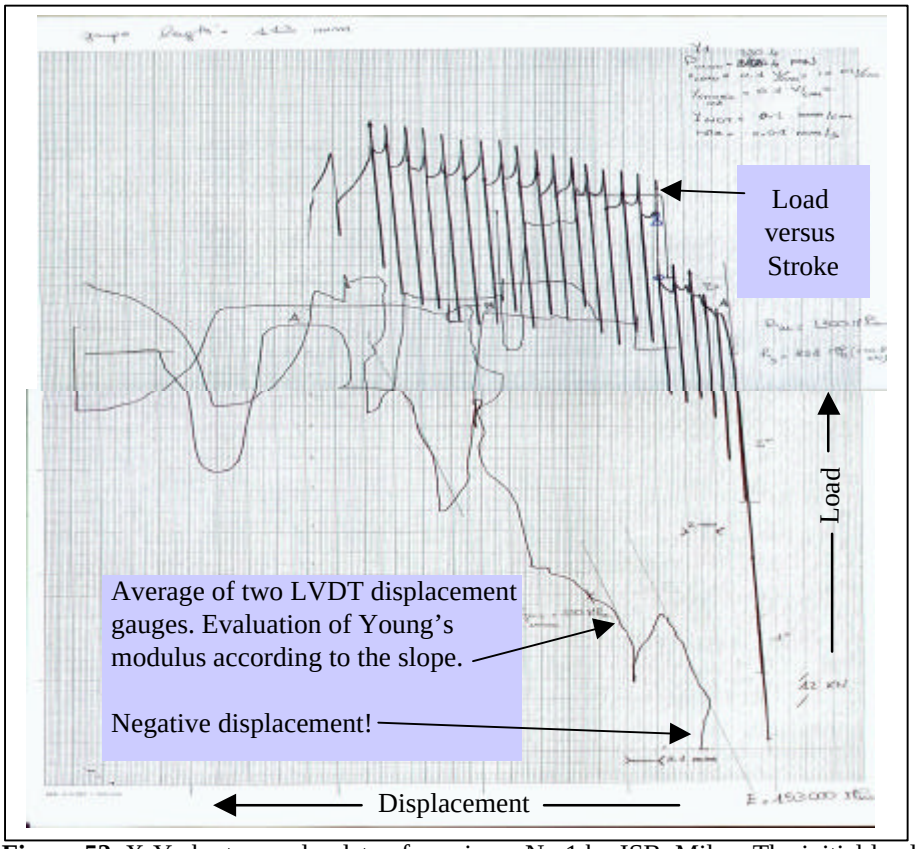

Figure 52. X-Y chart recorder data of specimen No 1 by ISB, Milan. The initial loading regime show a negative displacement of the LVDT system. Young's modulus has been determined from the shown linear portion and was evaluated to be 150 GPa.

The test with specimen No 2 having a diameter of 22 mm could be successfully evaluated with the Forschungszentrum Karlsruhe double extensometer system which failed fortunately only after ca. 24 % elongation. The LVDT system of ISB failed in the initial loading sequence. Again there was rapid movements and shocks in this initial phase either because of hydraulic jack system or machine feed back system. During this test the software acquired additionally the stress versus strain obtained by the stroke movement and it could be easily demonstrated that a direct determination of Young's modulus using the stress versus stroke displacement is almost impossible. In addition, the specimen orientation designation at ISB (X and Y) did not correspond to the former designations used at Forschungszentrum. The specimen designated by X at ISB corresponded well with the batches of Y (lower yield strength) values of Forschungszentrum designation and the batch designated with Y (specimen No 1 of ISB) corresponded to X orientation of Forschungszentrum batch. **Table 23** shows all to date collected tensile results of this one ton trial cast stainless steel. So far the discrepancy of the yield strengths measured simultaneously on the same specimen between ISB and Forschungszentrum Karlsruhe differ not much (less than 4 %). However, the differences of Young's modulus values are much higher (ca. 15 % higher in case of ISB). According to the nature of Young's modulus measurement this difference is understandable considering the requirement of a very high sensitive measurement system.

Table 23. Cryogenic temperature tensile test results of Type 316LN cast stainless steel

File and (Orientation)	Young's Modulus GPa	Yield Strength MPa	Ultimate Tensile strength MPa	Uniform Elongation %	Reduction of Area [C] %
CASTA-T1 (Y)	180	954	1206	10	22
CASTA-T2 (Y)	186	925	1233	9,5	22
CASTB-T1 (Y)	150	668	1090	31	23
CASTB-T2 (Y)	155	688	1133	23	23
CASTX-T1 (X)	196	859	1167	37	27
CASTX-T2 (X)	186	877	1108	12	15
CASTX-T3 (X)[B]	135	811	1069	28	33
CASTX-T5 (X)[E]	121	918	1111	35	
CASTY-T7 (X)[G]	132 FZK 153 Breda	936 FZK 898 Breda	1283 FZK 1300 Breda	27	-
CASTZ-T1 (Z)	158	744	1142	26	27
CASTZ-T2 (Z)	150	738	1196	34	25
CASTY-T1 (Y)	105	693	1096	34	31
CASTY-T2 (Y)	146	663	1112	37	39
CASTY-T3 (Y)[A]	158	652	900	23	30
CASTY-T4 (Y)[B]	107	769	1061	24	27
CASTY-T5 (Y)[B]	100	827	1184	27	31
CASTY-T6 (Y)[D]	184	770	1073	27	-
CASTX-T4 (Y)[F]	132 (Breda)	668	1094	24	-

A Tensile specimen gauge section 12 mm diameter. Test performed in liquid helium
B Coupon 155 T1
C Evaluated by averaging of the cross section appearance at 0° angle in tensile direction by microscope
D Gauge section 12 mm diameter. Test performed in liquid helium. Coupon 155 T1
E Gauge section 12 mm diameter. Test performed at 4.2 K gas helium. Coupon 155 T1
F 22 mm diameter at LHe (Breda, Italy) values determined by FZK extensometers, Direction X or Y ?
G 18 mm diameter at LHe (Breda, Italy) values determined simultaneously, Direction X or Y ?

Regarding the fact of the obvious compression component during the measurement of the specimen No 1 with the ISB's LVDT system (negative displacement, see **Figure 53**) this compression component may have overestimated the Young's modulus value. The two additional specimens with 18 and 22 mm diameter are also tested at ISB afterwards and similar tensile results are obtained as the previous one's.

9.5 Investigations of Young's Modulus by Non Destructive Testing

Within these investigation task it was tried to evaluate the materials Young's modulus value using a non destructive testing method owing to the problem of the low Young's modulus values of the so far determined results with the present trial cast steel. Especially, the uncertainty with the mechanical tests and the large scatter band of the determined values led to this independent measurement method. As known, the Young's modulus for Type 316LN alloys do not change much within a large temperature range below the ambient temperature. Nominally, for common stainless steel products at 4 K only around a 10 % increase of this quantity is to date observed compared to 300 K. Therefore, it was worthwhile to check this physical quantity using a sound vibration technique which determines by one touch testing technique the flexural vibration of an object after an impulse excitation of the sample. The equipment used was the Grindo Sonic, an ASTM Standards C323, C848, C747, and C215 compatible device. By simple machined plane bars the material can be immediately measured very fast, precise, and with a high reproducibility. The system analyzes the longitudinal, flexural, and torsional vibrations and determines, in microseconds, two periods of the fundamental vibration.
The general partial differential equation for a free bending vibration

$$E \cdot J \cdot \frac{\partial^4 f}{\partial x^4} = -\frac{g \cdot A}{g} \cdot \frac{\partial^2 f}{\partial t^2}$$

holds for a vibrating bar , where

E = Young's modulus
J = Bending inertia of cross section
γ = Density of the material
A = Area of cross section
g = Acceleration of gravity
x = coordinate in long direction of the bar
t = time

are.
The solution of this equation for a bar resting on supports with two free ends is given by where

$$E = 0.946 \cdot K_p \cdot \frac{g \cdot l^4}{a^2} \cdot f^2 \cdot 10^{-10}$$

and K_p an independent constant are and can be determined by the geometry of the bar using the following equation,

$$K_p = 1 + \frac{a^2}{L^2} \cdot (7.32 - 11 \cdot \frac{a^2}{L^2})$$

where a and L are the thickness and the total length of the rectangular shaped bar respectively.

Several rectangular cross-section bars have been machined for the purpose of the ambient temperature Young's modulus determination. Prior these tests standard 316LN and aluminum plate materials were also measured by this technique. A high degree of confirmation between those values and values determined by destructive tensile technique was evident. A high reproducibility could be observed also during many times of impulse excitation of the cast alloy bars in different orientations. The values so far determined by this method are all relatively high (usual 316LN values) and therefore, in case of this cast alloy the uncertainty still remains about the source of the differences between those obtained by non destructive technique and by mechanical tensile testing method.
Table 24 shows the geometrical conditions of the used bars and their results.

Table 24. Non destructive testing of the cast alloy bars using the Grindo Sonic device at 295 K

Orientation	Length mm	Width mm	Thickness mm	Mass g	Young's modulus GPa
X	100	15,01	15,01	17,8	175,8
Y	100	15,01	15,02	178,3	189,3
Y	142,8	19,05	6,76	146,1	183
Y	118,1	18,95	6,76	120,2	194
Y	120,7	12,6	7,22	86,9	191
Y	119,55	13,55	7,77	99,8	183
Y*	121,4	13,7	7,25	95	146
Y	120,85	12,75	7,78	94,9	187

*This block was cut after the test in four pieces in long orientation for the reason of tensile specimen machining

As shown in Table 24 a high degree of variation is obvious with respect to Young's modulus data. To check the differences between the tensile Young's modulus and the vibration Young's modulus one of the tested blocks were subdivided into four sections. From each section one standard tensile specimen were machined. Thereafter, room temperature tensile measurements were conducted with those four specimens. In addition, to cross check the performance of the mechanical testing system two well characterized standard specimens (AlMgSi1 and Manet [martensitic steel]) were also used during these investigations. The **Figure 53** below shows the determined results with these tests, which confirm the high accuracy of the entire measurement system.

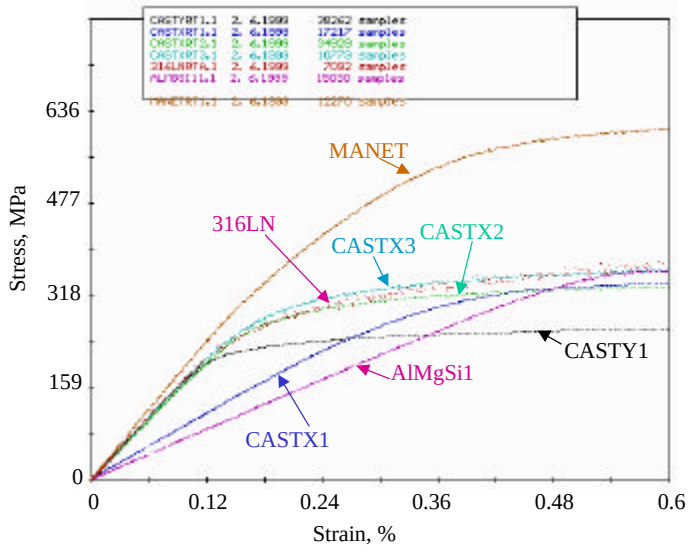

Figure 53. Stress- strain diagram of four specimens machined from previously sound vibration tested cast steel block. Additionally the diagram shows the plots of an Al-alloy and a ferritic steel at room temperature.

Material & file	Young's Modulus GPa	Yield Strength MPa
CASTYRT1	178	249
CASTXRT1	95	336
CASTXRT2	169	319
CASTXRT3	176	343
316LNRTA	186	343
AlMgSi1	72	359
MANETRT1	203	590

Table 25. Results of the room temperature tests with four cast steel specimens belonging to the same block. Calibration specimens are AlMgSi1 and MANET.

Table 25 gives the determined tensile properties of the six tests shown in **Figure 53**. In fact, the determined values for the two reference alloys match accurately the exact Young's modulus data which can be obtained by the literature. Out of four cast steel specimens one of them show a very low Young's modulus value of 95 GPa thus verifying the possibility of getting such low data. The average of four tests give also almost a similar value as determined by the sound vibration technique (154 GPa versus 146 GPa).

9.6 Thermal Expansion Measurements of cast steel material

These investigations were conducted with the available cryogenic proof extensometers. Prior the tests the apparent thermal shrinkage of the double extensometer system were checked by a low thermal expansion (LTE) glass material (Ceredur). This material has almost zero thermal expansion between room temperature and 4 K. The determined value of the apparent thermal shrinkage were than subtracted by the value of the actual measurement. In addition, several known materials thermal shrinkage were checked with the same technique between 295 K and 77 K (LN2). **Table 26** gives the results determined for a variety of materials.

Table 26. Thermal shrinkage investigation results between 295 K and 77 K for several materials

Apparent displacement of the set up for LTE (Ceredur) for a reference length of 8 mm	59.02 µm
Total displacement of the set up for Valinox (Type 316LN) for a reference length of 8 mm (Type 316LN aged)	81.44 µm 81.44 – 59.02 = 22.42 µm Thermal Expansion = 0.28 %
Total displacement of the set up for Incoloy 908 (aged) for a reference length of 8 mm	74.46 µm 74.46 – 59.02 = 15.44 µm Thermal Expansion = 0.19 %
Total displacement of the set up for CAST steel for a reference length of 8 mm (Type 316LN , Y-direction)	84.87 µm 84.87 – 59.02 = 25.85 µm Thermal Expansion = 0.32 %
Total displacement of the set up for CAST steel for a reference length of 8 mm (Type 316LN, X-direction)	86.56 µm 86.56 – 59.02 = 27.54 µm Thermal Expansion = 0.34 %

Using the same technique the shrinkage of the cast stainless steel was also determined between 295 K and 7 K automatically during the cool down phase of tensile testing. These determined values were 0.32 % for the cast steel in X-direction and 0.36 % in Y-direction. The estimated error of the thermal expansion measurement set up was around 10%. The discrepancy between the values of 77 K and 7 K shrinkage may be the nature of the used insensitive technique or material related. Future tests have been planned to elucidate the obtained data with an upgraded more sensitive system. However, it can be confirmed that the cast alloy has a slightly higher thermal expansion coefficient (ca. 10%) compared to plate or forged materials.

9.7 Fracture investigations with cast steel model 2 material

These tests comprised JETT tests (**J** **E**valuation on **T**ensile **T**est) with notched round bars machined from the available coupons in different orientations and one ASTM E 813-88 test using a 15 mm thick **C**ompact **T**ension (CT) specimen from the cast B coupon, where the crack plane was parallel to y-direction. Although the CT specimen test at LHe could be conducted successfully the obtained value is not valid and unrealistic. The crack changed its plane during the crack extension phase of specimen loading. Thus this confirms also the non isotropic nature of the cast steel. Therefore, it is not possible to measure this material at least with such small thickness CT specimens. Besides, the ASTM standard is valid strictly speaking only for isotropic materials. The JETT specimens, however, could determine the fracture toughness successfully owing to the technique which gives the local fracture toughness of a material, where non isotropic properties do not play a big role. **Table 27** shows the obtained results at 7 K using the JETT technique. According to these results the material exhibits an average fracture toughness value > 150 MPa√m.

Table 27. Fracture toughness investigation results with cast stainless steel at 7 K

File and Orientation		Converted Fracture Toughness, MPa√m
CASTA-J1 (Y)	179	179
CASTA-J2 (Y)	97	132
CASTB-J1 (Y)	182	181
CASTB-J2 (Y)	122	148
CASTL-J1 (Y)	125	150
CASTL-J2 (Y)	134	155
CASTV-J1 (Z)	94	130
CASTV-J2 (Z)	167	173
CASTQ-J1 (X)	136	156
CASTQ-J2 (X)	163	171

The fracture toughness results determined with small round bars (JETT tests) show a large scatter owing to the local anisotropic conditions. For these reason after the standard 15 mm compact tension specimen tests measurements were conducted at LHe up to 40 mm thickness specimens. All these results were also so far not valid according to the E 813 crack front profile. In addition, the fatigue precrack appearance reveal after the CT specimen fracture a quite different behavior than usual plate materials of similar type. However, a minimum macroscopic fracture toughness of > 200 MPa√m can hold certainly for this newly developed cast steel referring the test results obtained with big CT specimens.

9.8 Tensile and fracture investigations with forged model 1 material

Table 28 gives the determined tensile and fracture toughness results of the tested materials for model 1 mockup. The tensile tests with the series T601, L600, and R602 of Model 1 tube forging show a high yield strength and a scatter of the elongation results compared to the series of T604, 603, and R605. The latter received batch was from samples in fully annealed condition (1080°C/3 h, water quench) , whilst the first series were from a preliminary batch with presumable improper annealing (1050°C/4 h and most probable no water quenching). The first series showed also precipitates reflecting to the low elongation and the low fracture toughness results of the two measurements. Comparing the tensile results of the three tests with the radial orientation (R602) it is obvious that between 4 mm gauge diameter specimens, tests conducted at 7 K and a specimen with 12 mm gauge diameter tested at LHe there are no size or environmental effects within the given test conditions. Cryogenic fracture toughness results show also usual range of values which are common for this type of steel.

Table 28. Tensile and fracture toughness test results of the samples provided from the tube forging of Type 316LN material at 4.2 K and at 7 K.

Material designation test codes and sample orientation in ( )	Young's Modulus GPa	Yield Strength MPa	Ultimate tensile strength MPa	Uniform Elongation %	K_{IC} JETT MPa√m
Forg. T601 (trans.)	209/209	1185/1165	1625/1635	46.5/40.5	238/163
Forg. L600 (long)	204/207	1113/1062	1620/1624	47/61	206/192
Forg. R602 (radial)	207/207	1140/1168	1457/1418	13/7	218/210
Forg. R602 (radial) [A]	199	1155	1467	15	-
Forg. T604 (trans.)	210	1010	1523	44	-
Forg. L603 (long)	201	1083	1525	45	-
Forg. R605 (radial)	209	934	1473	48	-

[A] This specimen has a 12 mm Ø and the test was conducted in LHe, whilst all others are 4 mm Ø standard ones and tested at 7 K under gaseous helium environment.

9.9 Weld joint performance of cast steel, tensile behavior

To investigate the properties of the cast stainless steel welded with a selected weld wire using GMAW weld process two tensile specimens were machined in weld transverse direction, thus enabling to check the tensile properties of the HAZ (Heat Affected Zone) regime at 7 K. For this purpose the double extensometer system having nominal gauge lengths of 7 mm was placed at HAZ region within the weld fusion line (etched beforehand) in the middle of the gauge length. **Figure 54** shows the result of the first test. As shown during this test the extensometer gauge section have not detected a plastic straining, moreover after reaching the elastic limit several load drops (resulting from the cast material region) occurred inside the elastic line. The insert in this **Figure 54** shows the load versus time diagram. This diagram gives also the details that the extensometers show no significant displacement. The fracture of the specimen occurred well inside the cast material apart from the weld fusion zone. This test confirms that the weakest link in the material is the cast alloy and not the weld zone and also not the HAZ. During the second test the fracture of the specimen occurred inside the heat affected zone and the extensometers could detect in this case after a while, a plastic yielding resulting from the straining of the heat affected zone. The Young's modulus of both tests show also relatively high values compared to the pure cast regime.

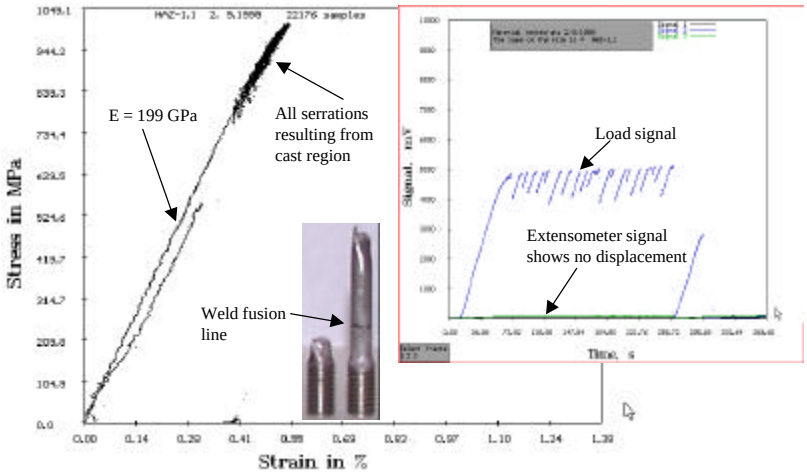

Figure 54. Tensile test performed at 7 K. The specimen consisted of base, weld, and HAZ zones. The extensometers were placed at the heat affected zone regime with the fusion line in the center. The insert shows the load, extensometer versus time diagram. The extensometer signals show no significant displacement.

9.10 Fatigue crack growth rate of cast and forged steels

To characterize the new cast steel of the one ton trial casting three CT specimens were machined from all three spatial directions in as received fully annealed condition. **Figure 55** represents all the results of these measurements performed at 7 K. For comparison reason several other investigated representative alloys of Type 316LN extruded and Incoloy 908

were plotted into the same diagram. In addition, the cast stainless steel showed no anisotropic behavior of the FCGR data and therefore all three orientation results are merged to one data set. The measurements carried out at 7 K show for the casting material a superior FCGR behavior compared with other alloys even with the aged Incoloy 908. The fatigued surface appearance of the tested cast steels differ also considerable from the 316LN type structural steels. The high resistance against the cyclic loading with respect to crack growth can be attributed to the completely different microstructure owing to the big grain sizes, a common feature of cast steels. Besides, during the course of these FCGR measurements also a new Japanese cryogenic stainless steel JK2 was investigated for the reason of cross check (between JAERI and Forschungszentrum Karlsruhe) and comparison with the selected materials of mock-ups (**Figure 56**). The cross check showed a circa 10 % difference between the JAERI and the Forschungszentrum tests above the $\Delta K \sim 30$ MPa$\sqrt{m}$ range, most probable due to the small size specimens of Forschungszentrum (4 mm thickness versus 12 mm of JAERI) which may result higher plastic constraints during the specimens cycling at high ΔK regime thus increasing the resistance against the crack propagation.

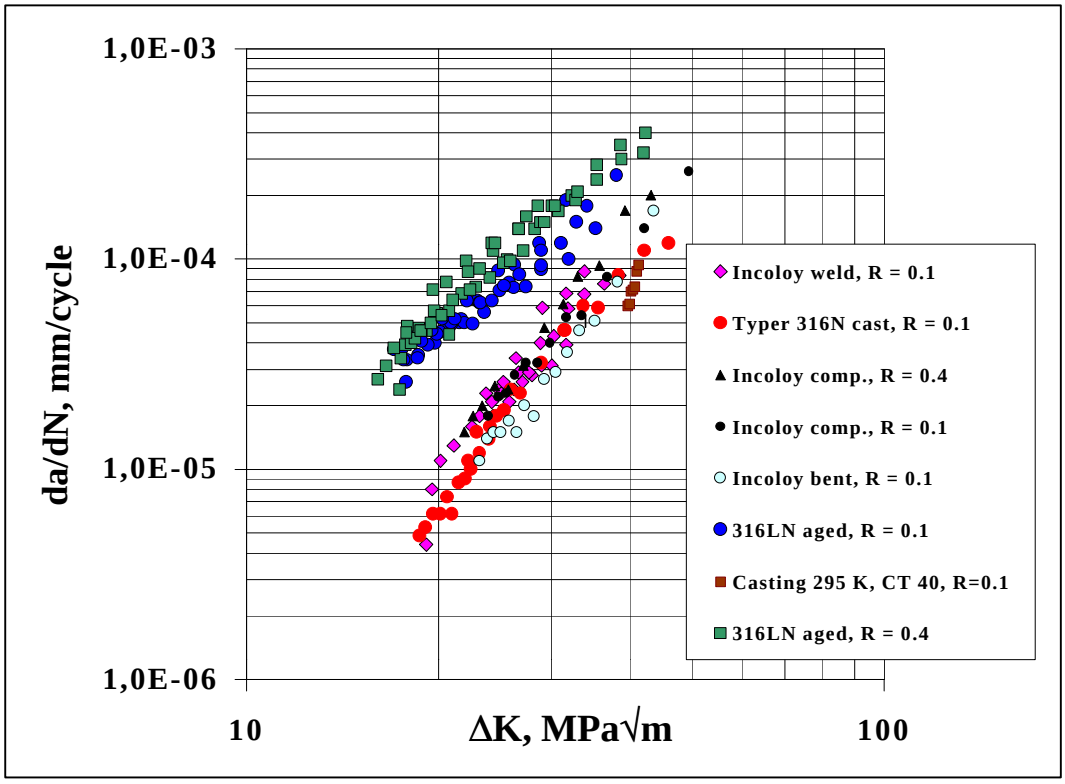

Figure 55. Fatigue crack growth rate of aged Type 316LN and Incoloy 908 jacket materials at 7 K and at different load ratios. The newly developed cast steel's FCGR represent the measurements at 7 K in all three spatial orientation.

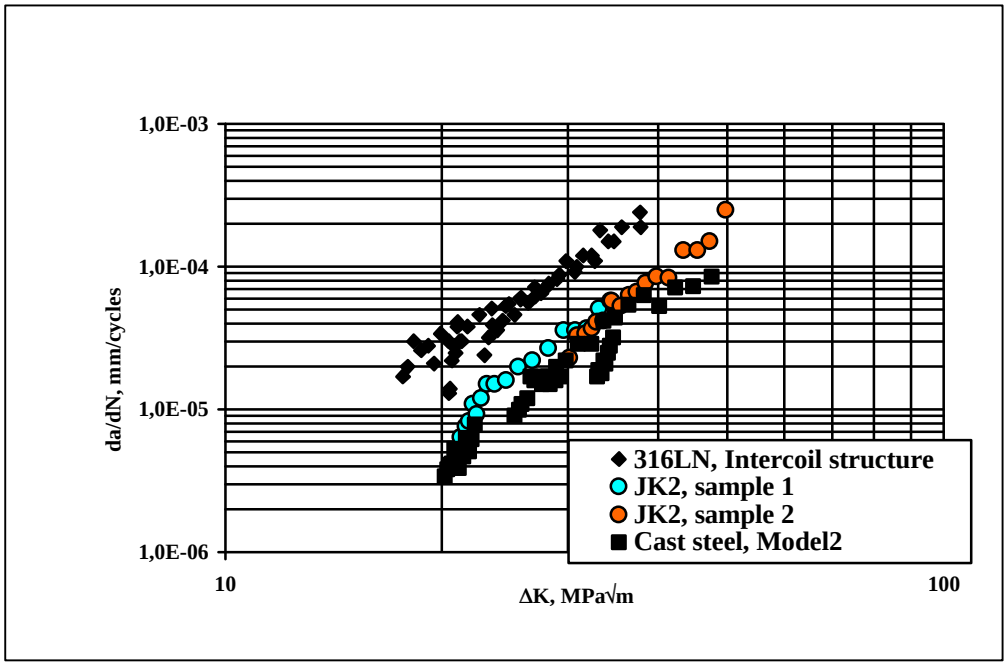

Figure 56. Fatigue crack growth rate of Type 316LN (plate material used in case of the intercoil structure) in comparison with the newly developed cast steel's FCGR and the Japanese stainless steel JK2 at 7 K.

For the forged model 1 Type 316LN stainless steel the results of the FCGR is given **in Figure 57.** The specimens for these test series were machined from the core of the big 40 t forging. In addition, the sample was cut from the bottom of the forged material thus showing bigger grains than usual. The FCGR results of the forged material is within the range of the cast stainless steel owing to the case of big grain sizes.

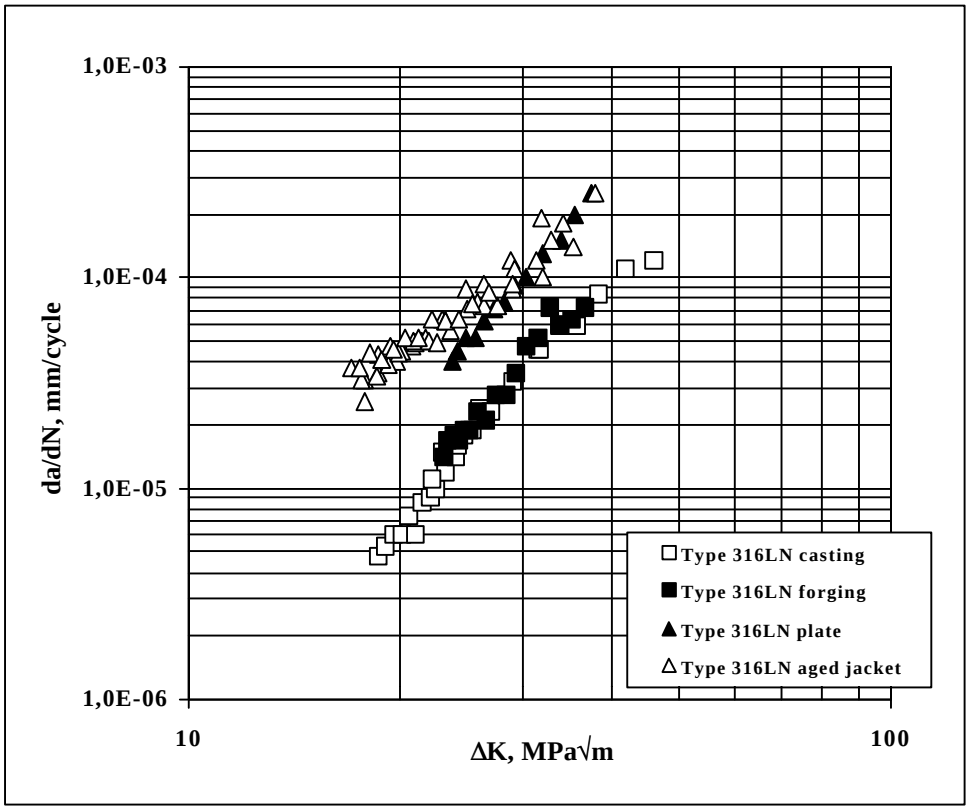

Figure 57. Fatigue crack growth rate of Type 316LN (forged materia, model 1) in comparison with the newly developed cast steel's FCGR. and common standard 316LN plate material at 7 K.

9.11 Mechanical test results with model 2 cast steel of 25 ton

Following the experiences of the trial casting with one ton weight the company Creusot Loire produced a casting for the model 2 as a final piece foreseen for the mock-up as shown in **Figure 46**. Similar cryogenic mechanical tests have been performed with this sample and the data is given in **Table 29**.

Table 29. Results on tensile properties of 25 ton cast steel mock-up between 4.2 and 7 K

File & specimen orientation	Specimen Type & Temperature	Young's modulus GPa	Yield Strength MPa	Ultimate Tensile Strength, MPa	Elongation %
Tcasty-1 (Y)	4 Ø, 7 K	159	944	1086	25
Tcasty-2 (Y)	4 Ø, 7 K	124	852	1055	40
Tcasty-3 (Y)	12 Ø, 4.5 K He gas	179	800	1231	26
Tcasty-4 (Y)	12 Ø, 4.2 K (LHe)	173	870	1183	17
Tcastx-1 (X)	4 Ø, 7 K	162	911	1216	33
Tcastx-2 (X)	4 Ø, 7 K	176	847	1048	27
Tcastz-1 (Z)	4 Ø, 7 K	214	877	1060	20
Tcastz-2 (Z)	4 Ø, 7 K	168	869	984	20

As given, the Table shows the results obtained with different size of specimens. In fact, the measurements are carried out also between 7 K and 4.2 K resulting no significant differences of the major engineering tensile behavior. For a final judgement, the average of all results with respect to trial casting and the 25 t casting were compared in Table 30 considering the spatial orientation.

Table 30. Comparison of two cast steels concerning their cryogenic mechanical properties

One ton trial and 25 t model 2 specimens with respect to their orientation	Young's modulus, GPa	Yield Strength MPa	Ultimate Tensile Strength, MPa	Elongation %
One ton trial (Y) versus model 2 (Y)	137 vs. 158	710 vs. 866	1082 vs. 1138	30 vs. 27
One ton trial (X) versus model 2 (X)	124 vs. 169	852 vs. 879	1055 vs. 1132	40 vs. 30
One ton trial (Z) versus model 2 (Z)	179 vs. 191	800 vs. 873	1231 vs. 1022	25 vs. 20

The results of **Table 30** shows so far that the yield strength variation regarding the orientation is less significant for the final casting. Also the Young's modulus values are more homogenous and higher in case of the 25 t mock-up. The fracture toughness properties at 7 K are also improved in case of the final casting as given in the following **Table 31**.

Table 31. Comparison of fracture toughness results between one ton trial and 25 ton final casting at 7 K

One ton trial cast and 25 t model 2 casting samples and specimens spatial orientation	Critical J-value	Converted average fracture toughness MPa√m
Cast steel A (Y) as rec. [0ne ton]	179 / 132	172
Cast B (Y) sol. heat treat. [0ne ton]	181 / 148/ 219	186
Cast (X) sol. heat treat. [0ne ton]	154 / 165	174
Cast (Y) sol. heat treat. [0ne ton]	130 / 140	160
Cast (Z) sol. heat treat. [0ne ton]	171	171
Cast (X) Model 2 [25 ton]	242 / 202	205
Cast (Y) Model 2 [25 ton]	193 / 241	203
Cast (Z) Model 2 [25 ton]	300 / 252	229

9.12 Conclusions

For structural Type 316LN cast steels there is no detectable size effect of the tensile properties at 4 K for specimens with diameters between 4 and 22 mm. For Type 316LN steels when tests are performed at 7 or 4.2 K (gas/liquid) there is also no detectable effect on tensile properties. Young's Modulus of the cast steel Type 316LN determined by tensile tests varies at 7 or 4 K between 100 and 185 GPa depending on orientation and position of machined specimens. Young's Modulus of the Type 316LN cast steel determined by nondestructive vibration technique at 295 K show values between 146 - 194 GPa. Measured thermal expansion of cast steel show between 295 and 7 K a ca. 10 % higher value compared to 316LN plate / forged materials. Fracture toughness tests performed with JETT technique show at 7 K an average fracture toughness value > 150 MPa√m. Tensile measurements conducted with specimens consisting of heat affected zone of a weldment show little or no straining of the heat affected zone. The weakest link of the weldment is in this case the base metal of the cast steel and not the weldment. The FCGR of the cast stainless steel and forged stainless steel show at 7 K low values comparable to the Incoloy 908 material. Finally, similar measurements performed on final 25 ton cast steel show a general improvement of all relevant cryogenic mechanical data.

10. Cryogenic mechanical characterization of 316LN base metal for ITER intercoil structures

10.1 Background

The subject deals here with the cryogenic characterization of a 80 mm thick, 2400 mm width and 4900 mm length plate material Type 316LN material provided by NOELL, Germany. The plate was produced by Creusot Loire Industrie (CLI), France with heat number 60679 designated as C516. These carried out investigations at 7 K comprised the characterization of the material with respect to tensile, fracture toughness, and fatigue crack growth rate measurements.

10.2. Test Procedure

The tensile tests have been performed using 4 mm diameter cylindrical specimens with 22 mm reduced section and M6 threaded ends. These tests were carried out with specimens machined from the sample in transverse, longitudinal, and vertical orientations. The position of the L-T (long-transverse) and T-L (transverse-long) specimens were approximately at near surface (circa in 10 mm depth) of the plate as well as plate mid section (circa 40 mm deep).

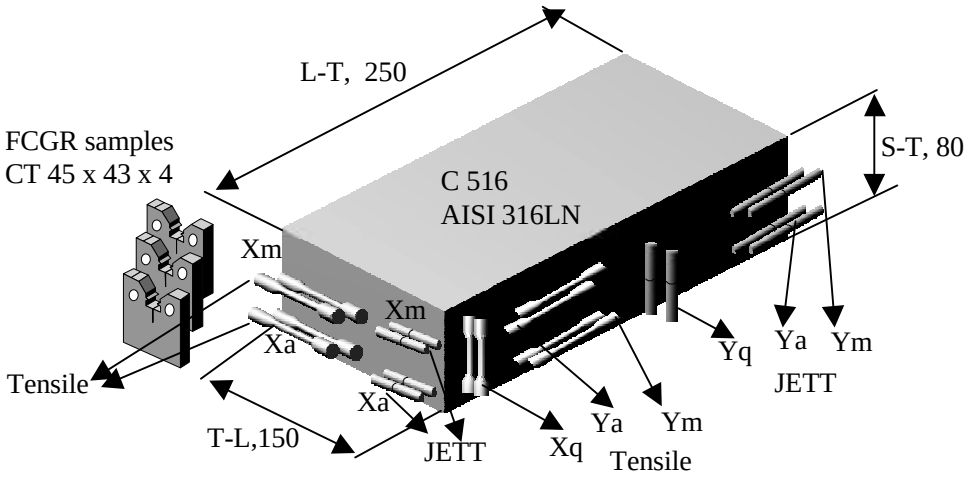

Figure 58. 80 mm thick Type 316LN metal sample and the position of the machined specimens

The specimens from S-T (short transverse) orientation were machined approximately from the plate center. The given orientation designations are according to ASTM. Measurements of the fracture toughness were performed by the JETT test, where the specimen orientation were similar to the tensile specimens.
The fatigue crack growth rate tests were carried out with small compact tension specimens from S-T orientation. **Figure 58** illustrates the received test sample of 250 mm x 150 mm x 80 mm with the position of the machined specimens.
The chemical composition of the investigated 80 mm thick plate is given in **Table 32**.

Table 32. Chemical composition of the investigated 80 mm thick plate Type 316LN

Mat.	C	Si	Mn	P	S	Cr	Mo	Ni	N
C516	.02	.49	1.58	.027	.0008	17.18	2.53	11.89	.16

10.3 Tensile measurement results

Figures 59 to 62 show all tensile tests carried out with the 80 mm thick plate sample using the specimens machined from different orientations. Each Figure contains the test results of two specimens machined from identical positions of the block. The stress region is enlarged between 1000 and 1700 MPa for the reason of better observation of the specimen to specimen scatter. In addition, **Figure 63** gives the details of the linear zero offset region responsible for the elastic properties of the tested material.

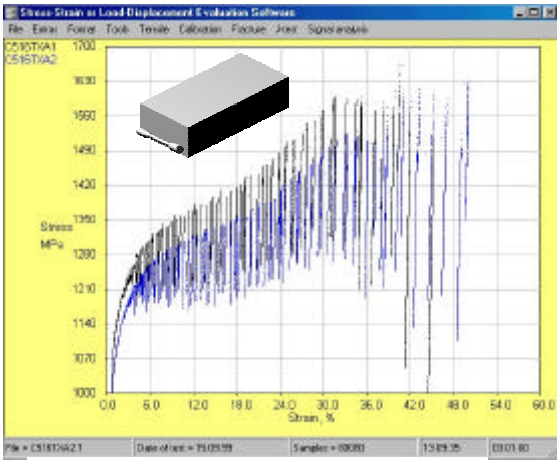

Figure 59. Results of stress strain measurements of the 80 mm thick Type 316LN sample at 7 K. Sample orientations are along the T - L direction and at near surface region. Designation of orientations according to ASTM.
T – L : transverse Long
L – T : Long transverse
S – T : Short transverse

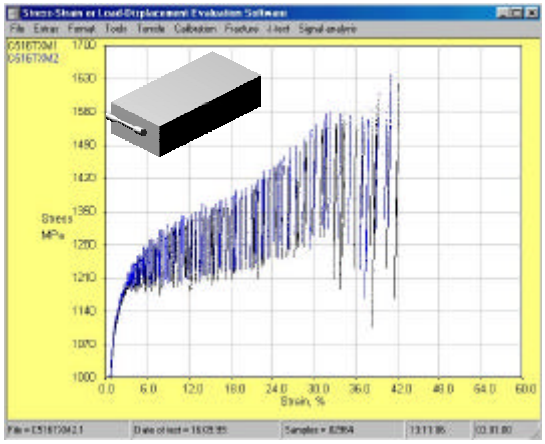

Figure 60. Results of stress strain measurements of the 80 mm thick Type 316LN sample at 7 K. Sample orientations are along the T - L direction and at mid plane region of the plate

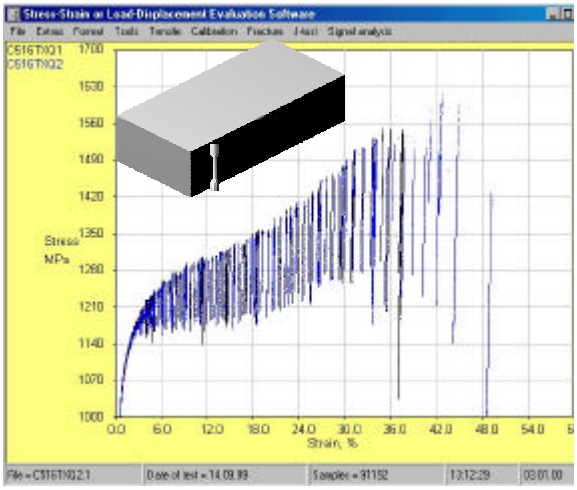

Figure 61. Results of stress strain measurements of the 80 mm thick Type 316LN sample at 7 K. Sample orientations are along the S - T direction and approximately from the mid plane region.

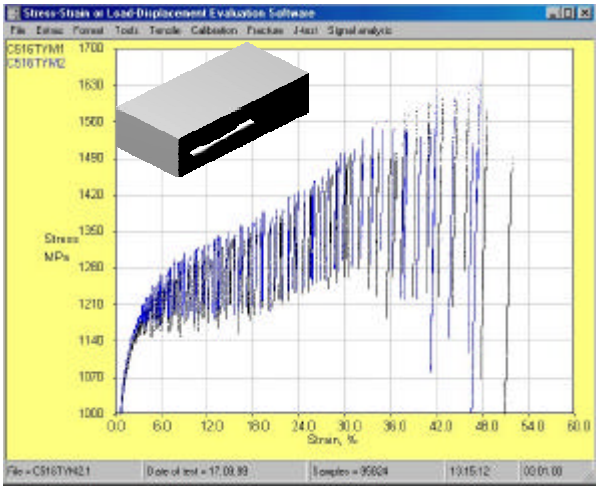

Figure 62. Results of stress strain measurements of the 80 mm thick Type 316LN sample at 7 K. Sample orientations are along the L - T direction and at mid plane region of the plate

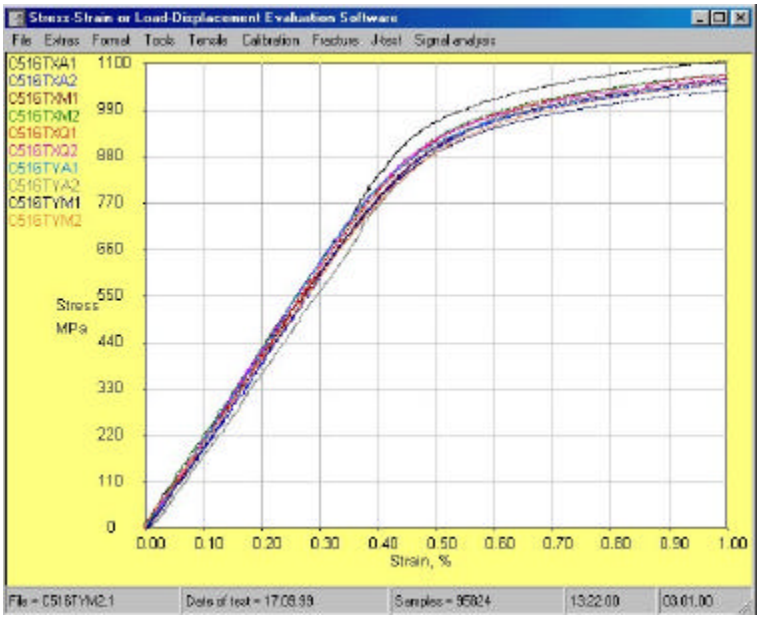

Figure 63. Results of stress strain measurements of the 80 mm thick Type 316LN sample at 7 K. In this diagram all tested sample results are shown out of the enlarged region between 0 % and 1 % strain.

Table 33 gives the results with the carried out tensile tests at 7 K. The scatter of the results are so far small with a statistical average and standard deviation of [204 +/-7] GPa for Young's modulus and [1007 +/- 20] MPa for yield strength, respectively. The material shows also a homogenous elongation in all three spatial orientations.

Table 33. Tensile test results of Type 316LN 80 mm thick plate sample at 7 K

Files	Specimen orientation	Young's Modulus GPa	Yield Strength MPa	Ultimate tensile strength MPa	Uniform Elongation %	Total elongation %
C516TXA1	T-L, surface	209	1051	1662	40	47
C516TXA2	T-L, surface	193	1002	1631	43	50
C516TXM1	T-L, mid plane	204	1000	1619	42	42
C516TXM2	T-L, mid plane	206	1015	1641	40	40
C516TXQ1	S-T	210	1009	1551	38	38
C516TXQ2	S-T	211	1003	1616	43	49
C516TYA1	L-T surface	210	991	1620	43	49
C516TYA2	L-T surface	192	1026	1565	42	45
C516TYM1	L-T mid plane	204	977	1614	44	52
C516TYM2	L-T mid plane	198	994	1639	42	48

10. 4 Fracture toughness measurements

For the fracture toughness measurements of the 80 mm thick Type 316LN plate material the JETT (EDM notched round bar) method has been applied. In **Table 34** all data obtained from the three orientations are collected together and the measured J-Integral test results are converted to K_{IC} corresponding to the crack plane orientation.

The achieved values of K_{IC} show a homogeneous fracture toughness of this investigated plate material.

Table 34. Fracture toughness properties tested by JETT method at 7 K.

Files	Specimen orientation	Critical J N/mm	K_{IC} MPa$\sqrt{m}$
C516TXA1	T-L, surface	251	226
C516TXA2	T-L, surface	306	250
C516TXM1	T-L, mid plane	280	239
C516TXM2	T-L, mid plane	255	228
C516TXQ1	S-T	232	218
C516TXQ2	S-T	246	224
C516TYA1	L-T, surface	220	212
C516TYA2	L-T, surface	296	246
C516TYM1	L-T, mid plane	290	243
C516TYM2	L-T, mid plane	259	230

10. 5 Fatigue Crack Growth Rate Measurements

The fatigue crack growth rate tests of the material was conducted using small compact tension specimens of the size 45 mm x 43 mm x 4 mm. Altogether three specimens were tested at 7 K. The results of these test are given in **Figure 64**. The drawn line gives the worse case of the investigated results and hence the Paris line coefficients are calculated using this trend line as $C= 2.1\ 10^{-9}$ mm/cycle and m = 3.15.

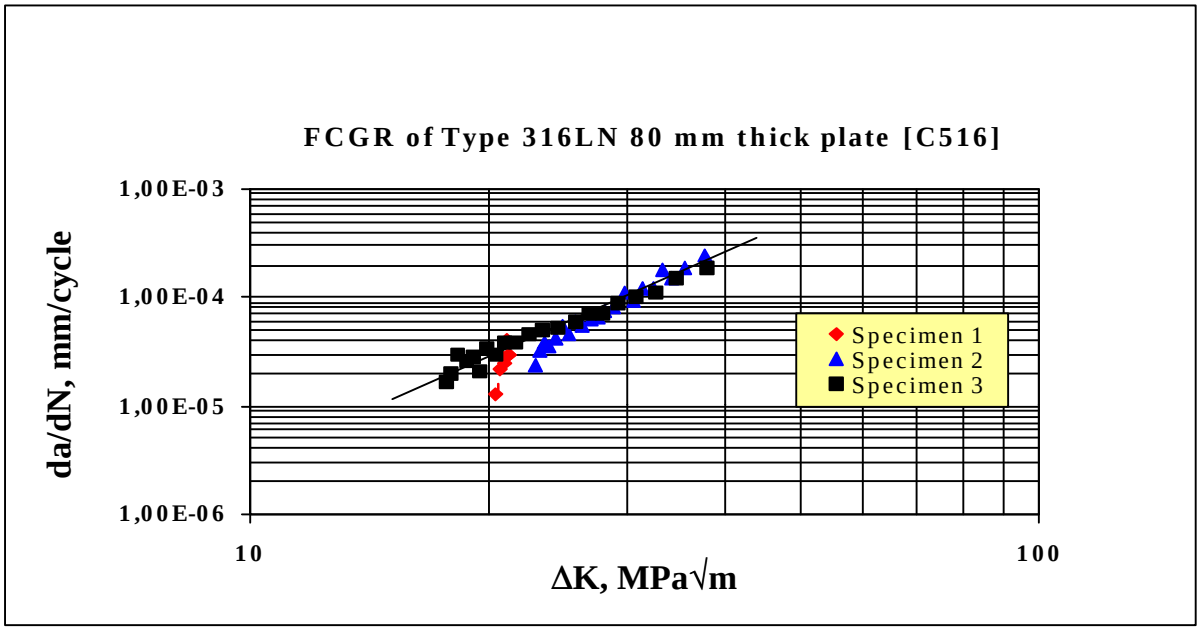

Figure 64. Fatigue crack growth rate test results of the material C516 (Type 316LN) at 7 K and at R = 0.1.

10. 6 Conclusions

The tensile properties of the investigated plate show a yield strength value around 1000 MPa considering all three orientations. The ultimate tensile strength and the uniform elongation values were obtained to be ~1600 MPa and >40%, respectively. The determined fracture toughness data show values >220 MPa√m in all three spatial orientations and the effect of orientation is negligible considering the scatter of the data. The fatigue crack growth rate data results at 7 K to Paris coefficients of C = 2.1 10^{-9} mm/cycle and m = 3.15, respectively.

11. Heat treatment investigations on Incoloy 908 jacketed TFMC superconductor samples

11. 1 Background

Parallel to the manufacturing of the Toroidal Field Model Coil (TFMC), designed with a stainless steel jacketed conductor, a complementary development program was started in Europe to use Incoloy 908 as a jacket material. This program included mechanical characterization of material at low temperatures, manufacture of a pancake using a dummy Incoloy jacketed conductor. The manufacture of the pancake was performed by Ansaldo (Genoa, Italy), using the tools used for the manufacture of the TFMC pancakes. The main difficulty in this manufacture comes from the phenomenon with Stress-Accelerated-Grain-Boundary-Oxidation (SAGBO)[2]. As the furnace used for heat treatment was using argon at atmospheric pressure, shot peening was applied to the whole outer surface of the conductor jacket and argon with very low oxygen content (<0.1 ppm) circulated inside the conductor. Nevertheless, despite these precautionary measures, after heat treatment cracks were discovered in the jacket as shown in **Figure 65**, and large crack extension occurred during transfer [3].

Figure 65 Cracks on the pancake jacket consisting of Incoloy 908 after heat treatment

The present heat treatment of the pancake showed that SAGBO still bears problems although the successful manufacturing of the Central Solenoid Model Coil (CSMC). Therefore the obtained experience from the CSMC heat treatment can't be transferred simply to other structures consisting of Incoloy 908 material. At Forschungszentrum Karlruhe a task was initiated to investigate the oxygen concentration changes during the heat treatment of original TFMC superconductor samples.

11. 2 Experimental setup

These heat treatment tests has been carried out in a resistance furnace specially installed for the aging process. The samples were placed in the temperature constant zone (+/-0.2 K) of an one side closed 150 mm diameter quartz tube. A turbomolecular pumping device maintained a vacuum of $3 \cdot 10^{-4}$ hPa at the process temperature of 923 K inside the quartz tube. The pressure was measured at the outlet, near the pumping unit and could be kept constant throughout the process. The oxygen concentrations and the temperature was measured in situ directly at the vicinity (circa 10 mm apart) of the specimens using a high precision commercial gauge (Zirox Company, Greifswald, Germany) based on zirconia emf cell capable of measuring oxygen concentrations lower than 10^{-20} ppm between 873 K and 1273 K. **Figure 66** shows details of the heat treatment setup in a schematic view used in a previous task for aging of tensile specimens. The aging process started after a temperature ramp up to 923 K and holding this temperature constant for the rest of the time. However, the oxygen could be recorded starting from 873 K. Oxygen content in ppm versus time data were acquired for several sample combinations, such as original as received non heat treated TFMC sample (**Figure 67**) or Incoloy 908 jacket removed from the superconductor strands and calibration tests with empty furnace.

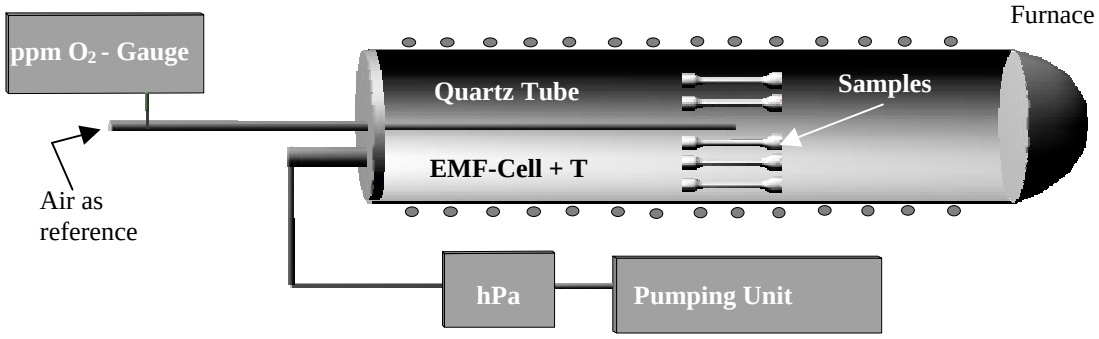

Figure 66. Schematic view of the heat treatment setup with turbo molecular pumping unit, oxygen emf cell with thermo couple, and pressure gauge. Here the specimens are tensile type.

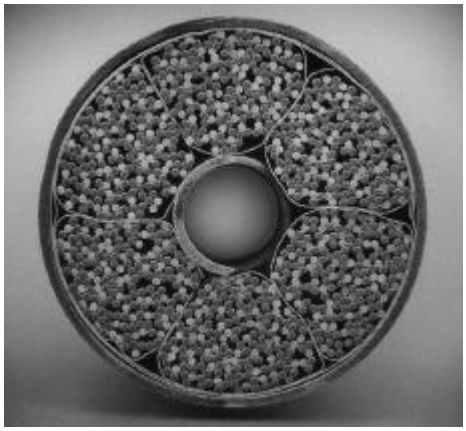

Figure 67. Incoloy 908 jacketed pancake superconductor in as received state

11. 3 Results of heat treatment action

The measured initial oxygen concentration of ~$1 \cdot 10^{-13}$ ppm (**Figure 68 and 69**) refers to an oxygen partial pressure of ~$1 \cdot 10^{-21}$ hPa (or ~$1 \cdot 10^{-25}$ MPa or ~ 1.10^{-24} bar) accounting to the pressure of $3 \cdot 10^{-4}$ hPa at the furnace outlet (with respect to air as reference of 210000 Vol ppm oxygen). The initially extremely low oxygen partial pressure is related to the rapid reaction of the oxygen with alloy constituents forming the reaction products (oxidation). This can be confirmed by the equilibrium oxygen partial pressures at 923 K of chromium and nickel according to the thermodynamics (Ellingham diagram [4, 5] as given schematically for Ni, Fe, and Cr in **Figure 70**) yielding for pure substances (chemical activity equal to unity) ~10^{-33} MPa and ~10^{-17} MPa, respectively. The nickel equilibrium oxygen partial pressure are thereafter much higher than the measured oxygen content by the emf cell. Therefore, in this initial stage of the aging the majority of the oxygen gas in the furnace atmosphere are involved with the oxide formation of the nickel surface and the emf cell region was oxygen depleted (low oxygen ppm) as the measurement shows. The oxidation phenomenon at the surface of the Incoloy 908 forces the diffusion of the oxygen along the grain boundaries of the material. The drastic increase of the measured oxygen concentration to ~2 ppm (or ~$3 \cdot 10^{-13}$ MPa) after a certain time at 923 K shows that the oxidation process is almost stopped and the equilibrium between the alloy constituents and oxygen partial pressure is maintained during the remaining aging time. The higher content of the oxygen is most probable given by the furnace system (leaks, pumping unit or else). These in situ measurements could verify these phenomena owing to the capability of the oxygen content determination at the very site of the aged alloy.

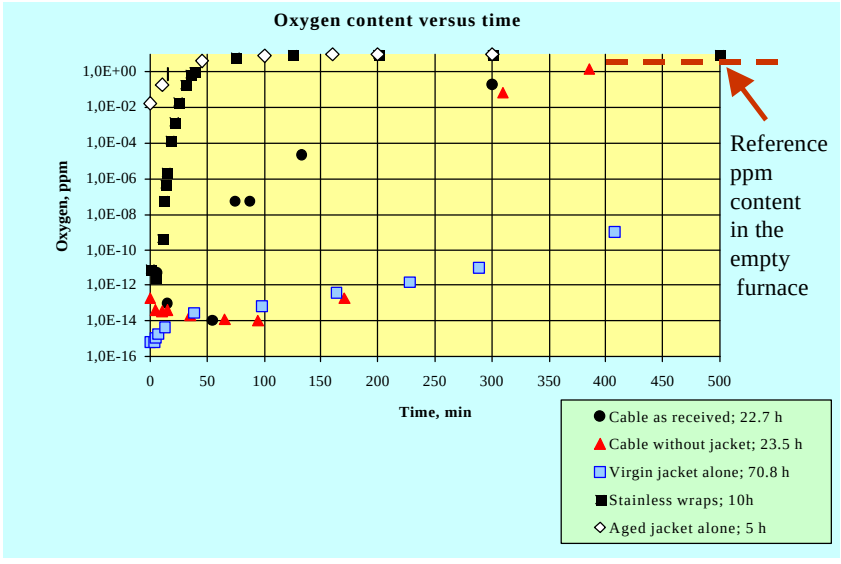

Figure 68. Oxygen content versus time diagram obtained for different samples during the 650° C aging process in a vacuum emf cell monitored furnace system in a close up view of 500 minutes

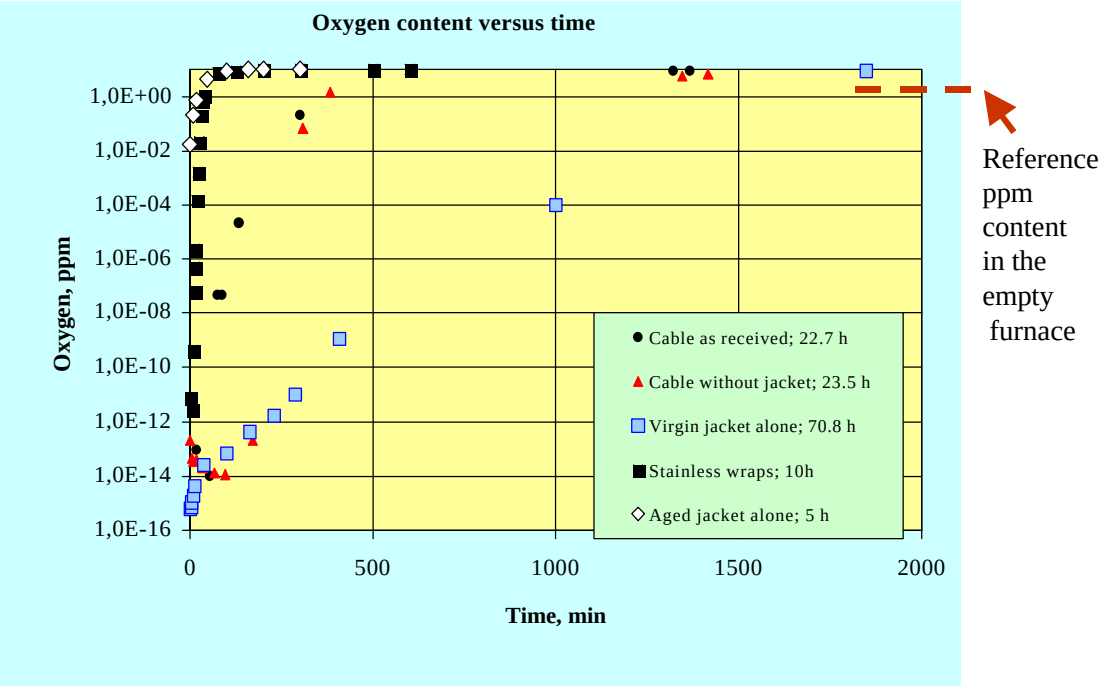

Figure 69. Oxygen content versus time diagram obtained for different samples during the 650° C aging process in a vacuum emf cell monitored furnace system up to 2000 minutes

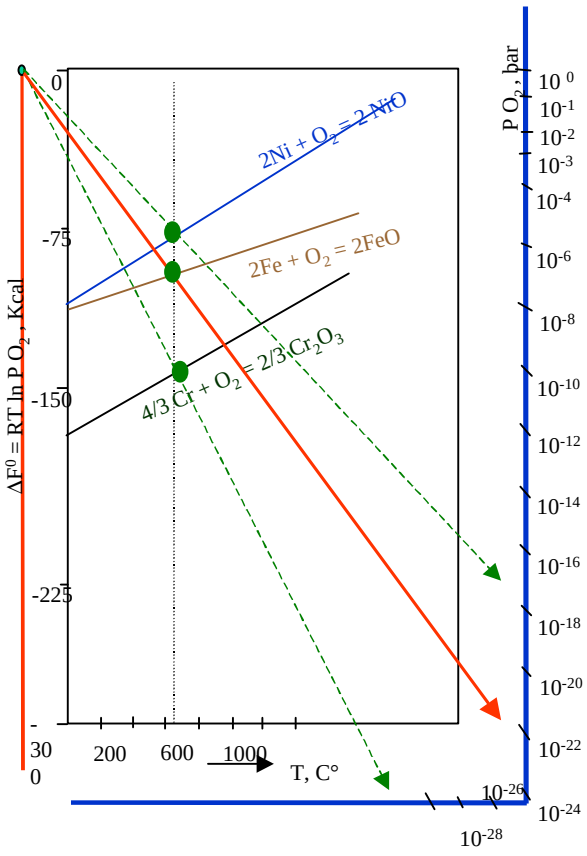

Note:
The chemical activities of all compounds in this diagram are unity

Figure 70. The standard free energy of formation of nickel, iron, and chromium constituents as a function of temperature. The nomogramm gives information about the oxygen partial pressure at thermodynamic equilibrium for pure substances where the chemical activities are unity.

As shown in both **Figures 69 and 70** the oxygen take up kinetics of the Incoloy 908 material in form of a jacket (tube) is very slow and takes several thousands of minutes up to thermodynamic equilibrium. Here the Incoloy 908 material determines the kinetics of the take up. Stainless steel structures (wraps) or an already aged Incoloy 908 tube (saturated with oxygen) reach in a very short time their thermodynamic equilibrium. The stainless steel reaches at around ~40 minutes whereas the once aged jacket structure reaches within some minutes the equilibrium. Cable without the jacket which consist of chromium plated superconducting strands or cable as received (complete cable including the jacket) show almost the similar kinetic behavior because the oxygen partial pressure conditions are determined by the chromium. However, this means that the oxygen gas still will diffuse through the jacket material (~ 2 ppm after ~ 500 minutes) because the high partial pressure. The diffusion of the oxygen into the jacket (thin walled tube) can be estimated using the following procedure.

Lacking of information with respect to the diffusion coefficient of oxygen into nickel metal at 650° C an assumption has been made by substituting the nickel/oxygen system with the iron/oxygen system. Diffusion coefficient of oxygen into iron can be ready calculated by the known activation energy and the D_o obtained by reference [6].

The D_o of oxygen diffusion into Fe is given as Do= 4 x 10-5 m^2/s

Activation energy is Q = 167 kJ/mol

At 700°C one obtains according to the data base a value D = 4 x 10^{-14} m^2/s

or 4 x 10^{-10} cm^2/s

This value refers to the bulk diffusion. Assuming that the diffusion will take along the grain boundaries, the grain boundary diffusion is in general 3 order of magnitude higher as in bulk lattice. So changing the above value to D = 4 x 10^{-7} cm^2/s estimates the grain boundary diffusion coefficient of oxygen atom into the nickel (or approximately into Incoloy 908) metal.

Assuming that the Einstein's equation of atom movement holds as given by the following equation

$$x\,[cm] = \sqrt{(\,D\,[cm^2/s]\,.\,t\,[s]\,)}$$

This results into: $x = \sqrt{(\,4.\,10^{-7}\,.\,3600.\,200)}$, with the aging of the metal for 200 hours.

The calculated result with 0.5 mm penetration of oxygen into the metal shows that the entire tube thickness will be fully penetrated by the oxygen and the jacket is therefore saturated with oxygen during the long period of the aging. The thin walled structure is therefore not representative compared to the CS jacket having a much thicker structure especially at the corner sections. Besides, the thin jacket tube incorporates a longitudinal weld seam which in case of CS jacket is not there. The weld seam may enhance internal tensile residual stresses thus acting detrimentally during the aging stage.

11. 4 Conclusion

The origin of cracks observed in the Incoloy pancake are a combination of an initial welding residual stresses and oxidation during heat treatment. Investigation of the oxidation indicates a fully penetration of the oxygen inside the jacket metal. A safe manufacturing of thin Incoloy 908 jacket would need first understand the mechanism of grain boundary diffusion and setting up conservative actions to avoid it.

12. Fatigue life investigations of a 80 mm heavy weldment for ITER intercoil structure

12. 1 Background

This present task deals with the estimation of the cryogenic mechanical performance of the 80 mm thick heavy weldment, welded by MAG process. The provided weld metal sample at 1999 by Noell company showed several weld process related defects. To check the weld metal performance in as received condition it was decided to perform fatigue life measurements at 7 K with the already machined common standard tensile specimens. X-ray diagnostics of the machined compact tension specimens showed in both long and transverse weld orientations statistical distributed defects in the entire weld metal (holes, bubbles, and pores).

12. 2 Specimens

The machined tensile specimens were 60 mm long with circa 20 mm long reduced section of 4 mm Ø. Both ends of the tensile specimens were metric threaded with M6. Altogether 4 specimens in weld transverse orientation and two specimens in weld longitudinal orientation were machined from different weld depths. **Figure 71** shows schematically the sample

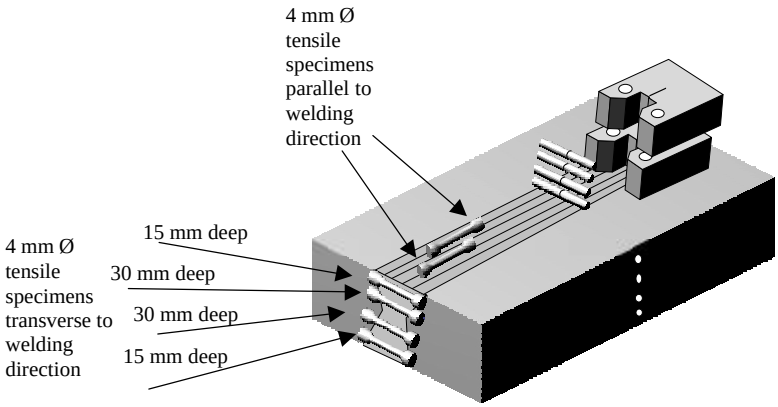

Figure 71. Illustration of the 80 mm thick weld metal and the position of the machined specimens

with the position of the machined specimens. Prior to the tests one was aware that the ratio 1.26 of threaded cross section (15.9 mm^2) to the test cross section (12.599 mm^2) will restrict the fatigue life test results in a way that the fracture occurrence will be more likely at the severe thread region and not at the smooth gauge section.

12. 3 Test Method

All fatigue life tests were carried out in a temperature variable helium flow cryostat equipped with a MTS servo hydraulic unit of +/- 25 kN load capacity. The tests were performed at a load ratio R (P_{min} / P_{max}) of 0.1 and at 7 K. Prior to the test of specimen No 2 the stress - strain behavior of the weld metal was measured with loading and unloading of the specimen twice up to 1 % strain. All other specimen were directly loaded to the envisaged stress level and the cyclic load was held constant throughout the experiment.

12. 4 Results and discussion

Table 35 shows the results of the first test conducted with the specimen No 1 machined from weld transverse orientation and 15 mm depth position. The load history shows that the specimen survived the given cyclic load.

Table 35. Fatigue life of Fravit weld metal obtained using 4 mm Ø (cross section 12.566 mm^2) tensile specimen at 7 K and R = 0.1

Specimen orientation, position, and number	Displacement range of the machine& specimen during cycling, mm	Frequency of cycling	Load range kN	Stress (max.) at gauge section MPa	Cycle number N	Comment
Transverse, from bottom 15 mm : No1	0.3930 - 0.2735	30	3.77 – 0.377	300	100 000	Survived
Transverse, from bottom 15 mm : No1	0.4320 - 0.2870	30	5.026 – 0.5026	400	10 000	Survived
Transverse, from bottom 15 mm : No1	0.4725 - 0.2915	25	6.28 – 0.628	500	10 000	Survived
Transverse, from bottom 15 mm : No1	0.512 - 0.2985	25	7.54 – 0.754	600	10 000	Survived
Transverse, from bottom 15 mm : No1	0.554 - 0.3100	20	8.796 – 0.8796	700	10 000	Survived
Transverse, from bottom 15 mm : No1	0.6790 - 0.3475	10	12.566 – 1.2566	1000	10 000	Survived

Figure 72 hows the stress strain diagram of the second specimen obtained prior to the cyclic fatigue loading.

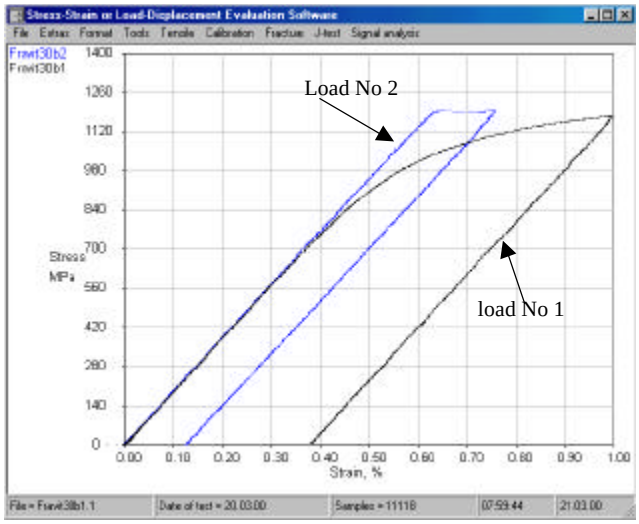

Figure 72. Stress strain diagram of weld metal in transverse orientation at 7 K. The second load sequence shows the strong strain hardening behavior of the material

The second loading shows the evidence of strong strain hardening behavior of the material. **Table 36** refers to the results of the static mechanical data. The yield strength of the weld metal with 1119 MPa shows that the weld metal has a considerable higher strength compared to the base metal of Type 316LN. Therefore the thread section (with a cross section of 15.9 mm^2) of specimens machined from transverse weld orientation and consisting of base metal is assumed to be the weak link of the system which could be confirmed by the tests.

Table 36. Mechanical properties of the weld metal obtained at 7 K in virgin state

Type 316LN weld metal (Fravit) transverse 30 mm depth from bottom	**Temperature** **K**	**Young's modulus** GPa	Yield strength MPa	Maximum achieved stress before unloading, MPa
Initial loading	7	192	1119	1175
Second loading	7	193	~1195	1197

Table 37 gives the results of all six tests. The failure analysis showed in all cases that the fracture occurs at the thread region rather than at smooth gauge section. Therefore in this **Table 37** also the calculated values of the stresses at the thread region are compiled.

Table 37. Fatigue life of Fravit weld metal obtained using 4 mm Ø tensile specimens at 7 K and R = 0.1 [cross section of the reduced gauge section =12.599 mm^2; at the root of thread section = 15.9 mm^2]

Specimen orientation, position, and number	Displacement range of the machine& specimen during cycling, mm	Frequency Hz	Load range kN	Stress max. at gauge section MPa	Stress max. at thread section MPa	Cycle number N	Comment
Transverse, from bottom 15 mm : No1	0.3930 - 0.2735	30	3.77 – 0.377	300	237	100 000	Survived
Transverse, from bottom 30 mm : No2	0.6790 - 0.3475	10	12.566 – 1.2566	1000	790	31019	Fractured at thread
Transverse, from top 30 mm : No3	0.8275 - 0.5285	15	11.31 – 1.31	900	711	35641	Fractured at thread
Transverse, from top 15 mm : No4	0.7030 – 0.4380	17	10.1 – 1.01	800	635	55779	Fractured at thread
longitudinal, from top 15 mm : No5	0.5580 – 0.3380	20	7.54 – 0.754	600	474	167732	Survived
longitudinal, from top 30 mm : No6	0.6890 – 0.4310	20	8.82 – 0.882	700	555	245116	Fractured at thread

Figure 73 shows the fractured tensile specimen under fatigue loading. The etched weld zone shows base and weld metal fusion zone. **Figure 74** gives the actual photography of the tested and failed specimen under fatigue loading.

Figure 73. Failure position of the specimen and the etched weld zone.

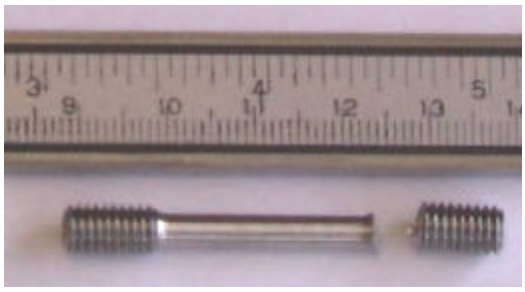

Figure 74. Failure position of the cyclic loaded tensile specimens at 7 K.

In **Figure 75** data with respect to stress versus cycle number are plotted in semi logarithmic scale. Between the transverse and long orientation specimens there is an obvious tendency indicating that the transverse specimens cyclic life are inferior to the longitudinal specimens life. This can be attributed to the following circumstances; the longitudinal specimens consist of pure weld metal having higher yield strength values compared to the base metal and

therefore this implies to a higher fatigue life. Contrary to that the thread region of the transverse specimens consist of base metal as shown in **Figure 73** and therefore these specimens are weaker compared to the specimens with pure weld metal. These tests are also not comparable with smooth section standard fatigue life specimens because of the failure of specimens at early stages due to the severe thread region. However, even with the existing high concentration stress at the thread region the material can bear stresses of circa 600 MPa for > 100 000 cycles at 7 K.

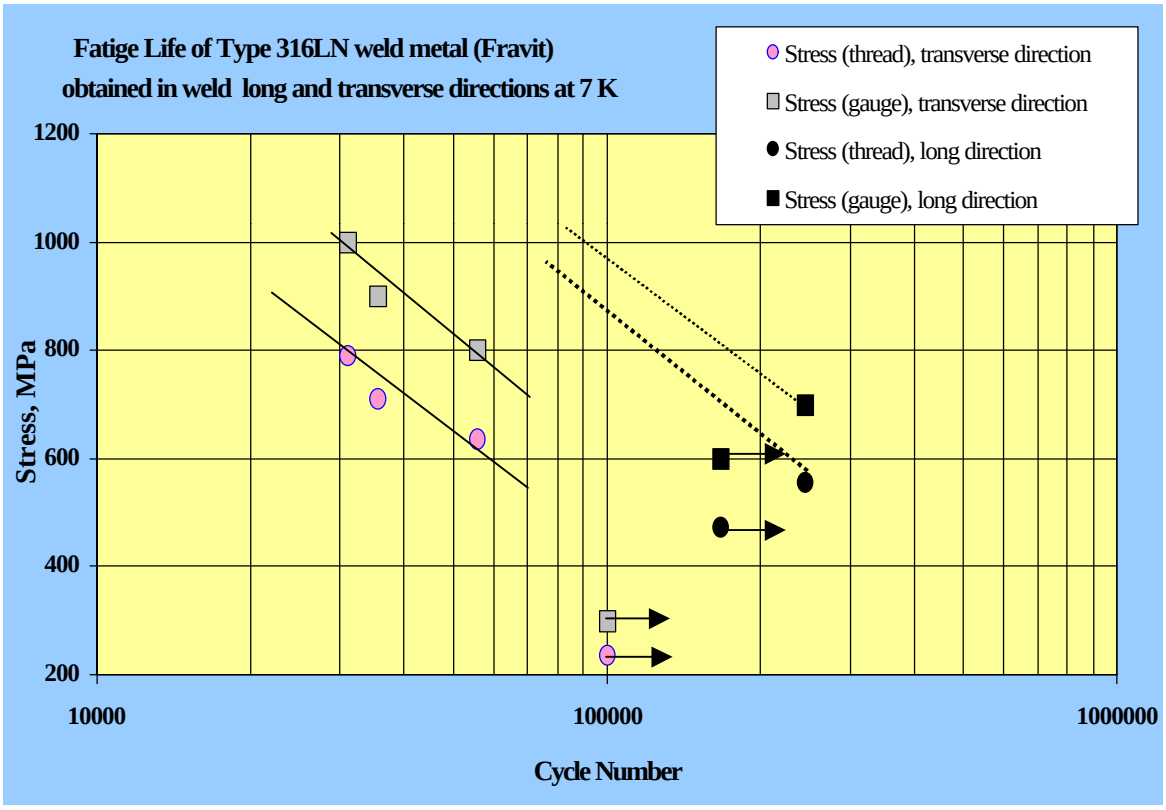

Figure 76. Stress versus cycle number of Fravit weld metal at 7 K obtained with usual standard tensile specimens machined in two different orientations. Arrows indicate survival of the specimens.

12. 5 Conclusions

Fatigue life tests at 7 K performed with standard tensile specimens of a heavy weld metal consisting of weld process related defects show specimen failure at thread region. The determined yield strength of the weld material at 7 K is ~1119 MPa which is significant higher than common 316LN base materials. In case of pure weld metal specimens (longitudinal orientation of the specimen) fatigue life is higher than the weld/base mixed specimens (transverse orientation). A cycle number of 100 000 at 600 MPa could be determined even considering the high stress concentration at the thread region.

13. Fatigue life investigations of weld metal for CS jacket materials Type 316LN

13. 1 Background

Knowledge about the fatigue life properties at 4 K especially of weld zones are rare. Therefore it is foreseen to perform measurements on fatigue life behavior of the CS jacket materials orbital weld zone. Preliminary tests were carried out with the reserve samples of

welded jacket materials provided during the manufacturing stage of the CSMC. The first set of these measurements comprised tests on 316LN (Valinox) CS jacket structures.

13.2 Specimens

The specimens for the fatigue life tests at 7 K were usual hour glass type flat and circular specimens carefully machined from the jacket material. However, the test section differed from the common hour glass configuration by allowing a 4 mm long parallel reduced section transverse to the welding orientation. **Figure 77** illustrates the machining positions of the specimens.

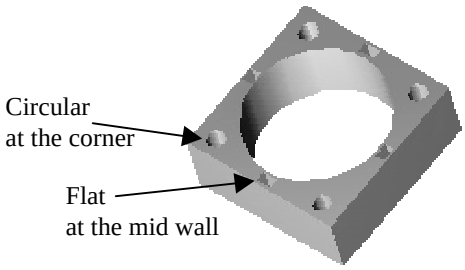

Figure 77. A section of the CS jacket and the details of the positions with respect to flat and circular test specimens.

Figure 78 shows the fractured flat and circular specimens. The center position of the specimens consist of entire weld metal.

Figure 78. Tested flat and circular Valinox weld metal specimens.

13. 3 Test method

The measurements were performed in a variable temperature cryostat allowing to cool down the specimen down to 7 K. The cyclic loading at 7 K was conducted using the servo hydraulic MTS machine (capacity 25 kN). The specimens were cyclic loaded up to fracture and the total cycle number was determined.

13. 4 Results and discussion

Nearly all specimens show a crack initiation from the surface region. A crack initiation from the bulk region of the specimen was observed only for some few specimens. **Figure 79** shows the fractured surface of three specimens showing the crack initiation, propagation, and the final fracture sites.

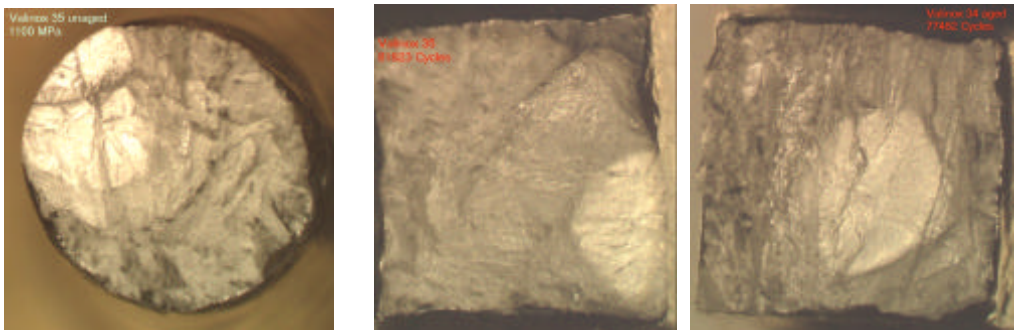

Figure 79. Type 316LN (Valinox) weld metal fatigue life tested cross sections. The far left and the center photography show circular and flat type specimens with crack initiation from the surface. The far right specimens fractured surface indicates an initiation of the crack from inside of the bulk region. A close up view under microscope reveals, however, the existence of a small pore which was the nucleation site of the crack.

In **Figure 80** the determined fatigue life of the weld metal from the CS jacket material (Valinox) is given. Between circular and flat specimens no significant differences could be observed. The specimen cyclic loaded at 900 MPa survived the 1 million cycle regime. The second time loading of this particular specimen at a load of 1000 MPa reveals however that the specimen has already consisted of a crack resulting from the previous loading. In the same **Figure 80** also measurements with the cast steel of the model 2 material is plotted. The low yield strength of the cast steel reflects also in a lower fatigue life range compared to the jacket material. Further tests are planned also with Incoloy 908 jacket material in near future.

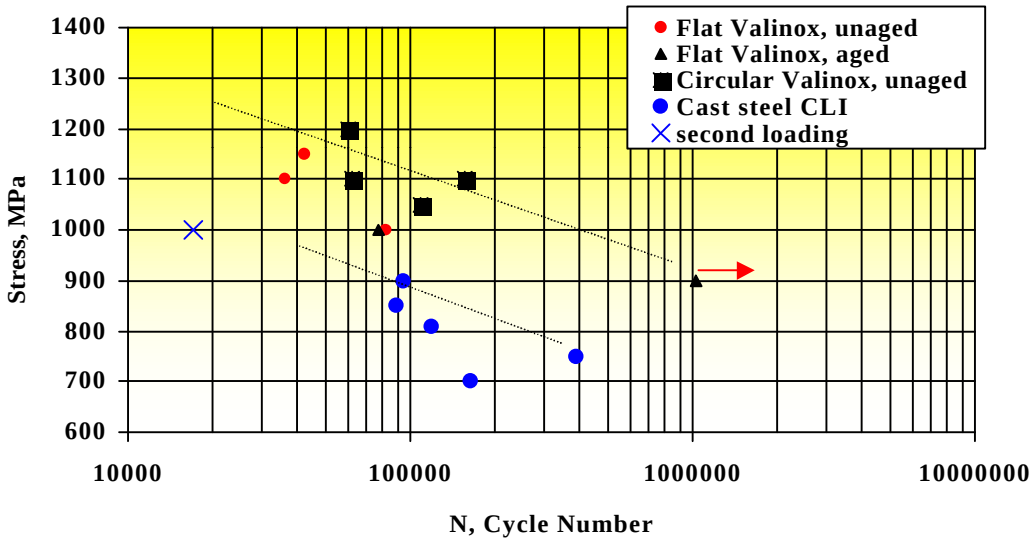

Figure 80. Fatigue life of Valinox welded material of CS jacket measured at 7 K. The survived specimens was loaded a second time with a higher cyclic load sequence. For comparison reason also cast steel results are plotted in this diagram.

13. 5 Conclusion

Fatigue life tests conducted with the CS jacket materials weld zone show in case of small flat and circular specimens a failure start from the surface region. Fatigue life tests with cast steel show that this steel is inferior compared to the jacket materials weld metal.

14. Determination of friction coefficient for ITER wedge plates at 7 K

14. 1 Background

For the design of the ITER intercoil structures wedges are necessary to couple the coils. The material of the wedge region consists of Type 316LN with a special surface roughness and the counterpart metal face would be additionally plasma nitride processed. For the design calculations the knowledge of the 4 K friction coefficient is a necessary. To measure the coefficient a special device was developed at Forschiungszentrum Karlsruhe thus allowing to test the pairs (plasma nitride surface / machined with a defined design roughness) at 7 K.

14. 2 Experimental setup

Figure 81 shows a schematic illustration of the designed device for the friction coefficient tests.

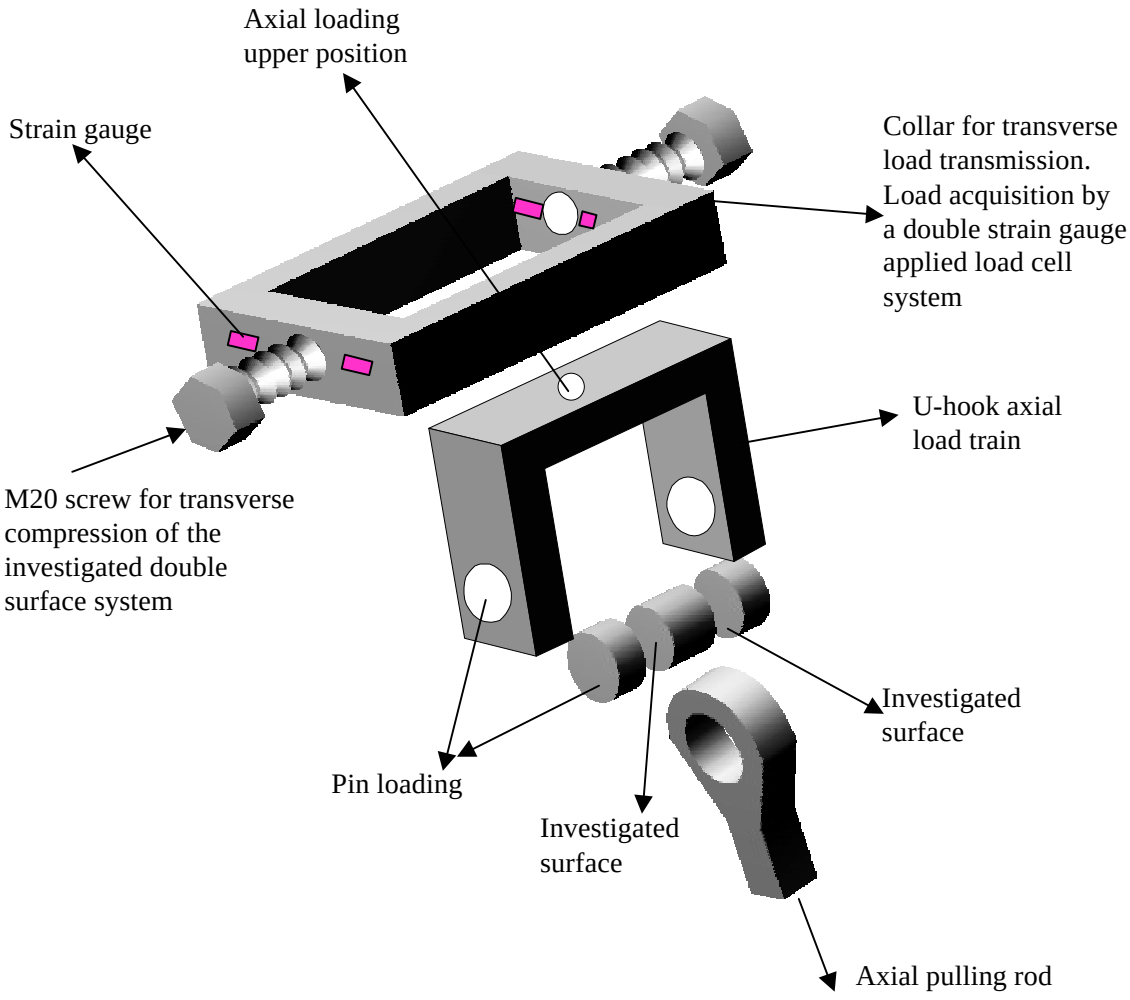

Figure 81. Axial loaded two test pair surfaces clamped together by a collar system which transfers the transversal force to the surfaces.

The illustrated collar system consists of two strain gauge bridge type displacement transducers which were calibrated prior to the tests (displacement of the collar versus the force) at room temperature and at 7 K to ensure the knowledge of the transverse force on the surfaces of the test samples. The investigated samples were nitride surface / machined surface and machined surface / machined surface.

14. 3 Results

During the axial loading the axial load versus axial displacement were recorded. At the first load drop which results from the slipping of the system the device was unloaded. The ratio of transversal force and the axial maximum load resulted into the friction coefficient (considering the two surfaces). **Table 38** gives the determined results with the test samples. The second test (file slip2) shows a very small friction coefficient. It can be assumed that this test is not valid because of some unknown cause. Decreasing the temperature from 295 K to 7 K results in a lower friction coefficient for both material pairs.

Table 38. Results with respect to friction coefficient μ between 295 K and 7 K for different surface conditions

File	Material combination	Temp. K	Transverse Load signal V	Transverse load kN	Ultimate Axial load kN	Friction coefficient μ
Slip1	Nitride surface/ machined surface	7	0.420	13.81	6.77	0.245
Slip2	Nitride surface/ machined surface	295	0.327	8.36	2.87	0.172
Slip3	Machined surface/ machined surface	295	0.325	8.31	4.38	0.264
Slip4	Nitride surface/ machined surface	295	0.360	9.21	5.17	0.280
Slip5	Nitride surface/ machined surface	295	0.433	11.10	6.92	0.311
Slip6	Nitride surface/ machined surface	295	0.238	6.09	3.90	0.320
Slip7	Machined surface/ machined surface	295	0.232	5.93	2.67	0.225
Slip8	Machined surface/ machined surface	7	0.275	9.042	3.30	0.182

14. 4 Conclusion

The friction coefficient for samples having plasma nitride hard surface and defined roughness surfaces of Type 316LN materials were determined successfully at 7 K. The friction coefficient decreases at 7 K approximately between 22 to 30 % compared to the room temperature values.

References

[1] A. Nyilas, "Final Report on ,Characterization of Jacket Material,", Contract NET/96-408, May 1997
[2] M. Morra et al., Incoloy 908. A low coefficient of expansion alloy for high strength cryogenic applications, Part 1 – Physical Metallurgy, Met. Trans. A., December 1992, pp. 3177-3192.
[3] P. Libeyre et al., Risks and benefits of Incoloy 908, To be published at SOFT 2000.
[4] H. J. T. Ellingham, Reducibility of oxides and sulphides, J. soc. Chem. Ind., Trans., (1944), 63 p. 125
[5] L. S. Darken and R. Gurry, in: "Physical chemistry of metals", Mc. Graw Hill Book comp. (1953)
[6] <http://dfw.jst.go.jp/difdb/home.html>

Institut für Technische Physik
Arman.nyilas@itp.fzk.de